UNSTEADY FORCES ON OSCILLATING HYDROFOILS

Thesis by

Gerhard Joachim Klose

In Partial Fulfillment of the Requirements

for the Degree of

Doctor of Philosophy

California Institute of Technology

Pasadena, California

1966

(Submitted 26 May 1966)

UNSTEADY FORCES ON OSCILLATING HYDROFOILS

by

Gerhard Joachim Klose

ABSTRACT

An experimental apparatus is described which has proved to be well suited to the determination of the unsteady lift forces on a hydrofoil oscillating in heave under a free surface.

Results are presented for tests covering a wide range of reduced frequency with several foil models in fully wetted, base-ventilated, and supercavitating flow. Tests were performed with aspect ratio one foils and also in two-dimensional flow. The effects of submergence depth below the free surface, angle of attack, and oscillation amplitude were investigated. The experimental findings for the fully wetted foils generally agree fairly well with the available theoretical results.

In supercavitating flow, the cavities were established by forced ventilation. The characteristics of the ventilated cavities under oscillation are discussed. The variation in the unsteady lift coefficients with cavity length, and the attendant unsteady cavity pressure, are also presented. The average values of the unsteady lift coefficients are found to differ appreciable from theoretical

calculations, and some factors which may contribute to this difference are considered.

The present work represents the first extensive set of unsteady force measurements on oscillating hydrofoils, and several new phenomena are revealed by the results. The implications of these findings for practical problems are discussed, and some suggestions are offered for further investigations.

ACKNOWLEDGMENTS

The author wishes to express his sincere appreciation and gratitude to Dr. Allan J. Acosta, whose guidance, help, and encouragement were indispensable to the successful completion of this program.

This research would not have been possible without the awards of Institute scholarships during the years 1960-65. Thanks are also due to the Office of Naval Research for supporting this work and providing research assistantships.

For their help given in many ways throughout this program, the author is indebted to the staff members of the Hydrodynamics Laboratory: Messrs. C. Eastvedt, H. Hamaguchi, T. Kiceniuk, J. Kingan, G. Lundgren, L. Whitcanack, and R. Wilson.

The assistance of Mrs. Phyllis Henderson, Mrs. Carolyn Knapp, Miss Cecilia Lin, and Mr. Carl Eastvedt in the preparation of the manuscript is gratefully acknowledged.

TABLE OF CONTENTS

UNSTEADY FORCES ON OSCILLATING HYDROFOILS

I. INTRODUCTION

A. Preliminary Remarks: Hydrofoils, Cavitation, and Hydrofoil Boats

A lifting surface (airfoil) operating in a water environment is called a hydrofoil. The distinction is useful, for, although hydrodynamics can use many results of incompressible, i.e., low-speed, aerodynamics, operation in water differs in several respects from operation in air.

The atmosphere is essentially unbounded and uniform, at least on the scale of any flying object. Bodies of water, on the other hand, have an upper surface which is a discontinuous transition to the atmosphere, and it has been convenient for the vast majority of watercraft to operate at this interface. A lifting surface travelling in water near the surface experiences a loss of lift due to the discontinuity of the fluid and in addition is affected by the surface waves which its own motion causes at the interface. These effects can be of substantial magnitude and make analysis of the flow more complicated than for operation far from the surface, as in aerodynamics.

Water further differs from air in that it can undergo a phase change. A liquid will turn into a gas when the vapor pressure is greater than the local ambient pressure; this is the boiling point.

This evaporation can be brought about either by heating the liquid, thus increasing the vapor pressure, or by decreasing the ambient pressure even without any temperature change. The occurrence of a vapor-filled bubble, or cavity, in the liquid is called cavitation.

On a lifting surface operating in water at high speed, decrease of the local pressure at points on the suction, or low-pressure, side of the foil to near the vapor pressure will cause the water to evaporate locally, forming a small bubble of water vapor. When operating at this condition, called incipient cavitation, water turbulence and vibration of the surface can cause pressure fluctuations so that bubbles will form and rapidly collapse. This bubble collapse near the surface of the body will gradually erode the material and causes the cavitation damage frequently seen on ship propellers and pump impellers, but this is not the concern of the present work.

When the local pressure is decreased further, generally by increasing the flow velocity, cavitation may spread over a considerable portion of the surface and cause a vapor-filled cavity which starts at the low-pressure point on the foil and extends downstream along the surface to a point where the pressure is sufficient to cause the cavity to collapse. This state, where the cavity extends over part of the length of the body, is referred to as partial cavitation. If the local pressure is still further decreased, the cavity will lengthen until it extends beyond the trailing edge of the body, and the flow is said to be fully cavitating. If in addition the lifting surface has a sharp leading edge from which the cavity springs, covering the entire

suction side of the foil, it is called a supercavitating hydrofoil.

Other cavity flow conditions include base cavitation, where a cavity extends downstream from behind the blunt trailing edge, or base, of a hydrofoil or support strut, with both sides of the foil fully wetted; and planing, which can occur for hydrofoils running at shallow depths of submergence where the spray sheet, the stream of water bounded by the water surface above and the upper cavity boundary below, breaks up and does not close the cavity off from the atmosphere, exposing the foil cavity to atmospheric air.

The cavitation state of a flow is characterized by a dimensionless parameter called the cavitation number, which is defined as

$$\sigma = \frac{p_o - p_c}{\frac{1}{2}\rho U^2}$$

where p_o is the free stream static pressure, p_c the pressure in the cavity, and $\frac{1}{2}\rho U^2$ the dynamic head of the flow. From the foregoing discussion it may be seen that longer cavities correspond to lower cavitation numbers.

At speeds below those necessary to cause cavitation, a gas-filled bubble may be established by ventilation, which means introducing gas from some external source into the low-pressure region of the foil. The pressure in such a ventilated cavity will be somewhere between the vapor pressure and the ambient static pressure, depending on the flow velocity and air supply rate. In surface ventilation, the cavity is ventilated by atmospheric air

through an intersection of the cavity with the free surface; this may be either the cavity of the foil itself (planing) or the cavity behind some body contiguous with the foil, such as a support strut. Alternately, the gas may be supplied artificially at a controlled pressure greater than atmospheric; this is called forced ventilation.

The cavitation state of a ventilated flow is indicated by the cavitation number, just as if it were naturally cavitating. The body only notices the presence of a cavity of essentially zero-density fluid, compared to the liquid, and whether the gas is water vapor or air is of no consequence to the forces generated. (This statement, as it turned out, is not exactly true in unsteady flows, but it definitely holds for steady flow.) The cavitation number is thus a scaling or similarity parameter for cavity flows much as Reynolds number is for single-phase flows such as in wind tunnel testing and hydraulics. This fact has greatly facilitated laboratory testing of cavitated bodies; by deliberately supplying air to the cavity, cavitation numbers can be achieved at relatively low velocities that with natural cavitation would only be reached at high flow velocities unattainable in many facilities.

The occurrence of cavitation has a substantial effect on the flow around bodies and the pressure forces generated, which increases with increasing degree of cavitation. As an example, the theoretical lift on a supercavitating hydrofoil is only 25 percent of that on a fully wetted foil. For this reason, much of the earlier work on high-speed flows was concerned with the prevention of cavitation at increasingly higher speeds through careful design of the foil shapes, in propellers

and pumps as well as hydrofoils. Nevertheless, if the foil is to generate any lift at all, it will always have a suction side and will have a critical speed where cavitation will occur. Since the just-barely-not-cavitating condition is close to incipient cavitation with its attendant performance deterioration and material damage problem, the emphasis has recently changed to deliberately designing foil sections for optimum supercavitating performance.

In some instances, moreover, cavitation or ventilation can be decidedly advantageous. An example is the use of base-ventilated struts with blunt trailing edges. Conventional airfoil-shaped sections required for fully wetted flow, such as the support strut in the present experiments, necessarily have long gradual tapers toward the trailing edge which limit the moment of inertia of the section. A shape designed for base ventilation typically has a modified parabolic cross section and maintains close to its maximum thickness over a large part of its chord length. Such a strut thus has a much higher moment of inertia and consequent rigidity, and its drag when base-ventilated is little higher than that of a fully wetted strut of the same maximum thickness.

The use of hydrofoils on high-speed boats was conceived as early as 1891 [1] since they promise much better lift-to-drag ratios at high speeds than more conventional hulls. The general idea is to use the normal hull for flotation at rest and low speeds, with the hydrofoils, which extend into the water deeper than the hull, generating increasingly more lift as the speed is increased until this lift is

sufficient to raise the hull entirely clear of the water. Since the drag caused by the hydrofoils is much less than that of a displacement hull, higher speeds can be economically attained.

One of the most noteworthy applications of hydrofoils was by the Wright brothers, in 1907. In an attempt to interest the Navy in their airplane, they equipped it with floats and tried water-based takeoffs from the Miami River. The airplane engine had a rather limited power output, and "hydroplanes" were fitted to the floats to raise them out of the water and decrease the drag at takeoff speed. Unfortunately, the experiment was unsuccessful; surface ventilation (planing) occurred at about 15 miles per hour with consequent decreased lift so that the floats did not rise clear of the water, and takeoff speed could not be attained. (2)

Although the German navy already had prototype hydrofoil boats in 1943 with displacements up to 80 tons and speeds around 50 knots (3), serious commercial development of these craft has only taken place in the last 15 years. The initial interest occurred primarily in Europe, where the private automobile had not yet blunted the need for public transportation, and was spurred on by the development of suitable propulsion machinery and the need of ship operators to compete with the increased speeds available in land and air transport. In western Europe hydrofoil boats are used mostly in coastwise service and on inland lakes while the Russians have found them very suited to rapid transport along their large river systems. In addition to their speed, these boats are well suited to operation in

enclosed bodies of water since they generate essentially no bow wave when foilborne even at full speed and thus cause less disturbance to the shore or other nearby craft than equally large conventional boats at normal speed. (For docking and low speed maneuvering, hydrofoil boats operate as displacement hulls.)

The first scheduled service with hydrofoil boats was introduced in 1955. Today, there are about 900 boats operating, of which 300 exceed 50 feet in length[1]. Most of these vessels are in regular scheduled service; in Russia alone there are 50 routes. While the fares charged on these boats are higher than on regular boats, their economics are based mostly on their high speed which allows perhaps three times as many trips per day and helps offset their higher construction cost.

The characteristics of hydrofoil boats are exhaustively described in References 1, 4 and 5. Only a brief familiarization will be given here.

There are all manner of ways in which to arrange hydrofoils on a hull. Historically the most frequently used has been the so-called "aeroplane" arrangement where a large foil near the front of the boat supplies about two-thirds of the lift, with the rest generated by a smaller foil situated at the stern. For convenience, the front foil is sometimes split so that there is a foil at each side of the boat. There are two basic types of hydrofoils, characteristically called surface-piercing and fully submerged.

Surface-piercing foils generally have a V or U shape when

viewed from the front, and their outer extremities, as the name implies, intersect the water surface. This is the type used by the largest European concern, Supramar, and has the advantage that it is self-stabilizing: if the boat sinks deeper into the water, more foil area is submerged and more lift is generated. The same feature, however, limits it to fairly smooth waters due to the lift fluctuations caused by waves encountered, which cause rough riding. In addition, all hydrofoil boats are limited by their foilborne hull clearance in the wave sizes through which they can operate. Nevertheless, in sufficiently large sizes (90 foot length) such boats are used for service between Italy and Sicily over open water. Surface-piercing foils are usually designed for fully wetted flow and are equipped with "fences" to prevent ventilation of the submerged parts of the foils from the surface. Typical speeds for vessels of this kind are around 40 knots.

Fully submerged foils are generally horizontal and flat and are supported by vertical nonlifting struts. They do not have the area-change self-stabilizing property of surface-piercing foils. A fully submerged hydrofoil does experience a decrease in lift as it approaches the surface, which is a stabilizing tendency, but this effect is very small unless the submergence is only a fraction of the chord length. At such small depths, the foil is quite sensitive to waves and accidental ventilation with consequent force change. In the very smooth waters of Russian rivers this is apparently not a problem; the Russian hydrofoil boats use very thin, lightly loaded foils of thic

system running close to the surface and augmented by small planing foils at the water surface. Their speed is typically also around 40 knots.

For rough water operation the only suitable system is fully submerged foils relatively far below the free surface. Due to their lack of submergence effect, they are quite insensitive to waves, as long as the hull rides far enough out of the water to avoid slamming on the waves, and thus provide a very smooth ride. The lack of any self-stabilization, however, requires some kind of feedback control system to maintain ride height and stability. Since shipbuilders have always built ships with inherent stability, there was at first great reluctance to rely on "gadgets" for this essential property, and progress in this kind of boat finally came mostly from American aircraft companies, which were more used to the concept. So far, only a few smaller commercial boats of this type have been built, but there is a great deal of activity with large military prototypes up to 500 tons displacement [1].

Fully submerged foils can be operated fully wetted up to a speed of perhaps 60 knots. At higher speeds, cavitation will occur and thus supercavitating foils will have to be used on boats designed for the 80 to 100 knot range. To avoid the abrupt force changes and cavitation erosion which occur during the transition from fully wetted to supercavitating flow, artificial ventilation would be used to establish the operating condition at a lower speed and provide a smooth transition to natural supercavitating flow.

Boats utilizing supercavitating foils are presently in the test-bed and design stage, and many problems have to be solved for optimum performance to be realized. The process of ventilation and amount of air supply required at various speeds is important; loss of the artificially sustained cavity on one of the foils would cause force changes that might severely affect the boat. Such a possibility was illustrated when the research boat "Fresh-1" capsized on a trial run due to the accidental occurrence of stall and consequent upper surface ventilation on one of her foils, which were designed for base ventilation [5].

The foil shapes required for supercavitating operation have sharp, extremely thin leading edges to promote cavity detachment from the leading edge. The limited strength of these sections has caused blade failures on supercavitating propellers where they were used and forced the adoption of modified shapes with lower efficiency but greater strength. On hydrofoils there will be corresponding hydroelastic problems such as flutter and divergence. Design information on the forces and unsteady characteristics of supercavitating hydrofoils will also have to be established before stability and control problems can be solved with certainty.

B. Previous Investigations

The object of this section is to illustrate the development of topics related to the present experiments. It is not intended nor feasible here to give a comprehensive review of the literature. An

introduction to further topics may be had by referring to References 6, 7, 8 and 9.

Fully wetted, steady flow - Incompressible aerodynamic theory has provided the natural starting point for hydrofoil analysis. The problem has been attacked by both conformal transformations and singularity representations, but even for the very basic problem of a hydrofoil in steady motion below a free surface, an "exact" solution has so far not been presented. A linearized solution for the two-dimensional hydrofoil has been developed by Bernicker [10] to include the effects of foil thickness and camber at arbitrary depth below the free surface, but the Froude number is assumed to be large and gravity effects are neglected. Another approach has been taken by Wadlin and Christopher [11] who worked out corrections to conventional airfoil theory to take account of the effects of submergence, aspect ratio and dihedral for a flat plate, neglecting the gravity effect; these agree well with experimental results. Experiments with finite aspect ratio foils have been performed by several investigators [11], [12], [13].

Fully wetted, unsteady flow - The fundamental work of Theodorsen [14] is also valid for oscillating hydrofoils at deep submergence. Woods [15] has treated the two-dimensional airfoil oscillating in an infinite fluid including the effects of thickness and viscosity. Laidlaw [16], starting from Reissner's exact integral equation for an oscillating lifting surface, has derived a new theory for the pressure distribution on rectangular wings with no

restrictions on aspect ratio or reduced frequency.

For two-dimensional foils at finite submergence, Crimi and Statler [17] used the conventional unsteady airfoil model of von Karman and Sears [18] and by considering the free surface radiation conditions solved the problem for various values of submergence and Froude number. The problem of an oscillating hydrofoil travelling beneath a surface with sinusoidal waves has been considered by Nishiyama [19].

Finite aspect ratio foils with free surface effect are included in the theory of Widnall [20]. Taking advantage of the capabilities of modern high-speed computers, she makes a direct attack on the integral relation relating the upwash to the lift distribution on the wing by assuming for the latter a set of modes with unknown coefficients which are found by satisfying the boundary condition of a known upwash at a set of control points on the surface; the required integrations are performed numerically.

The same method is also applied to supercavitating flows (see below), and it appears that every unsteady hydrofoil problem could be solved by this method, given the availability of sufficient computer time. Although the theory is developed for both two- and three-dimensional fully wetted hydrofoils, numerical results for the finite aspect ratio case are not worked out due to computing time limitations.

Some experiments with a fully wetted foil oscillating in pitch in a closed water tunnel have been reported by Smith and Sevik [21], who

found the magnitude of the unsteady lift to be generally less than predicted. Recently, extensive towing tank tests have been carried out by Cieslowski and Pattison [22] for fully wetted two-dimensional foils oscillated in heave and pitch, also including some flutter investigations. Runs with heaving motion were performed at various submergences and velocities, but the considerable scatter in the results obscures the effects of submergence and Froude number on the unsteady lift, the magnitude of which is again consistently below the theoretical value.

Supercavitating, steady flow - The subject of flows with separated wakes, also called free-streamline or cavity flows, arose with the invention of the hodograph mapping technique by Helmholtz and Kirchhoff almost a century ago. This method is based on the existence and conformal mapping properties of a complex potential for the velocity in two-dimensional, incompressible, irrotational flows, and it is suited to the solution of cavity flow problems since either the flow speed or flow direction is always constant on the boundaries of the flow.

The first application of this procedure was by Kirchhoff and Rayleigh to the case of an inclined flat plate in an infinite fluid [23]. The flow was assumed to separate at the leading and trailing edges of the plate, forming two free streamlines which bound a stationary wake extending to infinity. In practical cavity flows, however, the cavity pressure is less than ambient, which corresponds to a finite cavity length.

Since a closed finite cavity cannot exist in ideal flow theory, some artifice must be employed to obtain closure of the cavity. The various models which have been proposed for cavity termination include the Riabouchinsky and re-entrant jet models and the wake dissipation models of Roshko and Wu. A description of these is given by Tulin [9], where a new spiral vortex termination model is also presented. Fortunately, the details of the flow in the region of cavity collapse, which is typically highly unsteady and turbulent, have little effect on the flow about the hydrofoil itself as long as the cavity length is several times the length of the body. Thus, a choice between these models may generally be made for computational convenience or even aesthetic reasons, but all these non-linear theories present appreciable mathematical difficulties in the solution of practical engineering problems.

The application of free-streamline theory to supercavitating flows was greatly stimulated by the introduction of the linearized theory of Tulin and Burkart [24]. The body and cavity are assumed to be slender, the flow around them being considered as a perturbation on the main flow, and the slenderness is further utilized by applying the boundary conditions on the centerline of the system instead of on the boundaries, which are not known a priori in cavity flows. The simplifications resulting from this linearization allow ready computation of the forces acting on thin bodies and cambered surfaces in supercavitating flow, also permitting the solution of some cases with thickness by using the simple non-linear corrections devised by

Johnson[25].

Some recent contributions to the literature on steady supercavitating flows have been made by Johnson [26], who determined the effect of submergence depth and aspect ratio as well as thickness, and Auslaender [27], who investigated the characteristics of supercavitating hydrofoils with prescribed pressure distributions, running near the free surface but neglecting the gravity effect.

The linearized theory has been applied to a supercavitating flat plate operating in a channel of finite depth by Ho [28], considering the effect of a solid bottom together with the free surface. A similar investigation by Ai, Acosta, and Harrison [29] includes in addition the spray sheet contraction and the free surface rise upstream of the model, which become important at very small submergences. (In fact, planing flow will be maintained past a plate which has been raised until it is entirely above the level of the undisturbed free surface.) When the foil is one-quarter chord or more below the surface, the lift given by this theory is very nearly the same as that given by Ho [28]. A summary of steady supercavitating flow theory, as well as some further applications, has been given by Tulin [9].

Experimental results have been presented by Johnson [26] which show good agreement with his theoretical work. Kermeen [12] has conducted tests in a closed tunnel with foils covering a range of aspect ratios. Free-surface tests in which a supercavity was established by ventilation have been reported by Schiebe and Wetzel [30], who measured the forces and air entrainment rates,

and by Dobay [31], who found that surface disturbances or slight changes in submergence could cause sudden unpredictable changes in the cavitation state, such as from supercavitating flow to planing, of surface-ventilated foils at shallow submergences and discussed the implications of these findings for hydrofoil boat design.

Supercavitating, unsteady flow - It has been frequently remarked that free-surface flows become very difficult to treat exactly when the flow is time-dependent. This comes about because the boundary conditions on the unsteady free surface are non-linear and the location of the free surface itself is not known a priori. In addition, the surface of constant pressure is no longer a surface of constant speed when the flow is allowed to vary with time, and thus the hodograph method which is so valuable in the solution of steady cavity flows proves much less useful for the unsteady problem.

Considering the case of unsteady flows with and without a free surface, a quite essential difference may be pointed out. In the unsteady problem without a free surface, the time enters only as a parameter and thus the analysis is not basically different from the corresponding steady flow. For unsteady flows with a free surface, on the other hand, the time variation enters into the flow explicitly through the time dependence of the boundary conditions on the free surface. This considerably complicates the analysis since the flow at any one time depends on its entire previous history.

The combination of these factors has served to limit the solution of unsteady free surface problems to a few rather special

cases, which have been discussed by Wu [32]. Faced with such difficulties, it lies at hand to take advantage of the simplifications offered by a linearized theory. This was pioneered by Parkin [33], who combined Tulin's linear theory for steady cavity flows [24] with the linear oscillating airfoil theory of Woods [34] and solved the case of an unsteady supercavitating flat plate. While the theory has been constructed for arbitrary cavitation number, numerical results have been worked out only for cavitation number equal to zero [35].

Wu has applied the linearized theory for nonsteady cavity flows to the oscillating slender wedge with a finite supercavity [36], and Geurst [37] discussed the linearization of an unsteadily perturbed re-entrant jet flow and its application to the unsteady motion of a supercavitating hydrofoil at non-zero cavitation number. Describing the chordwise oscillation amplitude distribution by a power series, Martin [38] has derived expressions for the lift and moment in terms of the coefficients of this series for a thin supercavitating foil at zero cavitation number performing generalized oscillations. The results are applied to a rigid foil in heaving and pitching motion, and to a foil moving through a sinusoidal gust.

Although not strictly related to the present experimental work, Patton and Borden [39] have computed numerical results for the interesting problem of a hydrofoil at zero cavitation number oscillating in heave and pitch with a cavity starting at an arbitrary point on the upper surface, using a theory of Woods [40].

The initial reaction of a body in a steady cavitating flow, not

required to be slender, to a sudden acceleration has been studied by Wang and Wu [41], who used several wake models to investigate the small-time behavior of the unsteady cavity flow, including the effects of cavitation number and angle of attack. The same method was also used [42] to study the propagation of dynamic waves along the free surface of a two-dimensional cavity flow with small unsteady disturbances.

By an extension of the technique already described for fully wetted flow, above, Widnall [20] attacked the problem of a supercavitating hydrofoil in two- and three-dimensional flow. Numerical results were obtained for some steady flow cases as well as for foils of aspect ratio one, six, and infinity oscillating in heave and pitch. As in all the unsteady papers cited so far, there is no submergence effect due to a water surface; the fluid surrounding the body-cavity system is assumed infinite in extent.

The additional complication of finite submergence has only recently received some attention in unsteady supercavitating flows, with the Froude number always taken to be large, so that the free surface wave effect is neglected. Hsu [43] considered a two-dimensional foil at zero cavitation number, using the amplitude distribution power series method also used by Martin [38], and obtained numerical results for heaving and pitching motion and for flap oscillation [44]. He found that the effect of the free surface was much greater than had been anticipated, but there may be some errors in the analysis.[45] The solution for a two-dimensional

supercavitating flat plate oscillating under a free surface in the more general case of non-zero cavitation number has been obtained by Song [46], but the force coefficients are not given in readily usable form.

The amount of experimental work concerned with unsteady supercavitating foils has been extremely limited. Song [47] performed some tests with a flat plate oscillating in pitch, but mechanical difficulties restricted the reduced frequency to such low values ($k < 0.03$) that the usefulness for practical hydrofoil problems is doubtful. Song also measured the force coefficients on a steady supercavitating flat plate with an oscillating flap at zero cavitation number [45] and obtained fairly good agreement with analytical results derived from the linearized theory.

C. The Present Experiment

The problem of an oscillating hydrofoil travelling beneath a free surface is relevant to the stability and control of hydrofoil boats. Knowledge of the unsteady forces involved is required for the analysis of hydroelastic instability, such as flutter and divergence, and for dynamic response calculations. As the size and speed of hydrofoil boats continue to increase, availability of reliable design information will become steadily more critical if optimum configurations and control methods are to be achieved.

It may be appreciated from the above discussion of the previous investigations that many aspects of the unsteady hydrofoil problem

still await successful consideration. The separate influences of submergence effect, finite Froude number (free surface waves caused by the motion of the hydrofoil), and finite aspect ratio, all contribute to the complexity of the theoretical solutions, and in many cases where a problem has in principle been solved, the determination of accessible numerical results has been discouraged by the prohibitive computational effort required. This has been especially true for the case of supercavitating flow.

While the scope of the theoretical treatment has thus been restricted by these many factors, the extent of the experimental work is yet more limited. So far, only one set of tests [22] has been reported for the very basic case of a hydrofoil oscillating under a free surface in supercavitating or even in fully wetted flow.

There are several possible explanations for this rather disappointing state of affairs, not the least of which is simply mechanical. The mechanism required for oscillating the model and measuring the forces and other data would tend to be substantially more bulky and intricate than for corresponding steady flows. It would thus present some difficulty in performing tests of this kind in a towing tank, where all this equipment would have to be mounted on the travelling carriage. A great improvement in convenience, and perhaps even feasibility, is gained by performing the experiments in a channel where the water, with a free surface, may be made to flow past the model, allowing the equipment to remain stationary. The Free Surface Water Tunnel, which was used in the present experiments, is of course ideally

suited to this requirement, and the lack of previous experimental investigations may be at least partly attributed to the scarcity of comparable facilities.

In the almost total absence of other experimental results for oscillating hydrofoils with a free surface, an extremely wide scope of possible configurations was open to consideration. The two basic motions of a solid foil are heaving (vertical translation) and pitching (rotation about a transverse axis); of these, heaving is more closely related to the behavior of a hydrofoil boat in a seaway. Pitching is applicable to the boat control problem for the case where the whole foil is used as the control surface, but in actual practice the use of a fixed foil with a movable flap is more likely for this purpose.

It was decided to investigate the case of heaving motion of a hydrofoil in both fully wetted and supercavitating flow, including the effects of variations in several parameters, such as foil shape, depth of submergence, angle of attack, aspect ratio, flow velocity, and oscillation amplitude, covering at each setting a range of oscillation frequencies. A detailed description of these items is given in the section on Experimental Procedure.

Since the flow velocity in the Free Surface Water Tunnel is far too low for natural cavitation to occur on the models, ventilation was used to establish the cavities. The overall picture of the flow, and hence the forces on the foils, should be essentially the same as if natural cavitation were present. In addition, the forced ventilation case is applicable to real hydrofoil boats equipped with supercavitating

foils for operation at reduced speeds, where introduction of gas is required to maintain the cavity.

Experiments on oscillating airfoils analogous to fully wetted hydrofoils, though of course without a free surface, have been extensively performed in years past. However, the mechanical driving mechanisms usual in these airfoil tests have always suffered from unavoidable mechanical clearances and slack, which introduce disturbances into the resulting motion and cause high-frequency noise signals that are superimposed on the desired outputs. The electronically controlled hydraulic actuator used in the present tests overcomes these problems and also offers the advantages of compact size, easily and continuously variable oscillation frequency and amplitude, convenient mounting, large output force levels and particular suitability to the heaving motion required for these experiments.

Considerable thought was given to the method of recording and analyzing the data. The usual practice in oscillating tests has been to record all the pertinent signals with an oscillograph, and this was, in fact, done in the initial calibrations here. But some disadvantages quickly became apparent, such as the effort involved in analyzing the records, particularly if the signals contain much noise, and the sheer volume of the chart paper produced in any lengthy test program. The scheme used in this experiment (see the section on Equipment) permits direct read-out of the amplitudes of the fundamental frequency components of the signals, which

greatly facilitates both the conduct and the analysis of the tests.

Tests were carried out with foils of unity aspect ratio, which is in the range actually used on hydrofoil boats and may thus provide some data which is relevant to design problems, and then also with the foils oscillating between closely fitting side walls to simulate the two-dimensional case, which is more readily amenable to theoretical treatment.

As already remarked, many aspects of unsteady phenomena and cavitating flows still remain to be understood. The results of the present experimental tests are of interest for the comparison with theoretical work, where such exists, as well as providing some insight into the physical realities of the flows. In addition, they may point the way to desirable future investigations of both theoretical and experimental nature.

II. TEST EQUIPMENT

A. Water Tunnel - The experiments were carried out in the Free Surface Water Tunnel of the Hydrodynamics Laboratory at the California Institute of Technology. A detailed description of this facility is given in Reference 48, and thus only its main features will be described here.

The distinguishing feature of this tunnel, as implied by the name, is that the flow in the working section is confined by solid boundaries only on the sides and bottom, but is open to the atmosphere at the top so that a free surface exists in the working section. This permits the investigation of the effect of varying the depth of submergence of models.

An overall view of the water tunnel is shown in Fig. 1. The flow in the circuit is counterclockwise, that is, from right to left in the working section. The power is provided by a 75 horsepower variable-speed direct-current motor which drives a 42-inch propeller pump located horizontally in the lower return leg. The maximum flow velocity obtainable in the working section is about 30 feet per second. Velocity measurement is by means of a total head probe located in the contraction nozzle ahead of the working section.

The working section is 20 inches wide, 30 inches deep, and 8 feet long. The entire side and bottom surfaces of the working section are formed by Lucite windows to enable observation of the

flow. The depth of water flow in the working section in normal operation is 20 inches.

One of the main improvements in the tunnel since the writing of Reference 48 has been the installation of a skimmer at the entrance to the working section, which removes the upper one inch of the flow as it emerges from the nozzle and deposits it in the stilling chamber at the diffuser end of the working section. The boundary layer which is formed along the top surface of the entrance nozzle is thus entirely removed before the flow enters the working section, and velocity surveys confirm that the free-stream velocity of the flow is indeed maintained right up to the free surface, so that tests can be performed at very small submergences without encountering errors in the flow velocity. The skimmer is the semi-circular duct which can be seen at the entrance to the working section in Fig. 2.

Since large quantities of air may be introduced into the flow in the working section, either by ventilation of surface-piercing bodies or by deliberate introduction of air, the water tunnel has an elaborate air separator to ensure that all air bubbles are removed from the flow before recirculation.

For the investigation of two-dimensional flow, a pair of inserts were fabricated for the working section. These split the flow into three streams, the center one past the model, and the two outer ones which do not affect the flow around the model. To allow photographic and visual observation of the flow around the foil, these inserts were fabricated from Lucite; however, the pressure

fields generated by the oscillating hydrofoil caused considerable deflection of the inserts, and the gap between the foil and the walls, besides fluctuating, had to be set at an excessive value to avoid mechanical contact. The inserts were therefore stiffened, in addition to angle sections along their top and bottom edges, by 1/2 inch thick steel beams at the longitudinal location of the foil. These plates are on the outside faces of the inserts so they do not affect the flow in the center section, past the model. The inserts can be seen in any of the photographs of two-dimensional flow, such as Figs. 2 and 4.

The center section of the flow is entirely free of obstructions, the inserts being fastened only to the tunnel bottom and above the water surface. To prevent ventilation of the reinforcing beams from the surface, these are terminated just below the surface and a box-beam arrangement, using a carefully streamlined 1/8 inch steel plate, is used to span the free-surface interface.

D. Hydraulic Oscillator - The hydrofoil models are oscillated by a hydraulic oscillator which consists of a double-acting hydraulic piston with the admission of fluid controlled by a servo-valve which is connected to the piston chamber through passages in the cylinder body. The diameter of the piston rod is 1.000 inches and that of the cylinder is 1.120 inches. The usable force output capability, which is of course proportional to the hydraulic supply pressure, is about 300 pounds at a pressure of 5000 psi. The hydraulic oscillator was designed in cooperation with Team Corporation of El Monte, California, who also handled the fabrication.

The hydraulic fluid is supplied by a Dennison variable-displacement pump powered by a 10 horsepower motor and capable of delivering 10 gallons per minute at 5000 pounds per square inch. A view of this pump is shown in Fig. 5.

The hydraulic oscillator and servo-valve are mounted in a mounting box which in turn is mounted to the tunnel working section. A set of mounting adapters allows variation in the height of the mounting box on the tunnel rails, so that the submergence of the hydrofoil models can be set at any desired value. In addition, a static level control on the Servo Controller (see below) allows adjustment over a range of about one inch.

Rotation of the piston rod and attached strut (see next section) about the vertical axis must be prevented so that the hydrofoil does not develop a yaw angle. This is done by means of a nylon block, attached to the cross arm at the upper end of the piston rod, which slides in a closely fitting slot; it may be seen at the left end of the cross arm in Fig. 6.

A diagram of the hydraulic oscillator and its mounting is shown in Fig. 7 and a photograph in Fig. 6. The hydraulic oscillator can be seen mounted to the working section in Fig. 2.

C. Supporting Strut and Hydrofoil Models - The supporting strut is a symmetrical streamline section of NACA 0010 contour with 4 inch chord and 10 percent thickness which is attached to the piston rod of the hydraulic oscillator. This strut is designed to maintain fully wetted flow at all times, so that ventilation from the surface

will not occur along its trailing edge. Otherwise, air might travel from the surface along the strut to the foil, causing formation of a cavity. This would be undesirable in the fully wetted runs, obviously, and also in the tests with ventilated cavities since there it is desired to control the amount of air supplied to the cavity, which is not possible when the cavity is open to the atmosphere.

At its lower end, the strut carries the strut dynamometer, which will be described presently, to which in turn the hydrofoil models are attached. The foils are mounted centrally on the strut, the strut-foil combination thus forming an upside-down "T". The foils are all of the same dimensions in plan form, with a 6 inch chord and 6.10 inch span (for suitability for other tests), giving an aspect ratio of essentially unity.

Foils with several cross section shapes were made; these include a wedge with an apex angle of 8 degrees, a "flat plate" model of 1/4 inch thickness with the leading and trailing edges smoothly tapered to a sharp edge, and a plano-convex foil with the upper surface flat and the lower surface a circular arc, with a maximum thickness of 0.480 inches. All these foils have square side edges.

There are actually two of the wedge models; one is made of aluminum, as are all the other foils, but another one was made of wood (pine) waterproofed with epoxy resin, with a T-shaped aluminum reinforcing piece which forms the leading edge and provides strength in the area of the attachment bolts. This model was built to overcome the very considerable inertial mass of the aluminum wedge, since the

effect of this mass must be subtracted from the measured forces to obtain the lift coefficients.

Yet another model is the "rounded flat plate", designed to help investigate the effect of the sharp side edges on the "flat plate". This closely resembles the "flat plate", having also 1/4 inch thickness, but it has the side edges rounded to a semicircle of 1/8 inch radius and the leading edge rounded to a radius of 1/16 inch, with some taper. The trailing edge of this model, as well as of all the others (with the obvious exception of the wedge), is tapered to a point.

To allow the mounting of the foils at various angles of attack relative to the flow, wedge-shaped adapters can be inserted between the foil and the strut. All the foils have mounting holes with spherical seats, and the mounting screws are fitted with matching washers. This allows secure mounting of the foils despite the angular changes caused by the adapter wedges and insures precise alignment and repeatability of the mounting geometry.

The various foil sections and mounting adapters are shown in Figs. 9 and 10.

D. Strut Dynamometer - Measurement of the forces on the oscillating hydrofoil requires that a dynamometer be present somewhere between the foil and the actuator. In order to avoid the problems associated with having the foil attached by a long strut to the dynamometer and having to calibrate and compensate for the lever arm involved, it was decided to construct a dynamometer as part of the supporting strut, immediately above the hydrofoil itself. While

this requires the dynamometer to operate submerged, the water-proofing was not considered a particular problem.

The general layout of the dynamometer can be seen in Fig. 7 and also in Fig. 8, which clearly shows the flexures and the stressed elements before affixing of the strain gages. There are three active elements, two in the lift direction and one in drag. By adding the output of the two lift elements, total lift is given; subtracting the two outputs gives the pitching moment. These two quantities and the drag are the primary data of interest in hydrofoil problems.

Since the dynamometer was to be in the immediate vicinity of the foil, it had to be of the same contour as the strut in order to avoid distorting the flow. The maximum thickness of the strut is 0.4 inches, and the necessity of constructing the dynamometer within this width required some compromises.

Due to the limited width available, it was necessary to ensure sufficient strength through the gaged elements to resist roll moments which might be developed by the foil. This meant accepting the possibility of some interactions between the elements, but care was taken that the effect would be a minimum in the lift direction.

After the strain gages were attached to the active elements, thin sheets of steel were cemented in the recessed area on each side for mechanical protection, and the entire section was waterproofed after installation on the strut by wrapping the exterior surface with two layers of thin rubber sheet fastened with contact cement. The wiring from the strain gages passes upwards through the strut to the

top of the actuator, and the same hole is used to maintain a small internal pressure of air in the dynamometer to guard against leakage of water.

The completed dynamometer is very stiff in deflection and has no natural frequencies below 200 cycles per second. The design loads are 100 pounds per element, so that the total allowable load is 100 pounds in drag and 200 pounds in lift, which far exceeds any loads encountered in the present program.

E. Ventilating Strut - An auxiliary strut, mounted downstream of the test hydrofoil, carries a sting which projects forward to just behind the hydrofoil. It supplies ventilating air to the cavity and is also used for the measurement of both the average and the fluctuating cavity pressure. It may be seen in Figs. 3 and 4.

F. Instrumentation - An overall view of the instrumentation layout is given by the diagram of Fig. 11, which shows the interconnection of the various units. Photographs of the instrumentation and general working area are in Fig. 2. A detailed description of the components follows:

1. Servo Controller - The motion of the Hydraulic Oscillator is controlled by a servo-valve. The electrical signals for the servo-valve are generated by the Servo Controller in such a way as to cause the actual output motion of the Hydraulic Oscillator to be the prescribed waveform; in other words, it is a conventional feedback control system. The Servo Controller, built by McFadden Electronics, South Gate, California, Model Number 150A, may be set up so that

either the displacement or the oscillation velocity of the Hydraulic Oscillator conforms to the input waveform.

The comparison signals for the control of these feedback functions are generated by a displacement and a velocity transducer which are mounted to the cross-arm at the top of the piston rod of the Hydraulic Oscillator; they are the two rod-and-plunger devices visible at the right end of the cross-arm in Fig. 6. Both of the transducers are linear variable differential transformers (LVDT's); the displacement transducer is carrier-excited while the velocity transducer is self-excited. The output of the latter is also used for the measurement of the velocity amplitude of motion of the Hydraulic Oscillator, which is needed in the data reduction.

2. Return Signal Analyzer - This unit consists of a Variable-Phase Low-Frequency Oscillator and the Return Signal Analyzer (RSA) proper, as well as associated power supplies; the system is manufactured by Boonshaft and Fuchs, Hatboro, Pennsylvania, Model Number 711A.

The Oscillator generates a sinusoidal waveform which is used as the reference waveform by the Return Signal Analyzer; another output furnishes the command signal to the Servo Controller. This command signal is of the same frequency as the reference signal, but its phase relative to the reference signal is continuously variable throughout 360°; its amplitude is also adjustable. The frequency range of the Oscillator is from 0.01 to 1000 cycles per second, and its maximum output amplitude is 50 volts.

The Return Signal Analyzer performs a Fourier analysis of the signal applied to its input, which has just returned from whatever system is under test (whence the name of the unit), and resolves it into two components, one which is in-phase with the reference signal and one which is in quadrature phase (90^{o}) to the reference signal. Only that part of the signal which is of the same frequency as the reference waveform is detected by the RSA; all other frequencies are eliminated. The resulting rejection of noise and harmonics is specified at 40 db. This feature is convenient at very low signal levels, for instance for the dynamometer strain gage outputs in the present tests, which even with careful shielding picked up a large 60-cycle component. Since the fundamental frequency component of the signal is of primary interest, the fact that with the present apparatus all information about harmonics and other frequencies is lost is not an important drawback. (With some modifications, the oscillation and reference signals could be generated separately, and such investigations could then be carried out.)

The outputs of the RSA are the root-mean-square amplitudes of in-phase and quadrature components. They are given as DC signals which may be either positive or negative; a negative output will occur for instance on the in-phase channel if the return signal is 180^{o} out of phase with the reference waveform. The lowest full-scale sensitivity of the RSA is 0.05 volts; the DC output voltage is 10 volts for full-scale deflection at all sensitivities.

3. Digital Voltmeter - The output voltages of the RSA, as well as other DC voltages, were measured with a Non-Linear Systems Series 2900 Digital Voltmeter, which is basically a reversible digital counter with counting rate proportional to the input voltage (100, 000 pulses per second per volt). It is characteristic of digital devices that their accuracy is equal to the least count, that is, to one unit in the last column. The read-out of four decimal digits in this voltmeter thus represents a real and usable accuracy which was, in fact, essential to the acquisition of satisfactory data. At its most sensitive setting, the voltmeter has a least reading of 1 microvolt.

The voltmeter operates by sampling the input voltage for either 0.1, 1, or 10 seconds. The read-out is the total number of pulses recorded by the counter during this period and is thus proportional to the average voltage over the sampling time. AC voltages average to zero since the counter runs backwards for negative voltages.

4. Oscillation Amplitude Measurement Since it is the velocity of the heaving, or plunging, motion which causes the fluctuating effective angle of attack, it was decided to use the oscillation velocity directly as the measure of the amplitude of the motion. It is measured simply by applying the output voltage of the velocity transducer to the RSA.

5. Force Measurement - The forces generated by the hydrofoil are measured by strain gages applied to the active elements of the strut dynamometer. The excitation and balancing functions for the

strain gage bridges are performed by Microdot PB-290A Power and Balance Units and a Microdot VB-300 Power and Balance Monitor. The resultant bridge output voltage for each of the active elements is amplified by a factor of ten in Burr-Brown Model 1605 Operational Amplifiers. The signals of the two lift elements are then either summed, to give total lift, or differenced, to give pitching moment; any of the individual or combined signals can then be selected, are amplified again by a factor of 100 in Model 1605 amplifiers, and routed to the input of the RSA for measurement.

6. Cavity Pressure Measurement - It was desired to measure both the average cavity pressure and its fluctuations. A tube affixed to the ventilating strut and along the sting, terminating near the foil, sampled the average cavity pressure; this was measured relative to atmospheric pressure on a water manometer. Except when a measurement was being taken, air was bled through the cavity pressure line at a very low rate to keep the line clear of water droplets.

Measurement of the fluctuating cavity pressure requires the use of a transducer. The obvious location for this is the tip of the sting, and a Statham Model PM131 TC transducer was chosen for its small size, which allowed it to be mounted inside the 1-inch diameter sting with only the diaphragm exposed. This transducer has a rated range of ± 2.5 psi, and while the values of the fluctuating cavity pressure were not expected to be very large, the transducer had to be able to stand up under the full dynamic head of the flow, should the

cavity be swept away.

Erratic results in the first tests led to the discovery that water droplets trailing off the strut were hitting the diaphragm of the transducer in a periodic manner, giving an apparent fluctuating cavity pressure output. A splash shield was thereupon fabricated to protect the diaphragm from direct impact.

The low sensitivity of this transducer (8 millivolts/psi) necessitated amplification of its output by the same two stages of Burr-Brown amplifiers used for the forces in order to boost the signal level to a value sufficient for the RSA.

Seepage of water into the sting drowned out two of these transducers, and for the last series of tests a Wiancko Type P2-3142 transducer was used, mounted at the top of the ventilating strut and connected to the cavity by 54 inches of 1/4 inch I.D. tubing. It was ascertained that this remote location would have no significant effect on the cavity pressure measurements up to oscillation frequencies of 10 cycles per second [49]. The range of this transducer is ± 5 psi. It has the advantage of having a built-in preamplifier which boosts its output to 0.5 volts/psi, so that its signal needs no further amplification before analysis by the RSA.

7. Cavity Length Measurement - The bottom of the tunnel working section being a Lucite window, a mirror mounted at an angle below the working section allows observation of the cavity behind the hydrofoil from below. This, combined with the direct view from the side, made determination of the cavity length possible within 0.1

chord lengths in most cases (cavity length is non-dimensionalized in terms of the hydrofoil chord). A scale marked off in tenths of chord length was fastened to the bottom window of the working section to facilitate estimation of the cavity length.

8. Ventilating Air Supply - Compressed air for ventilating the cavity was taken from the Campus air supply, which has a nominal pressure of 90 psi and quite satisfactory short-term stability. The air was metered through a valve and its flow rate measured by a Fisher-Porter Flow-Rator, with a Heise 100 psi pressure gauge measuring the pressure at the Flow-Rator. The air was then piped to the ventilating strut and carried forward to the cavity through a 1/2 inch copper tube fastened along the sting.

Although the flow velocity through this tube was substantial at the higher air supply rates, extensive checks confirmed that the air blast impinging on the hydrofoils had no measurable effect on the fluctuating force measurements.

III. EXPERIMENTAL PROCEDURE

A. Initial Check-out and Calibrations

1. Hydraulic Oscillator - A displacement and a velocity transducer are attached to the cross arm at the upper end of the piston rod. The displacement transducer can be conveniently calibrated statically. The velocity transducer was calibrated by driving the Hydraulic Oscillator at the various test frequencies and determining the oscillation amplitude from the output of the displacement transducer; this was also checked by visual observation of the double amplitude through a traveling-stage microscope.

Testing of the Hydraulic Oscillator revealed a "hammering" sound and roughness in the output waveform when the Servo Controller was set to Position Feedback. This probably arises because, when the Controller notes a position discrepancy, it signals the servo-valve to instantaneously admit a discrete volume of fluid to correct the discrepancy, leading to instabilities in the servo-valve operation. In the Velocity Feedback mode, operation was smoother, with no roughness evident, as might be expected since the whole feedback loop involves one less integration in this mode. All the tests were run in Velocity Feedback mode.

During check-out of the Hydraulic Oscillator, the harmonic content of the velocity output waveform was investigated. It was found that the distortion in the output was minimized by reducing the hydraulic

power supply pressure from the initial 3000 psi to 1200 psi. The velocity output waveform then had less than 5 percent total harmonic content, mainly third harmonic, at all test frequencies. While the force output capability of the Hydraulic Oscillator is reduced by the lower supply pressure, the resulting force capacity was ample for all tests planned in the present program.

2. Strut Dynamometer - Initial static calibration of the strut dynamometer was performed by applying forces to a loading fixture which has adjustable points of application, so that for instance vertical loads could be applied exactly at the electrical center of the two lift elements.

Applying combinations of loads to the two lift elements and the drag element showed a strong interaction of lift loads on the drag readings. The amount of the effect was sharply different for the two lift elements, so that the point of action of a lift force would have to be known to allow correction of the drag readings. Since this was not possible in the present program, the measurement of drag forces was foregone.

The excitation voltage for the two lift elements was adjusted to provide equal output for equal forces from both elements, and the mixing potentiometers in the Burr-Brown amplifiers were set to give equal total lift output for equal forces applied to the two lift elements. After this, an oscillatory calibration of the dynamometer was carried out by bolting a known mass to the strut and oscillating the load at the various test frequencies. The inertia of the bare strut was determined

similarly.

The oscillatory calibration of the dynamometer was performed repeatedly during the course of the tests. This was necessitated by the occasional changes required in the waterproofing envelope surrounding the strut due to both gradual deterioration and mechanical damage; this envelope connects the active and inactive parts of the strut and thus affects the stiffness of the dynamometer, albeit only slightly. In addition, a small long-term wander seemed to occur in the dynamometer calibration, and occasional calibration checks were considered prudent.

B. Range of Parameters

It was desired to investigate the effect of depth of submergence and static angle of attack α_o on the fluctuating forces. Various values of oscillation frequency were to be used to cover a range of values of reduced frequency; in addition, the flow velocity in the water tunnel was to be varied so that the same values of reduced frequency would be obtained at different oscillation frequencies to ascertain that the reduced frequency is indeed the relevant parameter for correlating the fluctuating force coefficients. Tests were to be carried out both for the aspect ratio one foils and in two-dimensional flow, using the test section inserts previously described. Finally, these results were to be obtained both in fully-wetted flow and with ventilated cavities.

It seemed apparent and quickly became obvious that it was not feasible to carry out tests with every model at every submergence and angle of attack in every flow configuration. This was reinforced

by the discovery in initial tests with ventilated cavities that the fluctuating forces showed substantial changes with varying air supply rates to the cavity, which meant that for each configuration and at each frequency of oscillation a whole range of air supply rates would have to be covered.

Thus evolved the alternative scheme of picking essentially one configuration as a standard and varying the values of one parameter at a time. This was not strictly adhered to, but it provided the general plan for the sequence of experiments.

The four hydrofoil models are the "flat plate", the wedge, the plano-convex foil (used only in the initial fully wetted runs) and the "rounded flat plate". The oscillation frequencies were 3, 5, 8, 10, 15, 20, 30, and 40 cycles per second; in some of the ventilated runs, the intermediate frequencies of 8, 15, and 20 cycles per second were omitted. Submergences with the aspect ratio one foils were 0.25, 0.5, and 1.7 (the largest possible) times the hydrofoil chord, which is 6 inches; for the two-dimensional tests, geometrical limitations of the test section inserts and the hydraulic oscillator mounting limited the submergence to a single value of 1.2 chord lengths.

The static angle of attack could be varied over a range from -12° to $+12^{\circ}$. This range could of course only be used in fully wetted flow; to achieve ventilated cavities which spring from the leading edge generally required a minimum angle of 12° between the flow direction and the wetted surface. The static angle of attack α_o is measured from the centerline of the model, which means that in ventilated flow

the flow about the flat plate at $\alpha_o = 12^o$ is about the same as for the 8^o wedge at $\alpha_o = 8^o$. The angle of attack of the plano-convex foil is measured from the flat upper surface. At angles of attack below the value required for leading-edge ventilation, the wedge could be operated base-ventilated, with both the upper and lower surfaces fully wetted, although in fact base-ventilated runs were only carried out at $\alpha_o = 0^o$.

The normal flow velocity in the working section was arbitrarily picked as 11 feet per second. At this velocity, the reduced frequency ranges from 0.43 to 5.17 for oscillation frequencies from 3 to 40 cps. Correlation tests were carried out at a 50 percent higher velocity, 16.5 feet per second, where the reduced frequency ranges from 0.29 to 3.81. Thus a large range of values of reduced frequency would be thoroughly covered.

The amplitude of the oscillation is determined by the excitation voltage setting, which was usually 4.0 volts. This gave an oscillating angle of attack of 4 to 5 degrees at most frequencies, tapering off to somewhat less than 3 degrees at the highest frequency of 40 cycles per second. To check the effect of oscillation amplitude, some runs were made at 2.0 and 6.0 volts excitation as well. Since the lift coefficients are calculated per unit angle of attack (see below), they should be unaffected by amplitude as long as the oscillating angle of attack remains fairly small.

C. Data Runs

After the electronic equipment and other instrumentation had been set up, preparation for a data run consisted simply of mounting the hydraulic oscillator for the intended submergence depth and bolting a hydrofoil to the strut at the proper angle of attack.

For the tests of two-dimensional flow, the test section inserts first had to be installed in the working section. When the inserts are parallel to each other and to the tunnel walls, formation of boundary layers on the surfaces causes the free surface to rise in the downstream direction. It was found that the free surface in the center part of the section, around the models, can be kept nearly level by tapering the spacing between the two insert walls so they are about 3/16 inch farther apart at the downstream end than at the nozzle. While this causes the free surface in the two outer sections of the flow to rise still further, that does not affect the flow around the foils.

After the inserts were installed and centered in the working section, final adjustments were made after mounting of the hydraulic oscillator and hydrofoil so that the gap between the foil and the walls was 0.030 to 0.040 inches. Finally, for ventilated runs, the ventilating strut and sting were installed.

When the tunnel had been filled with water and the flow velocity had stabilized, the strain gage bridges were re-balanced to remove the steady force output level. In the fully-wetted runs, only the oscillation velocity and the force outputs needed to be recorded.

Zeroes were taken before and after each data point by stopping the oscillation, and two data points were taken at each oscillation frequency.

The basic procedure in the data acquisition procedure is to adjust the phase of the command signal to the hydraulic oscillator so that the oscillation velocity signal from the transducer is in-phase with the reference waveform of the Return Signal Analyzer. When now the force output is applied to the input of the RSA, the in-phase lift, relative to the actual motion, appears directly on the first channel and the quadrature lift on the second.

In the runs with ventilated cavities, the oscillation frequency was set and the air supply rate varied in steps from the minimum which would support the cavity to the maximum flow rate available, then back down to the minimum. This minimum varied considerably with configuration and oscillation frequency. Since the in-phase and quadrature lift were read out directly from the two channels of the RSA, it was possible to tailor the steps in air supply rate instantly for closer investigation of sudden force changes. Usually 10 to 15 different values of air supply rate were used to cover the range.

At each of these points, the values of oscillation velocity, in-phase and quadrature lift, in-phase and quadrature cavity pressure, air flow rate and supply pressure, average cavity pressure, and cavity length were recorded. It may be appreciated that covering a range of air supply rates at each of several oscillation frequencies for just one configuration was a fairly lengthy process, especially since

signals had to be applied to the RSA sequentially and some short time allowed for stabilization for each. This effectively limited the extent of the test program; nevertheless, a considerable variety of configurations was investigated.

Estimation of the cavity length presented some problem since the cavity changes length during the oscillation cycle and also varying amounts of water and froth are introduced into the cavity by the re-entrant jet. In general, however, the criterion used for the recorded cavity length proved quite workable, namely, the shortest clear cavity as it was seen by the unaided eye. These cavity lengths agree well with high-speed flash photographs taken during some of the runs.

D. Data Reduction

1. Forces - The equivalent mass of the active part of the strut was determined by an oscillatory calibration of the bare strut (no foil mounted) in air. The inertial mass of the hydrofoil models with the mounting bolts and wedge adapters for each configuration was found by weighing. The measured quadrature lift forces were corrected for the inertial force due to the strut and hydrofoil mass, which was calculated for each data point by using the measured oscillation amplitude. Calculation seemed both a more straightforward and reliable method than the scheme sometimes used of injecting a signal proportional to the correction term into the electrical signal generated by the force balance.

The forces measured by the strut dynamometer include the

contribution of the bottom part of the strut, between the dynamometer and the hydrofoil. It would have been a major project to measure these tare forces by oscillating the strut and foil separately with a small fixed gap between them, measuring the forces only on the strut. If drag forces were to be measured, the contribution of the strut to the total force would probably be significant. But it is plausible that the contribution of the bottom part of the strut to the lift forces is negligible, and hence such a tare force calibration was omitted in the present program. Thus the measured lift forces are attributed entirely to the hydrofoil.

Similarly, no attempt was made to correct for the disturbance to the flow about the hydrofoil caused by the presence of the strut. Not only would this have been a difficult task, but since in fact hydrofoils of configurations similar to those in these tests would normally be supported by just such a strut, there is no practical benefit to such a procedure.

Except for correcting the quadrature lift forces for the inertial force due to the hydrofoil and strut mass, as already outlined, no corrections to the measured forces were made, such as for tunnel interference effects, wall blockage, or nearness of the tunnel bottom. In these free-surface flows, such effects are expected to be small.

The forces were reduced to coefficient form by dividing by the dynamic head, foil planform area, and the equivalent oscillating angle of attack due to the transverse heaving velocity:

$$C_{L\alpha} = \frac{\text{Lift}}{(\frac{1}{2}\rho U^2) A \alpha_{osc}}, \qquad \text{where} \qquad A = 2 b s = cs$$

$$\text{and} \qquad \alpha_{osc} = \frac{V_{osc}}{U} .$$

The subscript $_r$ denotes the in-phase part of the lift, that is, the part which is in-phase with the oscillation velocity; the subscript $_i$ denotes the quadrature part.

2. Air Supply Rate - The reading of the Flow-Rator is corrected for the line pressure at its location to give the amount of air at atmospheric pressure which is entering the cavity, which itself is substantially at atmospheric pressure. The air supply rate coefficient is defined in a logical manner only occasionally used by other investigators:

$$C_Q = \frac{Q}{A_p U}, \qquad \text{where} \qquad Q = \text{corrected air flow rate}$$

A_p = projected foil area normal to the flow .

An air supply coefficient of unity would thus have the physical meaning that the amount of air injected into, and entrained away from, the cavity is equivalent to a stream of air of the width and projected height of the foil moving with the free stream velocity, so that the entire wake of the foil may be thought to be filled with air moving at the flow velocity.

The air supply system used in the present tests limited the maximum air supply coefficient to about 0.4, which is about ten

times the minimum required to sustain a typical oscillating cavity and was considered quite adequate.

3. Cavitation Number - The cavitation number is defined as

$$\sigma_k = \frac{p_o - p_c}{\frac{1}{2}\rho U^2} \quad , \qquad \text{where} \quad p_o = \text{ambient pressure}$$

$$p_c = \text{cavity pressure}$$

$$\tfrac{1}{2}\rho U^2 = \text{dynamic pressure}$$

In a free-surface flow, it may be rewritten in a form which permits more convenient computation:

$$\sigma_k = \frac{h_o - h_c}{\frac{U^2}{2g}} \quad , \qquad \text{where} \quad h_o = \text{submergence of model in ft.} H_2O$$

$$h_c = \text{cavity pressure (gage), ft.} H_2O$$

$$\frac{U^2}{2g} = \text{velocity head in ft.} H_2O$$

4. Cavity Pressure - To illustrate the relationship between the unsteady cavity pressure and the unsteady lift, it would be convenient to plot the unsteady cavity pressure on a basis which allows easy numerical comparison with the lift coefficient graphs. The equivalent-lift cavity pressure coefficient C_{pc} is so defined that a unit change in C_{pc} changes the lift force exerted by the hydrofoil by the same amount as a unit change in the lift coefficient $C_{L\alpha}$. In other words, if the changes in unsteady cavity pressure with air supply rate were solely accountable for the variations in lift coefficient, the plot of C_{pc} versus cavity length would have the same shape and numerical values as the $C_{L\alpha}$ graph. (The difference between the two,

then, is ascribable to factors other than the unsteady cavity pressure.)

$$\text{Lift} = p_c A \qquad \text{(due to cavity pressure)}$$

$$\text{Lift} = C_{L\alpha} \left(\tfrac{1}{2}\rho U^2\right) A\, \alpha_{osc} \qquad \text{(due to oscillation)}$$

Hence $$C_{L\alpha} \sim \frac{p_c}{\left(\tfrac{1}{2}\rho U^2\right) \alpha_{osc}} \equiv C_{pc} \quad .$$

As with the lift coefficient, the subscript $_r$ denotes the in-phase part and the subscript $_i$ the quadrature part.

IV. DISCUSSION OF EXPERIMENTAL RESULTS

The measured in-phase and quadrature lift forces, after correction as already described in the previous section, were reduced to coefficient form by dividing by the dynamic head, foil planform area, and the equivalent oscillating angle of attack due to the transverse heaving velocity:

$$C_{L\alpha} = \frac{\text{Lift}}{(\frac{1}{2}\rho U^2) A \alpha_{osc}} \quad , \quad \text{where} \quad A = 2bs = cs$$

$$\text{and} \qquad \alpha_{osc} = \frac{V_{osc}}{U} \ .$$

The subscript $_r$ denotes the in-phase part of the lift, that is, the part which is in-phase with the oscillation velocity; the subscript $_i$ denotes the quadrature part.

The manner of presenting the data corresponds to the standard practice in plotting unsteady forces, as first introduced by von Karman and Sears [18], namely, a polar diagram of the in-phase versus the quadrature lift coefficient, with the reduced frequency k as a parameter. An alternative method would be to plot the magnitude and phase angle of the unsteady lift coefficient against reduced frequency in separate graphs. While this has the advantage of allowing easier interpolation between data points, it turns out that the features of the present results are shown more clearly in the polar type of diagram

than in separate magnitude and phase plots. An illustration of this fact is given by Figs. 26 and 27, where the results have been plotted in both ways. It is evident that the large changes in the lift coefficient for the wedge foil are shown much more clearly in the polar diagram.

A. Fully Wetted Flow

1. Three-Dimensional Tests (Aspect Ratio = 1) - These tests were carried out in two groups of runs separated by almost a year. Since there was a considerable amount of duplication in these two groups, a very natural opportunity was provided for assessing the repeatability of the results. In every case, the force coefficients were reproduced within at worst 5 percent. In addition, the short-term repeatability was within two percent for runs that were separated by one or two weeks; in most cases the data points were so close together that they could not be plotted as separate points. While the long-term reproducibility was not as good as might be (and, in fact, was) hoped, the validity of the measurements is certainly well established in this way.

Tests which were performed to check the effect of variations in some parameter were always carried out in a group covering only a short span of time, so that the differences between runs varying any one parameter can be assumed to show the actual effect of the parameter variation, including at most the two percent short-term uncertainty.

a. Representative Results - Some introductory results are shown in Figs. 12 and 13, which are from the first and second

group of runs, respectively. Also shown on these graphs are the theoretical points calculated from Reference 16. These calculations are for infinite submergence and are compared here with experimental values for only 1.7 chord lengths submergence, which is the largest obtainable with the present apparatus. But it was expected that the surface effect has largely diminished at this depth, which is confirmed by a glance at Figs. 16 and 17, and thus a meaningful comparison can be made.

While the calculations extend only up to a reduced frequency of 0.5, it is already evident that the experimental quadrature lift for all the foils is lower than the theoretical values in this region. In contrast to this, the experimental in-phase lift is never smaller than the theoretical values and is, in fact, consistently larger for the wedge-shaped foil than either the values for the other foil shapes or the calculated values.

The large values of in-phase lift coefficient for the wedge foil compared to the flat plate are surprising. Unfortunately no other results, either experimental or theoretical, are available for such a foil shape. The wedge is essentially just a flat plate with the thickness uniformly increasing toward the trailing edge. In steady flow, airfoil theory predicts a lift increase with thickness [50], but in free-surface flows, an appreciable decrease of lift due to thickness is found as the surface is approached [10]. For unsteady flow, the theory of Woods [15] gives a small decrease in the in-phase lift coefficient due to thickness when viscosity is neglected. However,

all these theories assume an airfoil-shaped surface, specifically one with a sharp trailing edge, and are thus not really even applicable to the wedge foil.

It does not seem likely that thickness is the sole reason for the large in-phase lift of the wedge. In the absence of other applicable results, this finding must be considered unexplainable at present.

The vector magnitude of the experimental lift coefficient for the flat plate foil, which most nearly resembles the theoretical model, is about equal to the calculated magnitude, only the phase angle φ_L is somewhat smaller. The rounded flat plate has generally slightly lower values of in-phase lift coefficient than the flat plate, which is reasonable since the rounded side edges give this model a slightly lower effective aspect ratio than the square-edged flat plate foil.

Corresponding results for the other values of submergence are given in Figs. 14 and 15. Comparison of these curves shows that, although the numerical values of the lift coefficients change with submergence, the relative trajectories for the various foils are quite similar at each depth.

The most striking feature of the curves is the behavior for the wedge at a reduced frequency of about 4.5. This is not as pronounced in Fig. 12 as in the others, but it is evident in every case. This "knee" in the curve has good reproducibility (see Fig. 17) and appears to be a real physical effect. A discussion and explanation of this phenomenon will be deferred to Section f. below, after the other features of the fully-wetted tests have been described.

b. Submergence Effect - Experimental results at varying submergence are shown in Fig. 16 for the flat plate foil and in Fig. 17 for the wedge. Both the in-phase and the quadrature lift coefficient decrease as the foil approaches the surface. This seems to hold at all values of reduced frequency, except of course above the "knee" of the wedge curve.

At the present time, there exist no numerical theoretical results for the effect of submergence depth on a finite-aspect-ratio foil oscillating under a free surface. It might be reasonable to assume that the trend of the surface effect should be the same for a finite aspect ratio as for infinite aspect ratio (two-dimensional flow). This supposition, however, is not entirely confirmed by the two-dimensional theory of Reference 17, the results of which are plotted in Fig. 25. The in phase and quadrature components do, indeed, decrease as the submergence decreases for reduced frequencies above about 1.0; but for values of reduced frequency below 0.5, the theoretical quadrature part definitely increases with decreasing submergence. The present experimental findings do not show this tendency.

It may be that the theoretical results would be different for a low aspect ratio foil and would not show the same trend at low reduced frequencies as for two-dimensional flow. Since the submergence could not be easily varied in the two-dimensional tests (discussed below) where the theory is applicable, the present experiment does not provide a direct check on this theory.

Experiments of an exploratory nature were also performed quite close to the surface. It was found that fully wetted flow could be maintained over the flat plate foil for submergences as small as 0.04 chords, which is 1/4 inch. By utilizing the static position control of the Servo Controller, the submergence was continuously varied from 0.15 chords to zero (i.e., where the foil was breaking through the surface), and force data were taken in this range. These results are not shown in the Figures since the test conditions were not well controlled and a planned repeat run was not carried out; but it was well established that both the in-phase and quadrature components of lift decreased monotonically as the fully-wetted foil approached the surface, with both components reaching a value at the smallest submergence of 0.04 chords of about 75 percent of their values at 0.5 chords submergence.

The oscillations of the fully-wetted foils caused considerable displacements of the water surface, which naturally increased as the foil approached the surface. Although these were visually very noticeable, they proved hard to capture on still photographs since the wavelength of the generated waves at the lowest frequencies, where the effect is largest, is very long. An impression may nevertheless be gained from Fig. 18; in the second picture the foil is near its maximum downward excursion, and the deflection of the water surface is obvious by comparison. Thus the effect of the proximity of the water surface on the unsteady forces is not entirely unexpected.

c. Reduced Frequency - To establish that the reduced frequency is in fact the pertinent parameter in these tests, some runs were carried out with the free-stream velocity increased to 16.5 feet per second, half again its usual value of 11 feet per second. Recalling that the definition of reduced frequency is $k = \omega b/U$, it is seen that the same value of reduced frequency corresponds here to a 50 percent higher value of oscillation frequency. Figure 19 shows the results of this check. While the highest frequency is now no longer large enough to reach the "knee", the curves show only minute differences in their common range.

Parenthetically, it might be noted here that the "knee" was reached at the higher flow velocity in the two-dimensional tests, reported below, by increasing the oscillation frequency beyond the usual range. The "knee" occurred at roughly the same reduced frequency for the higher flow velocity. Thus the reduced frequency indeed appears to be a meaningful parameter for the correlation of these oscillation tests.

d. Oscillation Amplitude - To ascertain that the more-or-less arbitrarily chosen oscillation amplitude does not affect the findings in some unsuspected way, a series of tests was performed in which only the excitation voltage was varied. The values chosen were 50, 100, and 150 percent of the usual excitation voltage; this voltage is quite linearly related to the oscillation amplitude which results. These tests were performed with the wedge foil and the results are shown in Fig. 20. There are only small differences in

the coefficients for values of the reduced frequency below the "knee" although both components seem consistently higher at higher excitation.

For low-aspect-ratio foils, it is well known that the lift-curve slope for steady flow is not constant but increases with increasing angle of attack [11]. As the oscillation amplitude is increased in the present tests, the equivalent maximum angle of attack increases also, carrying the foil into a region of higher lift-curve slope. Thus the average lift coefficient would be expected to be somewhat larger for higher oscillation amplitude, which is borne out by the experimental results.

It is remarkable that the "knee" in the curve occurs at substantially the same point for all oscillation amplitudes, considering the generally irregular behavior of the coefficients at this point.

e. Angle of Attack - It was found that the angle of attack α_o at which the foils are mounted on the strut has a significant effect on the in-phase lift coefficient for all the foils. This is shown for the flat plate foil in Figs. 21 and 22 and for the wedge in Figs. 23 and 24.

For the flat plate, the curves for a given α_o are almost identical whether the angle is positive or negative (comparison of the two figures is facilitated by noting that the curve for $\alpha_o = 0^o$ is common to both plots). There are no systematic variations with reduced frequency in the quadrature component, although the close similarity of individual points on the positive and negative angle-of-attack curves is noteworthy.

The two plots for the wedge are from the first and second group of runs, respectively. In the first group, the "knee" in the curve was not as pronounced as in the second, probably because intermediate frequencies of oscillation were not tried there. It is interesting that even in the later runs the "knee" is rather less prominent when the angle of attack is not zero.

For values of the reduced frequency below about 3, that is, below the "knee" of the curve, the wedge, too, exhibits increasing in-phase lift coefficients with increasing angle of attack; again, the curve for $\alpha_o = -4^o$ (not shown) is essentially identical to that for $\alpha_o = +4^o$.

The reason for the increased in-phase lift with increasing angle of attack is found in the nonlinearity of the lift-curve slope for low aspect ratio foils (11). At a higher set angle of attack α_o, the oscillations take place on a steeper part of the lift-versus-angle of attack curve, and thus the measured fluctuating lift coefficient is larger. Note that whatever mechanism causes the relatively large in-phase lift of the wedge at $\alpha_o = 0^o$ does not materially affect the further increase with increasing angle of attack.

f. Results for the Wedge - As can be seen from the results discussed so far, the peculiar trajectory of the lift curve for the wedge in the region of reduced frequency of 4.5 is a feature which persists for all the changes in experimental parameters. At a certain fairly well reproducible reduced frequency, the in-phase component decreases abruptly to near zero and in some cases even becomes

negative; at the same point the rate of change of quadrature lift becomes temporarily negative and generally remains irregular as the reduced frequency is increased further.

The consistent occurrence of this "knee" in the runs with the wedge, and its total absence for the other foils, reinforce the conclusion that a real physical phenomenon is involved. The possibility that it is only an instrumentation effect may be ruled out, since the data points are all taken individually, and the only difference between runs is the foil attached to the strut.

It is both immediate and physically reasonable to ascribe this phenomenon to the vortex shedding associated with the blunt base of the wedge. The Strouhal Number fw/U corresponding to the "knee" of the curve is about 0.20 based on the base height of the wedge. Previous experimental investigations of the wake behind stationary wedges carried out by Young and Holl [51] gave a value of 0.2 to 0.25 for the Strouhal Number based on the observed vortex shedding frequency, and wake studies behind both stationary and oscillating cylinders transverse to the flow, by Bishop and Hassan [52], also gave Strouhal Numbers around 0.20. These latter tests were carried out at Reynolds Numbers from 4,000 to 11,000, while Young and Holl had values about 200,000, based on chord length. Considering the wide range of Reynolds Number covered by these investigations, it may reasonably be assumed that the same physical process occurs in the present tests which have a Reynolds Number of 500,000 or, at the higher flow velocity, 750,000.

Bishop and Hassan [52] also performed tests with cylinders oscillated in a range of frequencies bracketing the observed natural shedding frequency, in which various coupling effects between the frequency of the imposed motion and the natural frequency of the wake were observed, such as synchronization, frequency demultiplication, and beating. Based on these findings, they postulate the existence of a non-linear self-excited "wake oscillator", analogous to a mechanical oscillator. Their observations certainly resemble the behavior found in the present tests, and the "knee" in the lift curves for the fully-wetted wedge may justifiably be ascribed to such a phenomenon.

It is worthwhile to note at this point that when the wedge is base-ventilated, so that the base of the wedge is no longer in contact with the water, the "knee" vanishes completely, as would be expected; see Section B., below.

2. Two-Dimensional Tests - Due to limitation imposed by the equipment, as already discussed in the previous chapter, tests were performed at only one submergence for two-dimensional flow. The theoretical effect of varying the submergence of an oscillating hydrofoil is shown in the curves of Fig. 25 computed from the results of Crimi and Statler [17]. Their calculations were carried out for several values of submergence and Froude Number based on semi-chord (not submergence). In the present tests the submergence is 1.2 chord lengths and the Froude Number is 3.88. The closest calculated case is 1.0 chords submergence and a Froude Number of 4.0, which should be quite comparable.

It might be mentioned here that these calculations could not be successfully carried over to predict the trend of the submergence effect at low reduced frequencies for the aspect ratio one foil, in Section b. above. This hardly means that the theory is not valid; more likely, the submergence effect on an aspect ratio one foil is just not the same in every detail as that for an infinite aspect ratio (two-dimensional flow).

a. Representative Results - Some experimental results are shown in Fig. 26, along with the theoretical curve computed for the same values of reduced frequency from Reference 17. The experimental points have also been re-plotted in Fig. 27 in magnitude-and-phase form. It can be seen that the features of the curves are much more evident in the polar type of diagram.

Comparison of the two-dimensional results, Fig. 26, with tests of the aspect ratio one foils, say Fig. 13, points up both similarities and differences. The in-phase lift of the wedge is again substantially larger than that of the flat plate, and its quadrature lift is also somewhat larger. The "knee" in the curve for the wedge occurs at the same value of reduced frequency as in three-dimensional flow, reinforcing the conclusion that the blunt base is the probably cause of the discontinuity in the lift coefficients.

The theoretical results do not bear quite the same relationship to the experimental findings as for the aspect ratio one tests, where the flat plate had nearly the same in-phase lift coefficient as calculated. Here the in-phase lift of the flat plate is considerably lower than the

calculated curve, while that of the wedge is only slightly higher than calculated. The quadrature lift is lower for both foils than the calculated values.

The simulation of two-dimensional flow, as in the present tests, by a finite-span model supported between walls is inevitably imperfect. The gap clearance between the model and the walls reduces the lift, as does the boundary layer along the walls. There is flow interference due to the strut supporting the hydrofoil, and in addition, in the present tests there was some "breathing" of the two-dimensional inserts even after they had been stiffened, with the gap which was nominally set at 0.030 to 0.040 inches fluctuating by perhaps 0.010 inches at the lower oscillation frequencies.

For steady flow, some investigations by Bate [53] show the effect of end gap and support strut interference on the lift curve slope of a fully wetted hydrofoil in an arrangement similar to the present one. The lift decrease was roughly 3 percent for each 0.010 inches of gap. The effect of the mounting strut was determined by supporting the foil on a sting instead, which caused a 20 percent lift increase. While the numerical values cannot be directly applied to unsteady flow, the relatively low values of in-phase lift encountered in the present two-dimensional tests may easily be caused by a combination of such factors.

Some of the same effects may cause the differences between the experimental and theoretical quadrature lift coefficients. In experiments with an airfoil oscillating in pitch, Smith and Sevik [21]

found a similar discrepancy and ascribed it to a deficiency in the amount of non-circulatory lift after conducting oscillation tests in still water that showed the non-circulatory lift, which may also be called apparent mass, to be only 84 percent of its theoretical value.

It is not clear that the explanation is so simple, either for Smith and Sevik's tests or for the present ones. The tests of Reference 21 varied the reduced frequency by changing the flow velocity at a single constant oscillation frequency of 15 cycles per second. In the present experiment, tests were also conducted in still water at all frequencies. The measured apparent mass decreased from 101 percent of the theoretical value at 3 cps fairly smoothly to 80 percent at 40 cps, reaching interestingly enough the same 84 percent at 15 cps reported by Smith and Sevik.

A glance at the present results in Fig. 26 shows that the difference between the theoretical and experimental values does not disappear at low reduced frequencies, even when these are obtained by actually decreasing the oscillation frequency. Moreover, as noted by Grace and Statler [54], in free-surface flows the separation of the total forces into the usual quasi-steady, wake-induced, and apparent-mass contributions is no longer such a useful concept since the free-surface waves have very complex interactions with especially the wake and apparent-mass terms. Thus the differences between theory and experiment cannot be easily explained from the present findings.

b. Reduced Frequency - Tests at the higher flow velocity were performed with two-dimensional flow for both the flat plate and

the wedge foil, the results of which are shown in Figs. 28 and 29. There are again only small differences in the coefficients, confirming that reduced frequency is the primary parameter for the correlation of the unsteady force data.

In the tests with the wedge, the oscillation frequency in the high-velocity runs was increased above its usual range so that reduced frequencies in the "knee" range would be obtained. For such high oscillation frequencies, the force dynamometer calibration is not firmly established, nor was the oscillating mechanism checked out thoroughly, so the results are not numerically definitive. Nevertheless, the overall shape of the curve shows the "knee" clearly. There may be a small Reynolds Number effect on the vortex shedding Strouhal Number which is associated with the "knee", but the small difference in reduced frequency may also just be experimental uncertainty in this range.

B. Base-Ventilated Flow

Ventilation of the base of the wedge should have no measurable effect on the lift forces, since the flow about the foil itself is not materially changed, and thus only one check run was made to confirm this, with the aspect ratio one wedge. The results are shown together with those for fully wetted foils at the same test conditions in Fig. 30. Tests with air supply coefficients up to about 20 times the minimum required to sustain a cavity all gave the same lift with negligible scatter. There are only minor differences between the lift coefficients for the base-ventilated and the fully wetted wedge for reduced

frequencies below the "knee".

Since the "knee" in the lift curve for the fully wetted wedge has been associated with the vortex shedding of the blunt base, ventilating the base of the wedge should cause the "knee" to disappear and the lift curve to continue on a regular path, as for the other foils, when the reduced frequency is increased through the "knee" range. This is borne out by the experimental results shown in the graph.

C. Ventilated Cavities

As in the fully wetted runs, the tests with ventilated cavities were planned around one reference configuration from which changes in one parameter at a time would be made to investigate their effect. The reference setting for these sets of runs was the wedge foil at a centerline angle of attack of $+8^{\circ}$, which means that the face wetted by the water is actually at $+12^{\circ}$; the flow velocity was 11 feet per second; and the submergence was 0.5 chord-lengths for the three-dimensional tests and 1.2 chords for the two-dimensional setup.

The very first runs showed that a large variation in the measured lift forces occurred for changes in the air supply rate to the cavity, which of course also changed the cavity length. When undergoing oscillations, the cavity appeared quite unsteady; if this was accompanied by changes in the cavity pressure, a force in the lift direction would be produced since the cavity pressure acts on the suction side of the hydrofoil. Thus it immediately became desirable to measure the fluctuations in the cavity pressure.

As described in the Equipment section, this was initially done with a transducer mounted in the sting directly behind the cavity. However, water droplets impacting on the pressure diaphragm distorted the measurements and moisture affected the output of the transducer, and reliable measurements were only obtained for the last few sets of runs. The relationship of the unsteady cavity pressure to the lift coefficients will be taken up in a later section.

The presentation of the results with ventilated cavities follows the same form used in the fully wetted runs, namely, a polar plot of in-phase versus quadrature lift coefficient, with the exception that a whole group of points is now given at each value of reduced frequency to show the effect of cavity length. The direct variation imposed was in the air supply rate, which in turn causes the cavity length changes, but it is thought that the flow about the foil is affected primarily by the cavity length. This conclusion was reinforced by the finding in the two-dimensional runs that sometimes cavities of two distinctly different lengths were both stable for the same air supply rate (this will be further discussed below). For such cases, the lift coefficients showed the usual large changes with cavity length; therefore the use of cavity length as the parameter along the lift coefficient trajectories seems warranted.

The repeatability of results for these ventilated runs was not as good as in the fully wetted case. This is not surprising, since there are more variables affecting the flow when a cavity is present. The cavity detachment and entrainment are quite sensitive to small

changes in flow direction, for example, and small but noticeable changes in the entrainment region would sometimes occur when the position of the ventilating sting, which projects forward into the cavity and passes through the entrainment region, was changed. Thus small differences in the results obtained from two ostensibly identical set-ups can be expected.

In fact, the long-term repeatability for runs separated by several weeks appeared to be within about ten percent, which is considered quite satisfactory. An example is provided by comparing Figs. 35 and 38. Keeping in mind the large variations in the lift coefficients with cavity length, the differences are not really very large; it is notable how the general character of the trajectories traced out by the data points is retained in the repeat runs.

High-speed flash photographs of the cavity were taken for a variety of oscillation frequencies and air supply rates for the wedge foil in both two- and three-dimensional flow. A selection of these has been included here to illustrate some of the features of the flow and will be described in the appropriate sections below. High-speed motion pictures were also taken at several flow conditions, to get a better idea of the time history of the oscillating cavity, and some of these findings will be discussed.

1. Three-Dimensional Tests (Aspect Ratio = 1)

a. Representative Results - The lift coefficients for the reference configuration, the wedge foil at one-half chord submergence, are plotted in Figs. 31 and 32. Also shown, where available, are the

theoretical values calculated from Reference 20 for each value of reduced frequency corresponding to the experiments; these are for infinite submergence but should provide a starting point for comparison. It can be seen that the measured in-phase lift coefficient is very much larger than the theoretical value; the quadrature part is in general somewhat smaller than predicted. These differences will be discussed below.

The striking feature of the present results, as already mentioned, are the large variations in the lift coefficients with cavity length. The curves at the lower values of reduced frequency are all quite similar. Starting from the shortest sustainable cavity, the in-phase lift coefficient decreases with increasing cavity length while the quadrature lift remains fairly constant; then with further cavity length increase, the in-phase lift shows less change but the quadrature part starts increasing. This is especially noticeable at the lowest reduced frequency, where the quadrature part is almost tripled for a small change in cavity length; this is accompanied by a three-fold increase in air supply rate, but there is no change in the average cavity pressure. The only apparent change in the flow picture is some fattening of the cavity, but nothing obvious was observed visually that could be considered to account for these large changes. Since the same behavior is found at other reduced frequencies for this set-up and also at other configurations, there is no doubt that it is a real effect.

At higher values of reduced frequency, as on Fig. 32, the trajectories assume more complicated shapes. While the physical sig-

nificance of the shape of the curve is not clear at the present time, the range of lift coefficients which might be encountered is well indicated. In one particular configuration (the wedge at a velocity of 16.5 feet per second), three runs were made at a reduced frequency of 4.28, each separated by about four weeks. The trajectory, not shown in the figures, had roughly the same shape as for k = 4.28 in Fig. 32, with an additional loop. The numerical values of the lift coefficients shifted by about 10 percent over the course of these runs, but the trajectories were virtual duplicates of each other. The influence of cavity length on the unsteady forces thus appears to be a consistent physical effect even at very high reduced frequencies.

It may be appropriate here to mention again the procedure used in the runs, which was to start at the lowest air supply rate that would support a cavity, increase it up to the maximum, and then decrease it by steps back down to the minimum. Ideally, data points obtained at a given cavity length should of course be the same, whether the air supply rate is increasing or decreasing. A glance at the graphs shows that there is indeed little deviation, which demonstrates the very good consistency of the data within any one run.

Consideration of the large differences between the theoretical and the measured values of lift coefficient, the effect of the unsteady cavity pressure, and some comments about the loops in the curves for high reduced frequencies will be taken up in the Discussion below, after results of the other ventilated tests have been described.

The cavity behind a three-dimensional foil is composed of two distinct parts. There is a cone-shaped cavity due to the tip vortex at each side edge, with a quasi-two-dimensional cavity spanning the distance between them. Air entrainment from the cavity occurs by two different mechanisms corresponding to the character of these parts. The tip vortices persist for a large distance downstream from the foil, and their core is ventilated, carrying air out of the cavity. These vortices are quite stable and remain evident even when the foil is oscillated.

Entrainment from the two-dimensional part of the cavity occurs in the turbulent air-water mixture (re-entrant jet) at the end of the cavity. In steady flow, this region has a rolling motion, not unlike a breaking wave, which is also retained when the foil is oscillating slowly, although then the size of this region varies during the cycle and the cavity undergoes a surging or "sloshing" motion. At high reduced frequencies, the rolling motion has too much inertia to react to the oscillations, and entrainment occurs by a "flinging" motion at the end of the cavity; the oscillations in the cavity surface caused by the foil motion increase in amplitude in the downstream direction until finally a segment of the cavity is cut off from the main bubble and entrained away.

These characteristics are well illustrated by the high-speed flash photographs of the cavity behind the aspect ratio one wedge, shown in Figs. 33 and 34. The reflection in the mirror mounted below the working section shows the bottom view of the cavity. Fig. 33a shows

the cavity behind a stationary foil at nearly the minimum air supply rate; the ventilated tip vortices are seen especially well in the bottom view. Fig. 33b-d shows the foil oscillating at a relatively high reduced frequency (2.86) with increasing air supply rate. The tip vortex cavities remain in evidence at all times, but as the air supply rate is increased, the additional entrainment appears to be due mostly to the "flinging" effect of the two-dimensional part of the cavity. (Although the pictures may give the impression that the oscillation amplitude is increasing from Fig. 33b-d, the amplitude is actually constant, but the whipsaw-effect increases with larger cavity lengths.) Photographs of a typical cavity for low values of reduced frequency are shown in Fig. 34, again for air supply rate increasing from the minimum. The ventilated tip vortices are especially noticeable in the side views of Fig. 34a, b. Pictures b and c, both taken at the same conditions, illustrate the variation during the cycle; the former is taken near the bottom of the excursion and shows the quasi-steady cavity, while the air entrained away by the "sloshing" can be seen in Fig. 34c where the foil is just starting downward again. After the disturbance of the "sloshing," the tip vortex cavities are always re-established for the rest of the cycle.

b. Changes in Parameters - Sets of runs of the same extent as for the wedge at 0.5 chords submergence, above, were performed for a considerable variety of configurations and flow conditions. Other foils used include the flat plate and rounded flat plate, both of which were tested at both positive and negative angle of attack, that is,

with the cavity above and below the foil, respectively. To check the effect of submergence, tests were carried out with the wedge at 0.25 and 1.7 chords submergence in addition to the 0.5 chords submergence runs described above. Different values of reduced frequency were attained at the same oscillation frequencies by increasing the flow velocity from the standard 11 feet per second to 16.5 feet per second, as in the fully wetted runs. Also, the effect of oscillation amplitude was investigated by sets of runs with 50 and 150 percent of the standard excitation.

Unfortunately, the vast amount of data obtained from all these sets of runs has one common characteristic, which is that none of it differs appreciably from the results for the reference configuration described in the previous section. The shapes of the trajectories at each value of reduced frequency are fairly similar, and the differences in the numerical values of the measured lift coefficients are as a rule not much larger than the estimated amount of the repeat uncertainty. For this reason, the results of these runs are not shown in the figures. It was felt that presentation of these curves would merely result in a multiplicity of quite similar graphs which would not really contribute any useful information.

After this introduction, some comments are perhaps in order. Except for the contouring near the leading and trailing edges of the flat plate foil, the flow past the flat plate with a cavity should be about the same as that for the cavitated wedge when their wetted surfaces are at

the same angle to the flow, as in the present tests. The contouring causes some effective camber which would tend to reduce the lift; and, in fact, both $C_{L\alpha r}$ and $C_{L\alpha i}$ are slightly lower than for the wedge. The rounded flat plate, with its radiused leading and side edges, has slightly lower values of $C_{L\alpha r,\ i}$ yet, as might be expected. These trends are generally true throughout the reduced frequency range, although it must be remembered that the differences, while consistent, are little larger than the repeat uncertainty.

The tests at the higher flow velocity gave results that fit in well with results at the standard velocity for corresponding values of reduced frequency, confirming once again that reduced frequency is the primary correlating parameter. Runs at different oscillation amplitudes showed no significant differences.

After the substantial effect of submergence which was found in the fully wetted tests, it was rather surprising to find very little systematic depth effect in the cavity runs. This is apparently due to the presence of the bottom of the working section; the total depth of flow is of course constant, at 3.3 chord lengths, and thus the bottom is approached more closely as the submergence below the free surface increases. For steady flow of a supercavitating flat plate in a channel of this same depth, the theory of Ai, Acosta, and Harrison[29] predicts only 3 percent variation in lift coefficients for the three submergences used in the present tests; the effects of the free upper surface and the solid lower wall are apparently nearly compensatory. If these results hold

also for unsteady flow, they would explain the absence of a measurable depth effect for these ventilated runs.

2. Two-Dimensional Tests

A set of runs was performed with the wedge foil at 1.2 chord lengths submergence, the results of which are shown in Figs. 35, 36, and 37. Some repeat runs were carried out about two months later and are shown in Fig. 38. As has already been mentioned, there are only small numerical differences between the runs and the general character of the trajectories is closely reproduced, indicating quite good repeatability. Compared to the theoretical values, the measured in-phase lift coefficient is in general considerably larger and the quadrature component substantially smaller; both are relatively somewhat lower than in the three-dimensional tests, above.

The most noticeable feature of the two-dimensional results is the very large range of variation of the lift coefficients with cavity length, even as compared to the three-dimensional tests. In addition, the minimum air supply rate required to sustain a cavity was generally much higher, the minimum cavity length somewhat higher, and the cavitation numbers in a higher range than for the three-dimensional tests. These findings confirm the idea formed from flow observations that the tip vortex cavities in three-dimensional flow tend to stabilize the two-dimensional part of the cavity, since they are themselves quite stable. On the other hand, the maximum cavity lengths at high air supply rates were much larger for the two-dimensional tests. It is

possible that the downwash over the central part of the cavity caused by the tip vortices in three-dimensional flow helps to break up the cavities, and its absence may account for the longer cavities obtained in two-dimensional flow.

Photographs of the cavity in two-dimensional flow at a reduced frequency of 1.43 are shown in Fig. 39. Pictures b and c show one of the cases where two different cavity configurations are both stable, depending on which is established, that is, whether this air supply rate is approached from below or above. These two cavities correspond to the two flow conditions separated by the dashed line for k = 1.43 in Figs. 35 and 38. Cavities of intermediate length cannot be established. There did not appear to be any well-defined differences in the entrainment region of the two flows which would account for the existence of the two flow conditions. The unsteady character of the entrainment mechanism complicates both analysis and observation of entrainment phenomena, and the present knowledge about the process of air entrainment is still incomplete.

3. Discussion

For both two- and three-dimensional flow with ventilated cavities, there are large differences between the measured lift coefficients and the theoretical values. The quadrature component for both flow conditions is on the average about 20 percent lower than predicted. This is a common experience in tests with oscillating foils; it was also found in the previously discussed fully wetted runs, and similar results have been reported for fully wetted flow by Smith and Sevik[21] and Cieslowski

and Pattison [22]. This may be due to real fluid effects and breakdown of the Kutta condition at the trailing edge of the foil, and in the flows with a free surface, the surface effect may decrease the apparent mass contribution.

The outstanding feature of the present results, however, is the large value of in-phase lift compared to the theoretical value, for which zero cavitation number and infinite fluid extent are assumed. In this unsteady flow, most of the in-phase lift component can be considered to be due to the quasi-steady lift associated with the oscillating angle of attack caused by the heaving motion. Hence some steady flow results may be relevant to the explanation of this aspect of the present unsteady flow.

Three factors which may contribute to the large differences between the theoretical and experimental values of the in-phase lift are the flow boundaries, cavitation number, and angle of attack. Considering the influence of the solid bottom and upper free surface in the water tunnel, the calculations of Ai, Acosta, and Harrison [29] show the lift coefficient for all the present submergences to be increased by about 40 percent over the value expected in an infinite fluid. The cavitation number in the three-dimensional tests varied from 0.07 for the longest cavities to about 0.15 for the shortest, ranging as high as 0.30 for the two-dimensional runs. In steady flow, Widnall [20] calculated a 20 percent increase in lift coefficient for each 0,1 increase in cavitation number. The theory for unsteady supercavitating flow assumes

zero angle of attack, but in the actual flow the wetted surface has to make a minimum angle of 12^{o} with the flow direction for leading-edge ventilation to be realized. The non-zero angle of attack would also cause the lift coefficients to be higher than predicted. Thus a combination of all these effects would give a substantially higher value of lift coefficient than obtained from the original theory, but further investigations will be necessary before the reason for the observed large values of in-phase lift coefficient can be stated with certainty.

The other striking feature, of course, is the large range covered by the lift coefficients with changes in the cavity length. It is fair to say that the magnitude of this variation was rather unexpected. While it was recognized that with very short cavities the oscillation imposed on the foil-cavity system might cause some fluctuations in the cavity pressure and thus in the lift forces, it was supposed that such effects would decrease for sufficiently long cavities, say over twice the chord length, and that then the lift coefficients would show no appreciable variation with air supply rate, the cavity conditions closely approaching those of supercavitating flow.

On further reflection, and aided by hindsight, this supposition seems less well founded. The salient difference between flows with natural cavitation and with ventilation is, of course, that in the former the cavity is filled with water vapor while the ventilated cavity is supported by some external gas, in this case air. The water vapor may be assumed to be instantly convertible back into water, both along the

cavity walls and at the end of the cavity, but this cannot be said for an air-filled cavity. Rather, the only way air can leave the cavity is through entrainment in the water-air mixture at the end of the cavity. This entrainment region has a certain inertia and tends to remain stationary; also, while the entrainment mechanism can adjust itself to a different air entrainment rate (usually accompanied by a change in cavity geometry), this is not an instantaneous process.

On a supercavitating hydrofoil, such as in the present tests, the cavity springs from the leading edge and extends to far behind the foil, covering the entire suction side of the foil and leaving only the pressure side in contact with the water. When the foil is now oscillated in a heaving mode, observation shows that at most oscillation frequencies the cavity tends to become thinner when the foil moves into the cavity and fatter when it moves away from the cavity. Since the air-filled cavity is a constant-volume system on a short-time scale due to the inertia of the entrainment mechanism, it would get shorter as it gets fatter and longer when it gets thinner. However, the entrainment region appears to anchor the end of the cavity, so to speak, and resists rapid changes in length. The result is that the cavity volume increases when the foil moves out of the cavity and decreases when it moves inward, with attendant fluctuations in the cavity pressure since the entrainment and the air supply, and thus the amount of air in the cavity, are relatively constant. The suction side of the foil is exposed to this pressure, which thus contributes a fluctuating lift force.

To investigate the relationship of the unsteady cavity pressure to the variations in lift coefficient, a cavity pressure coefficient C_{pc} has been defined such that a unit change in C_{pc} causes the same lift force on the hydrofoil as a unit change in the lift coefficient $C_{L\alpha}$. Thus, if the unsteady cavity pressure plotted on this basis exactly duplicates the lift coefficient graph, then the variations in lift coefficient with cavity length would be entirely accounted for by the cavity pressure fluctuations.

Results of oscillating cavity pressure measurements are shown in Fig. 40 for the force data runs of Fig. 38. Taking note of the difference in scales, varying amounts of resemblance between the two sets of curves are apparent. On the plot for k = 0.43, it is notable that the large increase in $C_{L\alpha i}$ for long cavities is not accompanied by a corresponding increase in C_{pci}. A quite different situation occurs for k = 0.71 where the trajectory of cavity pressure covers a far larger range than would account for the variations in lift coefficient, yet the curves show many similarities. Here, the quadrature part of the cavity pressure has a substantial negative value at all cavity lengths, which would tend to lower the values of the quadrature lift coefficient and may explain why the range of $C_{L\alpha i}$ is so low, barely exceeding that for k = 0.43. On the other hand, the average C_{pci} (about -1.0) is much greater than the difference, estimated at 0.3, between the $C_{L\alpha i}$ actually measured and the value which might have been expected, based on the other measurements. At k = 1.43, there is a close similarity both in the shape and numerical values of the two curves, so

that in this case the lift trajectory may very well be due mostly to the unsteady cavity pressure.

These cavity pressure measurements are typical of those obtained also at other flow conditions. It is safe to say that, while the general trend indicates a definite connection between the oscillating cavity pressure and the unsteady lift coefficient, the present results do not show a reliable quantitative relationship. Further investigations of this point would be desirable. As an example, the pressure may not be uniform throughout the cavity because of the large changes in the cavity contour during oscillation. An attempt at measuring the local cavity pressure by mounting a pressure transducer directly in the wedge foil in the present tests was terminated when the suitable transducers which were available showed large, irregular outputs due to the oscillation accelerations.

A reflection of the oscilloscope trace of the regular cavity pressure transducer output was included in the field of view of the previously mentioned high-speed movies. The usefulness of the cavity pressure output for quantitative measurements was limited by some uncertainties in the calibration and noise contained in the signal. Nevertheless, frame-by-frame analysis of the films showed that the conclusions of the previous discussion of the unsteady cavity behavior are generally correct at low reduced frequencies, that is, that the cavity volume decreases when the foil moves into the cavity, and the cavity pressure tends to be highest when the cavity volume is decreasing. At higher oscillation frequencies, however, the phase relationships between the

foil motion, cavity volume, and cavity pressure become less consistent, especially at larger cavity lengths. This is probably due both to the entrainment mechanism and the dynamic waves in the cavity surface, which also make the accurate estimation of the cavity length and thickness from the films somewhat difficult.

Even if the changes in the lift coefficient could be traced to the unsteady cavity pressure, this would provide at best only emotional satisfaction since the fluctuating cavity pressure is of course also not known a priori. Anyway, it is reasonable to assume that other factors contribute to the unsteady lift forces; for instance, little is known about the dynamic pressures acting on the foil, and the effect of the oscillations and shape changes of the cavities. Successful prediction of the unsteady forces in ventilated flows will require a great deal of further advances in the understanding of these flows.

Finally, a word about the loops in the lift coefficient trajectories. A measure of skepticism greeted the first group of graphs which showed this feature. However, there is no basis for questioning the validity of the data, and it may be pointed out that the loops were not measured directly, but merely resulted from combining the separate data points. Recalling that half the data points are taken at increasing, and half at decreasing, air supply rate, a glance at the graphs will confirm the internal consistency of the results.

An interesting related result is worth mentioning. Geurst[37] has carried out calculations for an oscillating supercavitating hydrofoil with finite cavity length and has given Nyquist diagrams of the

functions governing the variations in lift, pitching moment, and cavity length. The curves for the latter show loops in the trajectories, quite similar to those shown here, which Meijer [55] was able to confirm experimentally. Admittedly, these are not directly related to the present tests, where lift instead of cavity length is the quantity of interest, and cavity length rather than reduced frequency is the parameter. Nevertheless, the physical phenomenon is similar in the two cases, and thus a certain family resemblance in the curves is not too surprising, though notable.

In conclusion, it may be recalled that the intent of the present experiments was the simulation of natural cavitation by forced ventilation. The equivalence of these two conditions in steady flow is well established, but the results obtained here with ventilated cavities raise some questions about the validity of such an assumption in unsteady flow. Further investigations need to be carried out to clarify this point. Probably the most direct way to resolve the problem would be to perform tests with oscillating hydrofoils in a closed water tunnel, in which the ambient pressure can be changed, so that both natural and ventilated cavities can be established at essentially identical flow conditions.

V. SUMMARY AND CONCLUSIONS

An apparatus has been designed and developed which is well suited to the determination of the forces acting on a hydrofoil that is forced to undergo oscillations. The present set-up was particularly constructed for the case of heaving motion (vertical translation), but the principle is equally applicable to pitching motion (rotation about a transverse axis). While this would require a different hydraulic actuator and force dynamometer, the design of these should pose no problems, and an even wider field of possible investigations would be opened.

A significant aspect of the present experimental work is the extremely good consistency of data obtained, especially with fully wetted flow. This allowed the sure determination of some quite small effects that would have been obscured if the scatter had been of the same magnitude as appears to be usual in tests of this kind. The rejection of noise and all frequencies other than the fundamental one, and the direct digital read-out provided by the equipment, as opposed to the commonly used oscillograph, greatly improved both the convenience and accuracy of the data acquisition.

With this apparatus, the unsteady lift forces on a hydrofoil oscillating in a heaving mode under a free surface have been measured over a wide range of reduced frequency for a variety of configurations, including foils of aspect ratio one and infinity (two-dimensional flow)

in fully wetted, base-ventilated, and supercavitating flow. By using different combinations of the flow velocity and oscillation frequency, it was determined that the reduced frequency is indeed the governing parameter for the unsteady force coefficients.

In fully wetted flow, the effects of foil shape, submergence, oscillation amplitude, and set angle of attack were found to be generally in agreement with expectations. However, the in-phase lift of the wedge is 20 to 30 percent higher than predicted and measured for the flat plate foil, and the quadrature lift is somewhat lower than the theoretical value for all the foils, which seems to be a common experience in tests of oscillating hydrofoils. In addition, the lift trajectory for the wedge shows a sharp break at a reduced frequency of about 4.5, which has been associated with the vortex shedding of the blunt base. It would be instructive to test a series of wedges with various values of base height in order to further study this phenomenon.

In two-dimensional fully wetted flow, both the in-phase and quadrature lift coefficients are somewhat lower, compared to the corresponding theory, than in three-dimensional flow. This can probably be ascribed to the imperfections inherent in simulating two-dimensional flow by oscillating a finite-span model between stationary side walls.

Base ventilation of the wedge caused no changes in the unsteady lift compared to the fully wetted wedge, but the knee in the curve entirely disappeared. This would be expected, since the base cavity

disables the mechanism which causes the vortex shedding interaction in fully wetted flow.

Supercavitating flow in the present tests was established by supplying air to the cavity, since the flow velocity in the water tunnel is too low for natural cavitation to occur. The length of these ventilated cavities varied with the air supply rate. Large variations in the unsteady lift coefficients were found with changes in cavity length, and the curves traced out by plotting the in-phase versus the quadrature lift coefficient, with cavity length as a parameter, assume fairly complicated shapes at the higher oscillation frequencies; they are, however, quite reproducible.

Measurement of the unsteady cavity pressure showed that, while the trend of the changes in cavity pressure had similarities to the variations in the lift coefficients, a quantitative correspondence cannot be said to exist. Further investigations on unsteady flows with ventilated cavities are needed to increase the knowledge of the physical processes involved in these flows.

As in the fully wetted tests, the average quadrature lift coefficient for ventilated foils was also found to be lower than the theoretical value. The in-phase lift, on the other hand, was somewhat larger than the expected value for two-dimensional flow, and about twice as large as predicted for the aspect ratio one foils. Some of the factors which may contribute to this discrepancy have been discussed.

It was pointed out in the introduction that very little experimental work has been previously reported on oscillating hydrofoils. The present work thus provides significant new information, not only

for confirmation of theoretical results where applicable but also especially in those cases where the behavior found in the tests was not expected from theoretical considerations.

Several of these new phenomena have a bearing on practical problems. The vortex shedding associated with the blunt base of the fully wetted wedge may be involved in the "singing" of propeller blades. For foils with ventilated cavities, the variations in the unsteady lift coefficients with cavity length are not at all predicted by the available theory, and the average value of the unsteady lift is greatly underestimated. In consequence, the transient forces on a hydrofoil boat encountering waves can be expected to be substantially higher than would be predicted from theory alone, which means the boat will ride less smoothly and also require larger control forces. For supercavitating propellers, the blade strength may become even more critical when these unsteady forces are considered than it already is.

There is an urgent need for further investigations in the field of unsteady ventilated hydrofoils. Theoretical work at low reduced frequencies could perhaps be based on the assumption, suggested by present experiments, that the mass of air within the cavity rather than the cavity volume is constant. Additional tests with ventilated cavities would help to further define the range of forces generated, and experiments on supercavitating hydrofoils with natural cavitation are essential for establishing the correspondence between natural and ventilated cavities in unsteady flow.

REFERENCES

1. C. Beason and A.K. Buckle, "Hydrofoil Vessels," Hovering Craft & Hydrofoil 5, 6, March 1966, pp. 4-25.

2. M.W. McFarland (editor), "The Papers of Wilbur and Orville Wright," McGraw-Hill Book Co., 1953, Vol. 2, pp. 1137-38.

3. "Baron Hans von Schertel," Hovering Craft and Hydrofoil 2, 6, March 1963, pp. 10-12.

4. P.J. Yangos, "An Appraisal of Hydrofoil Craft for the Benefit of the Aeronautical Engineer," Hovering Craft & Hydrofoil 4, 4, January 1965, pp. 6-22.

5. E.R. Lacey, "A Progress Report on Hydrofoil Ships," Hovering Craft & Hydrofoil 3, 7, April 1964, pp. 22-31.

6. Second Symposium on Naval Hydrodynamics, 1958, ACR-38, Office of Naval Research, Washington, D.C.

7. Fourth Symposium on Naval Hydrodynamics, 1962, ACR-92, Office of Naval Research, Washington, D.C.

8. SNAME Hydrofoil Symposium, 1965 Spring Meeting, Soc. of Naval Arch. and Marine Eng., New York, 10006.

9. M.P. Tulin, "Supercavitating Flows - Small Perturbation Theory," J. Ship Res. 7, 3, January 1964, pp. 16-37.

10. R.P. Bernicker, "A Linearized Two-Dimensional Theory for High-Speed Hydrofoils Near the Free Surface," J. Ship Res. 10, 1, March 1966, pp. 25-48.

11. K.L. Wadlin and K.W. Christopher, "A Method for Calculation of Hydrodynamic Lift for Submerged and Planing Rectangular Lifting Surfaces," NACA TN 4168, 1958.

12. R.W. Kermeen, "Experimental Investigations of Three-Dimensional Effects on Cavitating Hydrofoils," J. Ship Res. 5, 2, September 1961, pp. 22-43.

13. J. Feldman, "Experimental Investigation of Near-Surface Hydrodynamic Force Coefficients for a Systematic Series of Tee Hydrofoils, DTMB Series HF-1," David Taylor Model Basin Report 1801, 1963.

14. T. Theodorsen, "General Theory of Aerodynamic Instability and the Mechanism of Flutter," NACA Report 496, 1935.

15. L.C. Woods, "The Lift and Moment Acting on a Thick Aerofoil in Unsteady Motion," Philos. Trans. Roy. Soc. London, Series A, 247, November 1954, p. 131.

16. W.R. Laidlaw, "Theoretical and Experimental Pressure Distributions on Low Aspect Ratio Wings Oscillating in an Incompressible Flow," M.I.T. Aeroelastic and Struct. Res. Lab., Tech. Rep. 51-2, September 1954.

17. P. Crimi and I.C. Statler, "Forces and Moments on an Oscillating Hydrofoil," Cornell Aero. Lab. Report No. BB-1629-S-1, August 1962; see also Fourth Symposium on Naval Hydrodynamics, 1962, pp. 477-494.

18. T. von Karman and W.R. Sears, "Airfoil Theory for Non-Uniform Motion," J. Aero. Sci., Vol. 5, August 1938.

19. T. Nishiyama, "Unsteady Characteristics of the Submerged Hydrofoil Performing Heave or Pitch at Constant Forward Speed under Sinusoidal Waves," Fourth Symposium on Naval Hydrodynamics, 1962, pp. 495-525.

20. S.E. Widnall, "Unsteady Loads on Hydrofoils Including Free Surface Effects and Cavitation," (Thesis), M.I.T. Fluid Dyn. Res. Lab. Report No. 64-2, June 1964.

21. F.E. Smith and M. Sevik, "An Investigation of the Forces on an Airfoil Oscillating in Pitch about the Quarter Chord," Penn. State Univ., Ordnance Res. Lab. TM 607.2441-02, March 1964.

22. D.S. Cieslowski and J.H. Pattison, "Unsteady Hydrodynamic Loads and Flutter of Two-Dimensional Hydrofoils," SNAME Hydrofoil Symp., 1965 Spring Meeting, Paper No. b.

23. H. Lamb, "Hydrodynamics," 6th ed., Dover Publications, New York, 1945, p. 102.

24. M.P. Tulin and M.P. Burkart, "Linearized Theory for Flows about Lifting Foils at Zero Cavitation Number," David Taylor Model Basin Rep. C-638, February 1955.

25. V.E. Johnson, Jr., "Theoretical and Experimental Investigation of Supercavitating Hydrofoils Operating near the Free Water Surface," NASA TR R-93, 1961.

26. V.E. Johnson, Jr., "The Influence of Depth of Submersion, Aspect Ratio, and Thickness on Supercavitating Hydrofoils Operating at Zero Cavitation Number," Second Symposium on Naval Hydrodynamics, 1958, pp. 317-365.

27. J. Auslaender, "The Linearized Theory for Supercavitating Hydrofoils Operating at High Speeds Near a Free Surface," J. Ship Res. 6, 2, October 1962, pp. 8-23.

28. H.-T. Ho, "Linearized Theory for a Supercavitating Hydrofoil Operating in a Fluid of Finite Depth," Hydronautics, Inc., Tech. Rep. 119-7, June 1963.

29. D.K. Ai, A.J. Acosta, and Z.L. Harrison, "Linearized Theory of a Two-Dimensional Planing Flat Plate in a Channel of Finite Depth - 1," C.I.T. Hydro. Lab. Rep. No. E-110.2, April 1964.

30. F.R. Schiebe and J.M. Wetzel, "Ventilated Cavities on Submerged Three-Dimensional Hydrofoils," Univ. of Minn., St. Anthony Falls Hyd. Lab., Tech. Paper No. 36, Series B, December 1961.

31. G.F. Dobay, "Hydrofoils Designed for Surface Ventilation - An Experimental Analysis," SNAME Hydrofoil Symp., 1965 Spring Meeting, Paper No. f.

32. T.Y. Wu, "Unsteady Supercavitating Flows," Second Symposium on Naval Hydrodynamics, 1958, pp. 293-316.

33. B.R. Parkin, "Fully Cavitating Hydrofoils in Nonsteady Motion," C.I.T. Eng. Div. Report No. 85-2, July 1957.

34. Y.C. Fung, "An Introduction to the Theory of Aeroelasticity," John Wiley and Sons, New York, 1955.

35. B.R. Parkin, "Numerical Data on Hydrofoil Response to Non-steady Motions at Zero Cavitation Number," J. Ship Res. 6, 3, December 1962, pp. 40-42.

36. T.Y. Wu, "A Linearized Theory for Nonsteady Cavity Flows," C.I.T. Eng. Div. Report No. 85-6, September 1957.

37. J.A. Geurst, "Linearized Theory of Two-Dimensional Cavity Flows," Ph.D. Thesis, Tech. Hogeschool Delft (Netherlands), May 1961.

38. M. Martin, "Unsteady Lift and Moment on Fully Cavitating Hydrofoils at Zero Cavitation Number," J. Ship Res. 6, 1, June 1962, pp. 15-25.

39. J. Patton and A. Borden, "Computation of Oscillatory Loads on a Supercavitating Hydrofoil," David Taylor Model Basin Report 1840, August 1965.

40. L.C. Woods, "Aerodynamic Forces on an Oscillating Aerofoil Fitted with a Spoiler," Proc. Roy. Soc. London 239, Series A, March 1957, pp. 328-337.

41. D.P. Wang and T.Y. Wu, "Small-Time Behavior of Unsteady Cavity Flows," C.I.T. Hydro. Lab. Report No. 97-3, March 1963; see also Arch. for Rational Mech. and Analysis 14, 2, 1963, pp. 127-152.

42. D.P. Wang and T.Y. Wu, "General Formulation of a Perturbation Theory for Unsteady Cavity Flows," C.I.T. Hydro. Lab. Report No. E-97.7, March 1965.

43. C.C. Hsu, "Fully Cavitating Hydrofoils in Non-Steady Motion Under a Free Surface," Hydronautics, Inc., Tech. Rep. 119-5, August 1963.

44. C.C. Hsu, "Non-Steady Hydrodynamic Characteristics of a Supercavitating Hydrofoil Under a Free Surface," Hydronautics, Inc., Tech. Rep. 463-2, April 1964.

45. C.S. Song, "Supercavitating Flat Plate with an Oscillating Flap at Zero Cavitation Number," Univ. of Minn., St. Anthony Falls Hyd. Lab. Tech. Paper No. 52, Series B, November 1965.

46. C.S. Song, "Two-Dimensional Supercavitating Plate Oscillating Under a Free Surface," J. Ship Res. 9, 1, June 1965, pp. 40-55.

47. C.S. Song, "Measurements of the Unsteady Force on Cavitating Hydrofoils in a Free Jet," Univ. of Minn., St. Anthony Falls Hyd. Lab. Tech. Paper No. 49, Series B, June 1964.

48. R.T. Knapp, J. Levy, J.P. O'Neill, and F.B. Brown, "The Hydrodynamics Laboratory of the California Institute of Technology," Trans. ASME 70, July 1948, pp. 437-457.

49. A.S. Iberall, "Attenuation of Oscillatory Pressures in Instrument Lines," National Bureau of Standards Res. Paper RP 2115, Vol. 45, 1950.

50. I.H. Abbott and A.L. von Doenhoff, "Theory of Wing Sections," Dover Publications, New York, 1959.

51. J.O. Young and J.W. Holl, "Effects of Cavitation on Periodic Wakes Behind Symmetric Wedges," ASME Paper No. 65-FE-15.

52. R.E.D. Bishop and A.Y. Hassan, "The Lift and Drag Forces on a Circular Cylinder in a Flowing Fluid," Proc. Roy. Soc. London 277, Series A, 1964, pp. 32-75.

53. E.R. Bate, Jr., "The Effect of Gap Clearance and Support Strut Interference on the Lift Curve Slope of a Hydrofoil," C.I.T. Hydro. Lab. Int. Mem. E-118.14M (not available for distribution), November 1962.

54. J.M. Grace and I.C. Statler, "Free-Surface Effects on the Apparent-Mass, Quasi-Steady, and Wake Contributions to Hydrofoil Loads," Cornell Aero. Lab. Report No. BB-1629-S-2, August 1965.

55. M.C. Meijer, "A Summary of Experiments on Non-Steady Cavitation, Performed at the Shipbuilding Laboratory of the Technological University of Delft, Netherlands," C.I.T. Hydro. Lab. Int. Mem. 110.7 (not available for distribution), August 1963.

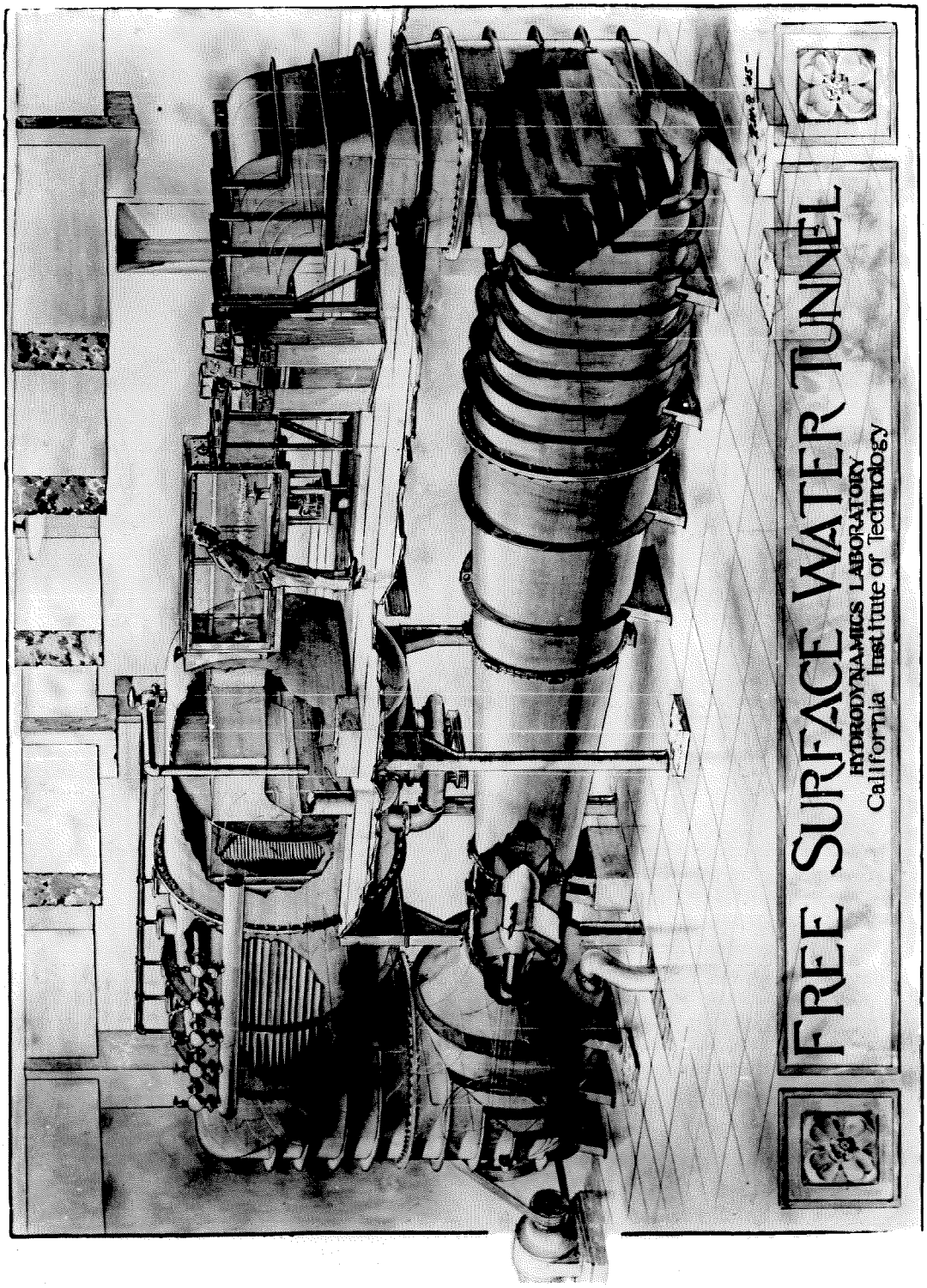
FREE SURFACE WATER TUNNEL
HYDRODYNAMICS LABORATORY
California Institute of Technology

Fig. 1

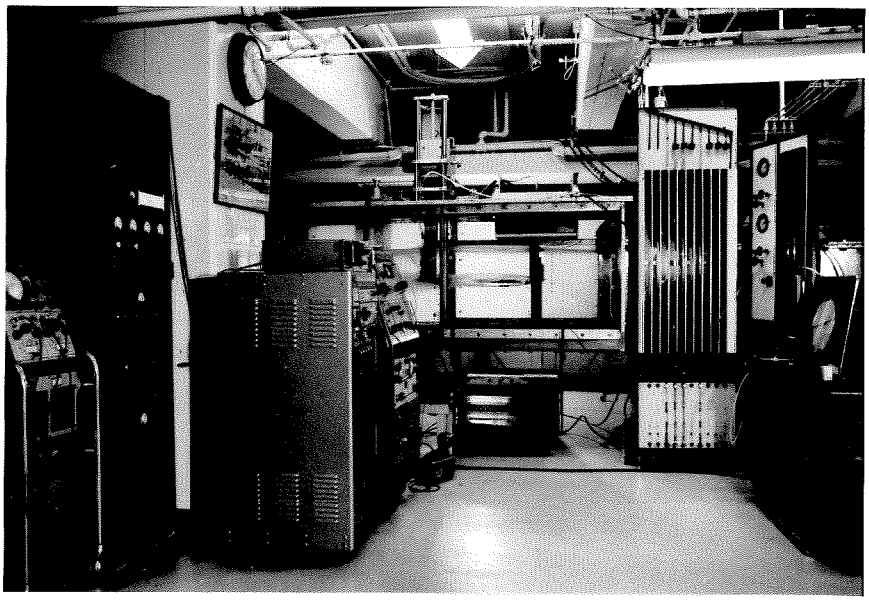

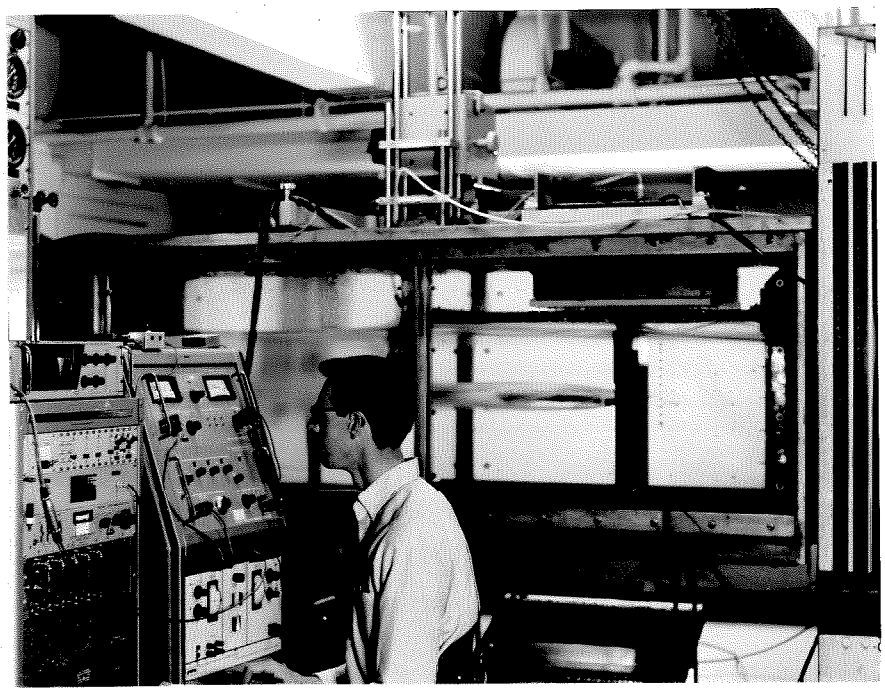

Fig. 2 - Views of the working section and test equipment.

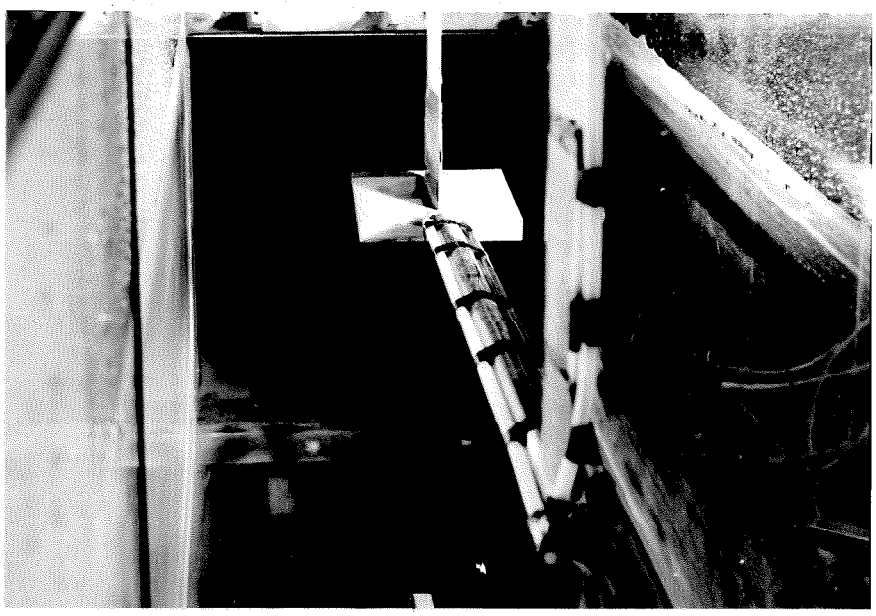

Fig. 3 - View looking forward and down into the working section set up for three-dimensional tests.

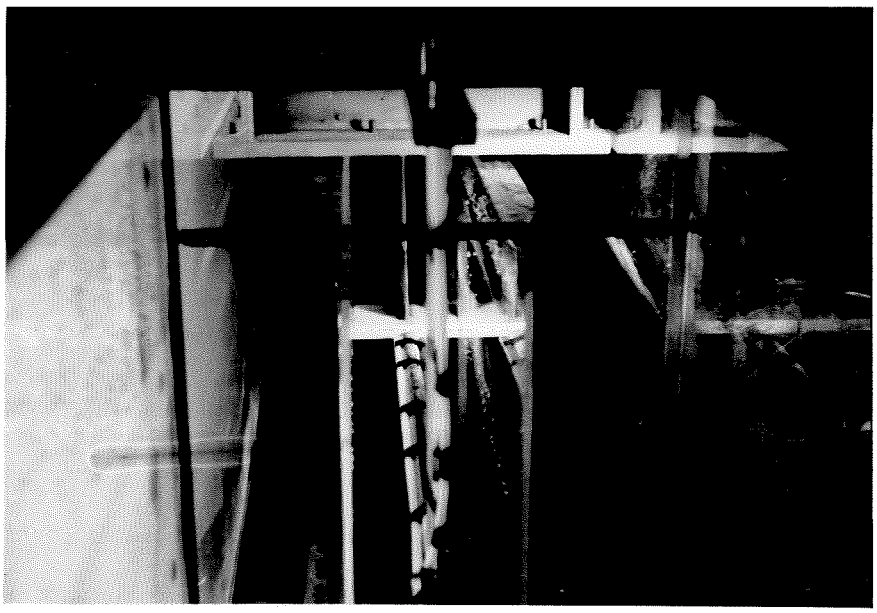

Fig. 4 - View looking forward and down into the working section with inserts installed for two-dimensional tests.

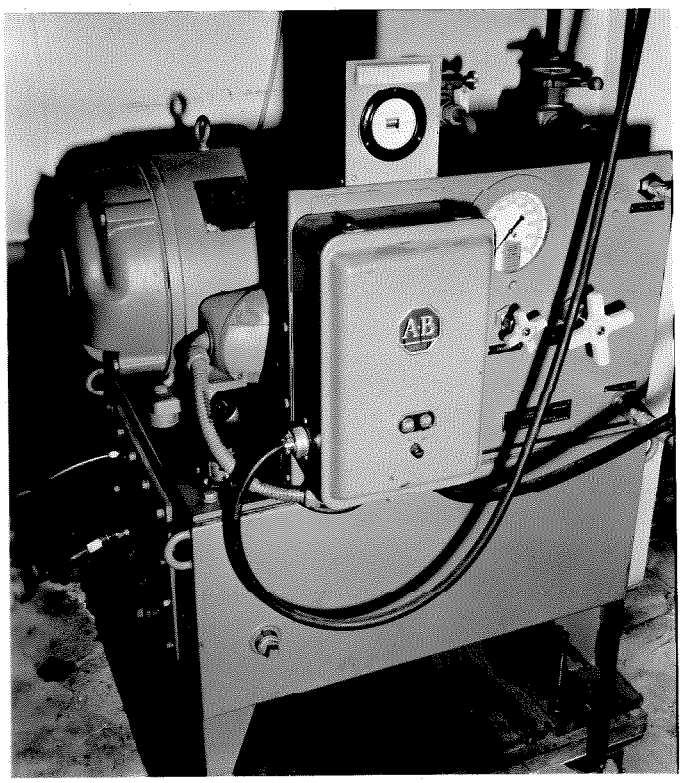

Fig. 5 - The hydraulic power supply.

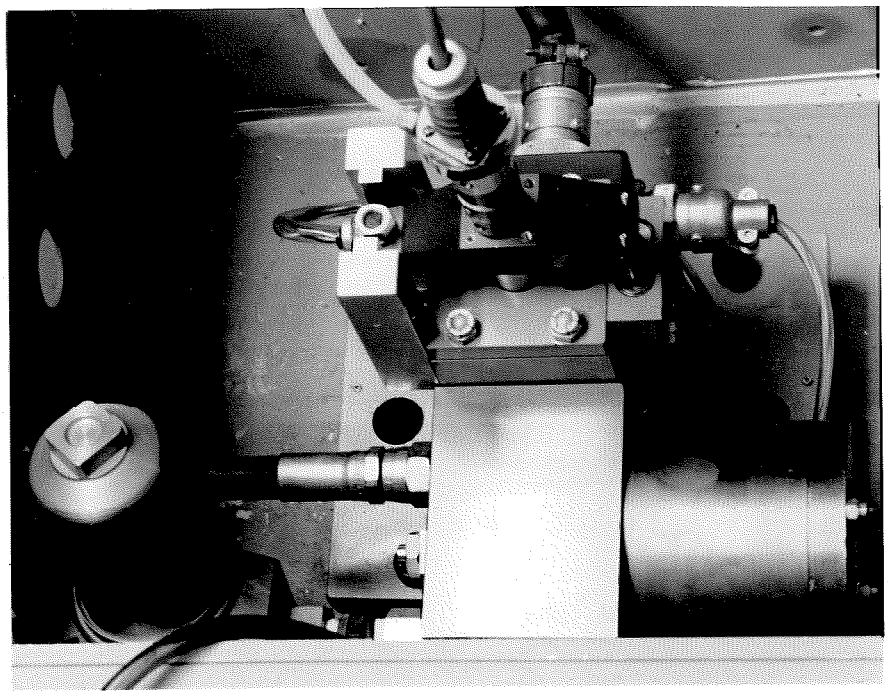

Fig. 6 - Top view of the hydraulic oscillator.

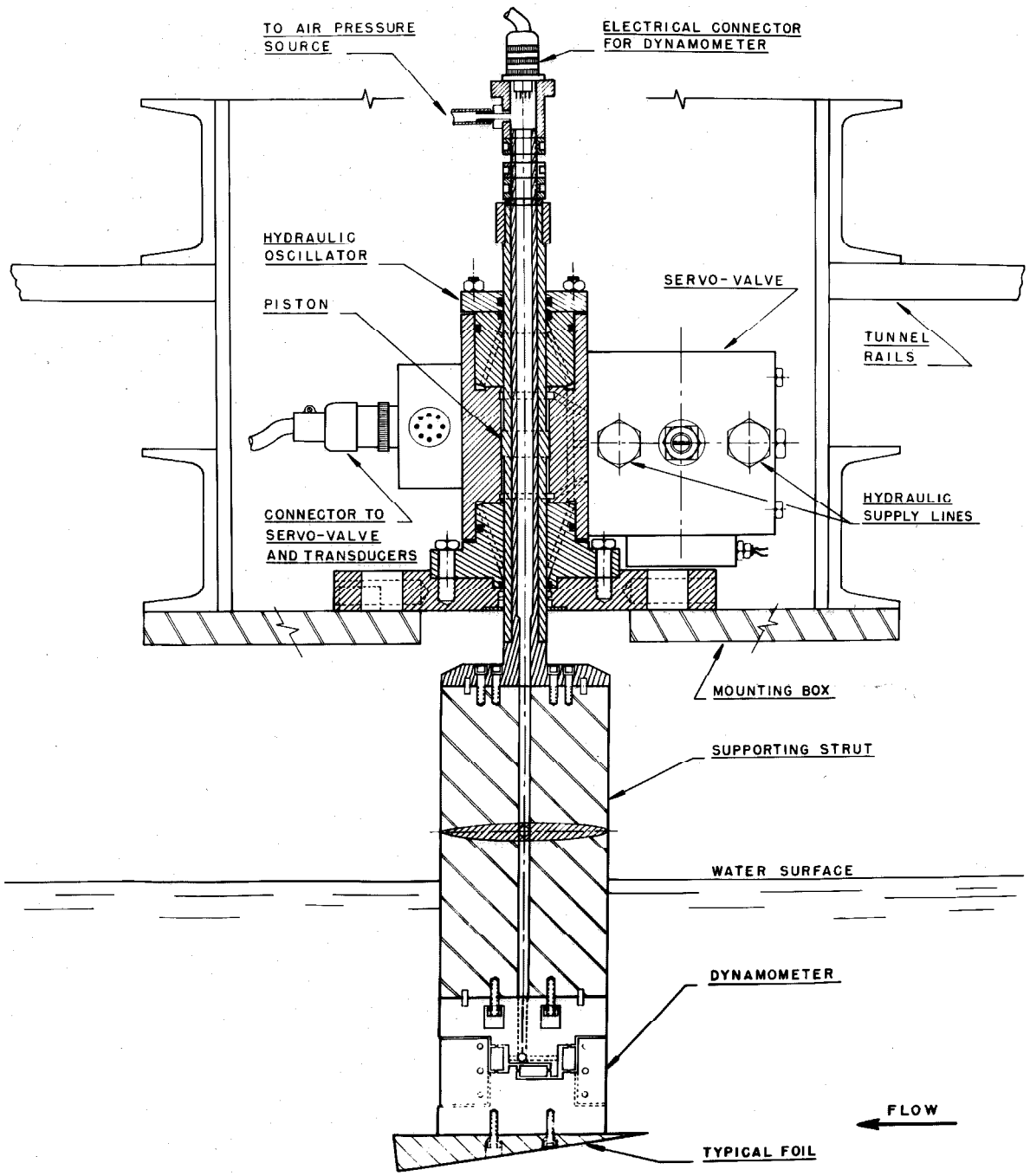

Fig. 7 - Cross-section drawing of the hydraulic oscillator, showing the tunnel mounting, strut dynamometer, and hydrofoil.

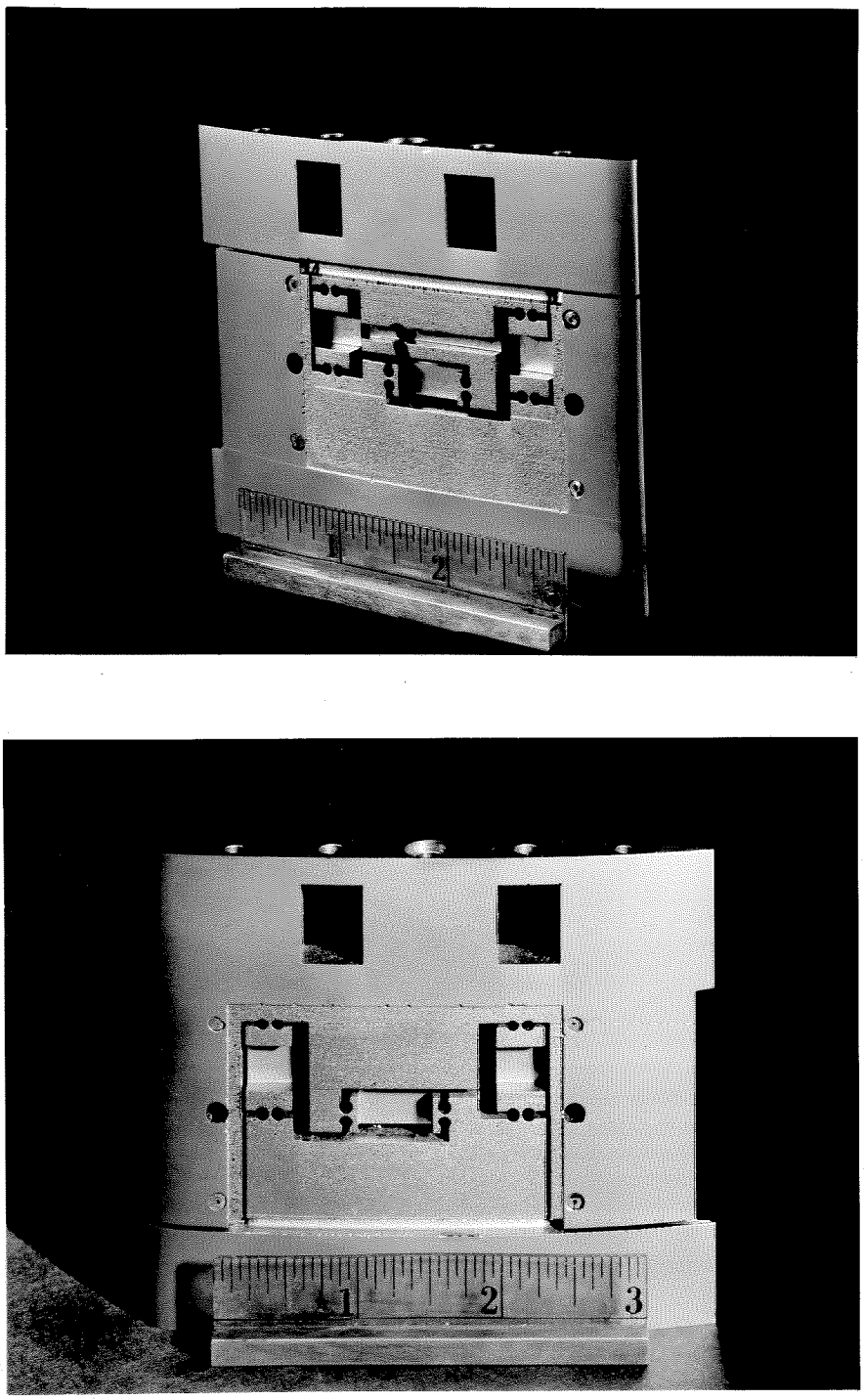

Fig. 8 - The strut dynamometer, seen from both sides, before affixing of the strain gages.

HYDROFOIL MODELS

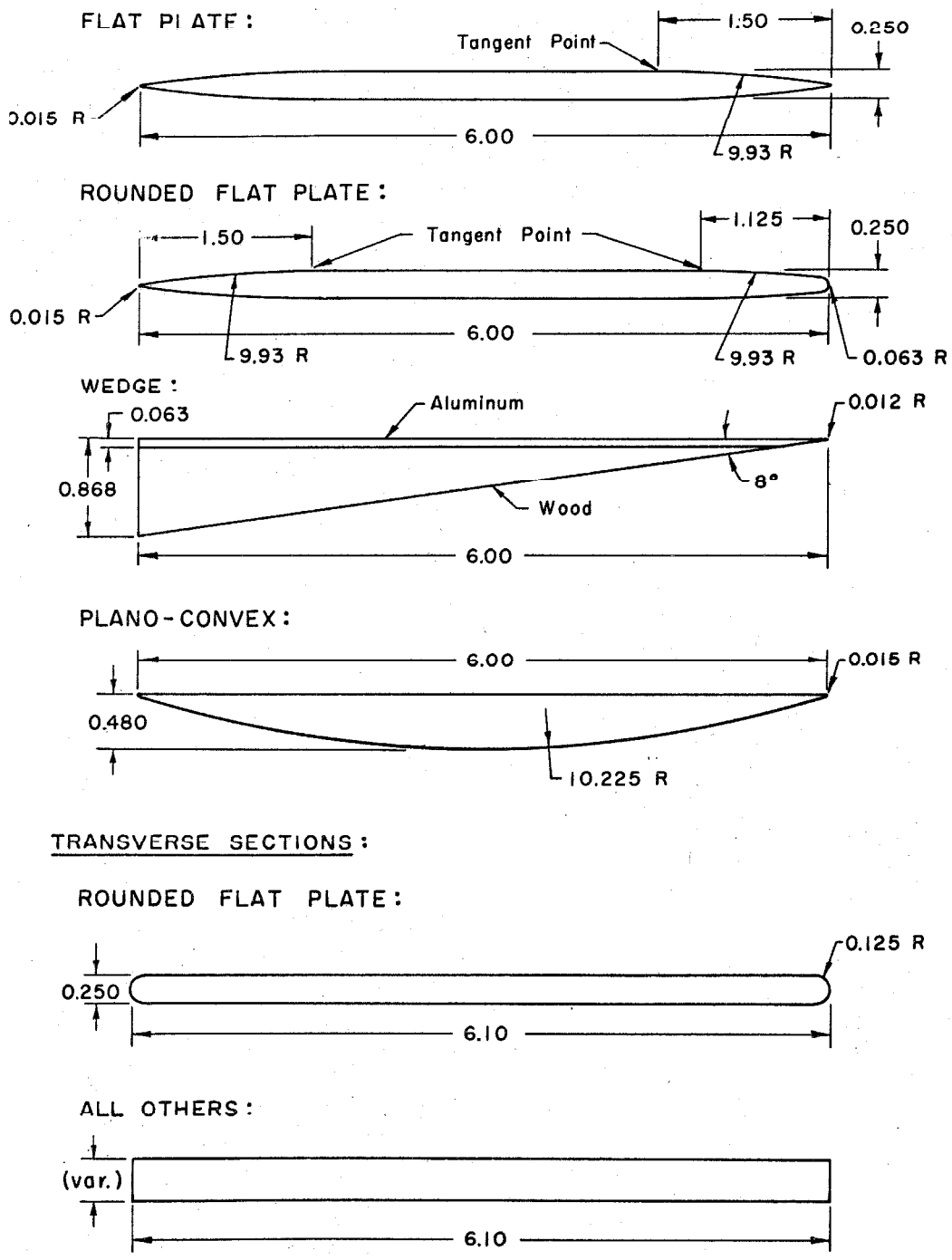

Fig. 9 - Specifications of the various hydrofoil models.

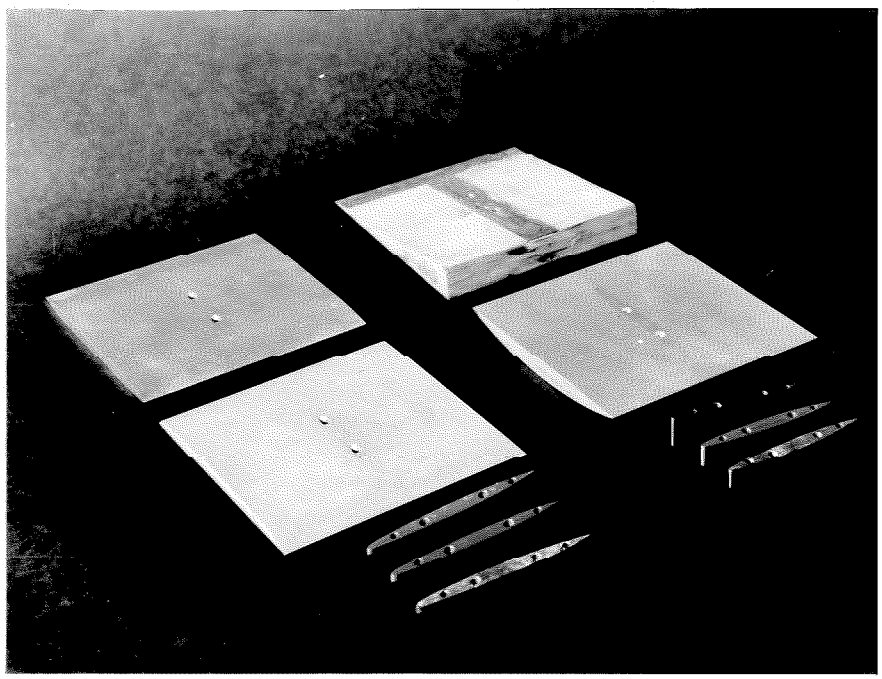

Fig. 10 - The hydrofoil models and mounting adapters.

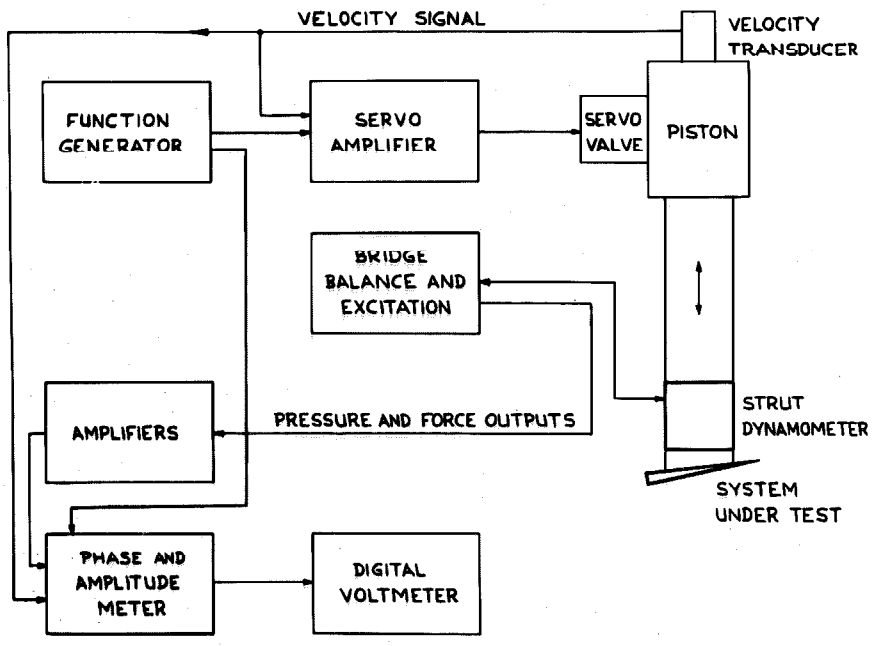

Fig. 11 - Diagram of the electronic equipment for hydraulic oscillator and data acquisition.

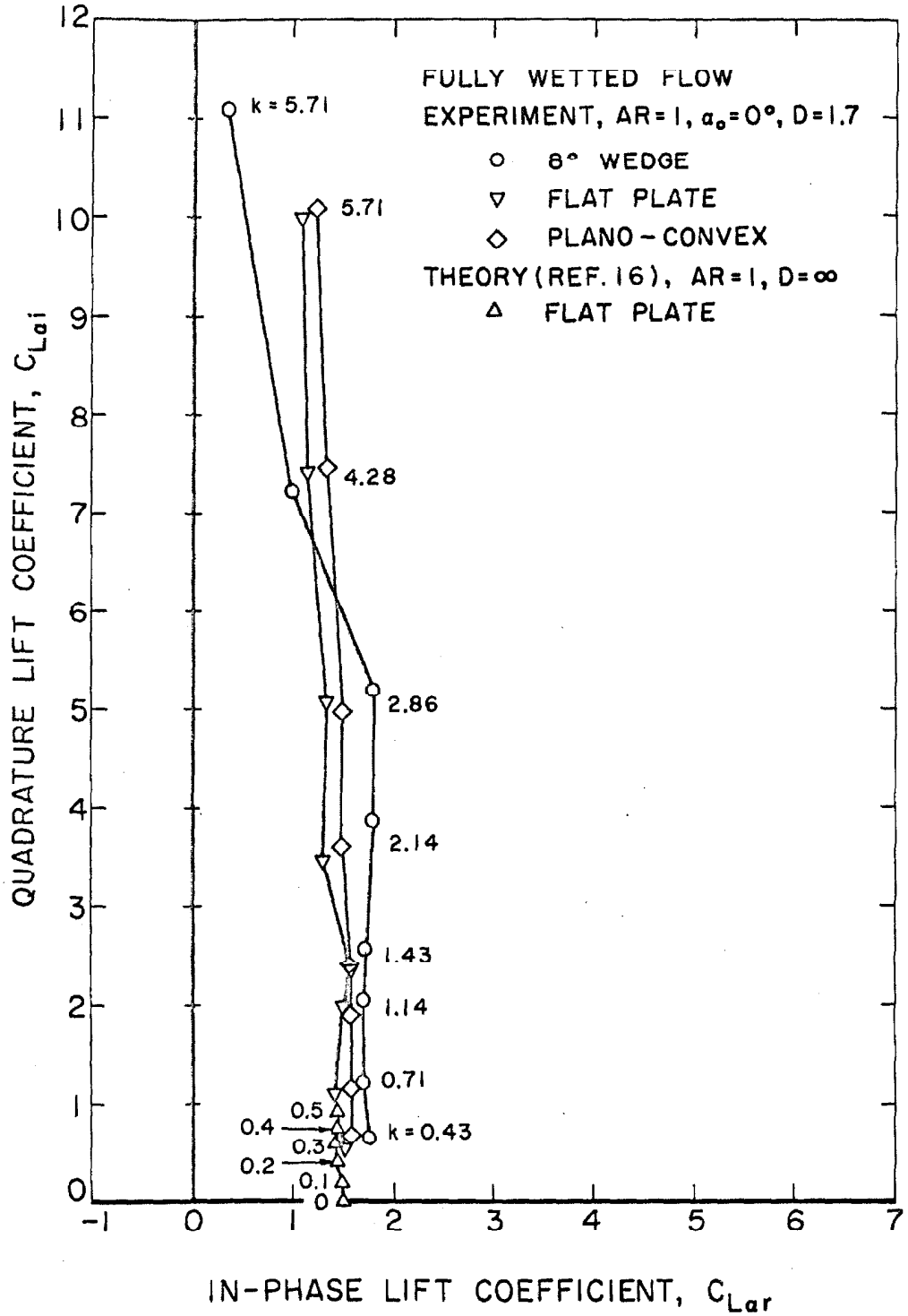

Fig. 12 - Variation of the unsteady lift coefficients with reduced frequency for several aspect ratio one foils in fully wetted flow at 1.7 chords submergence (first group of runs).

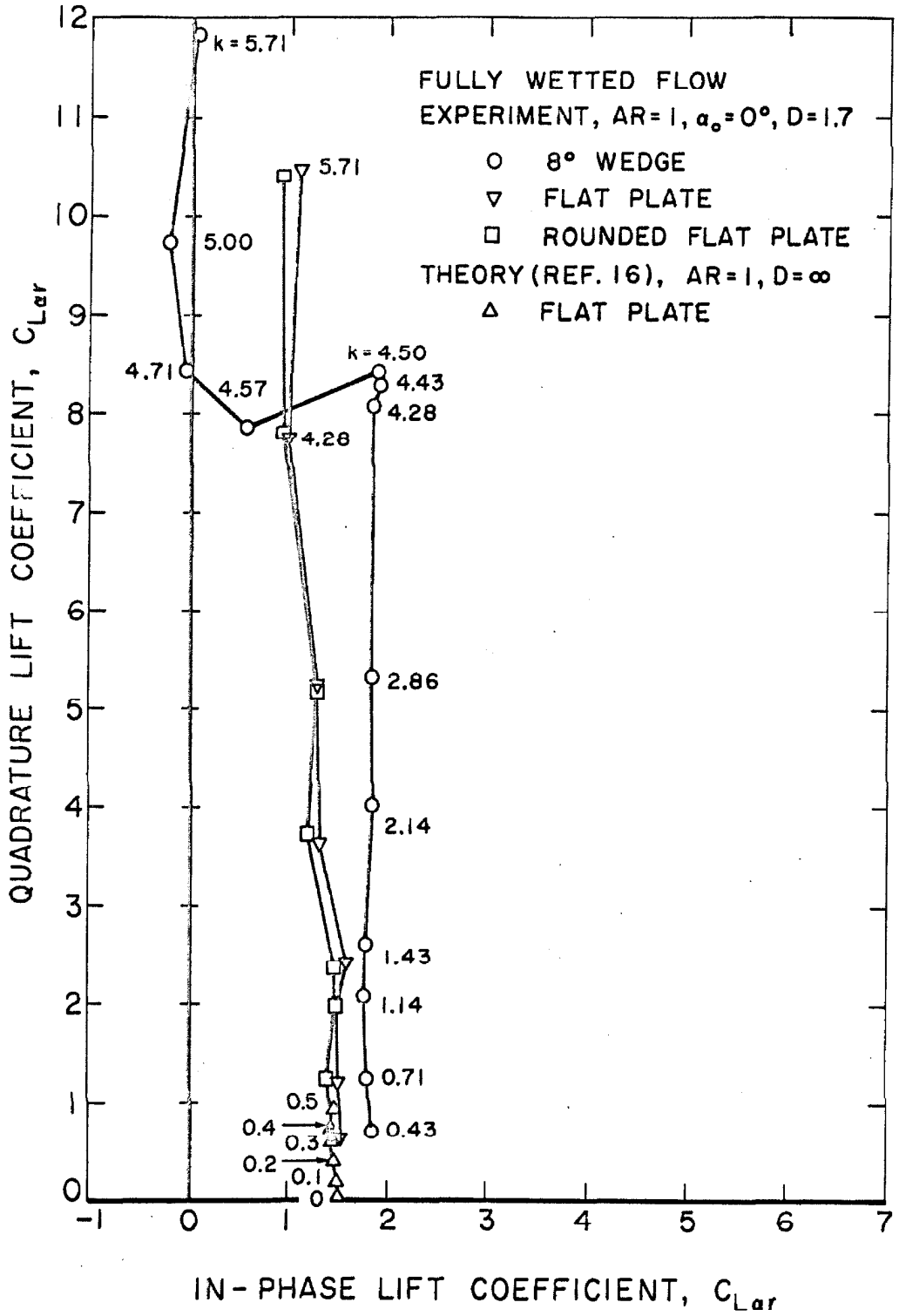

Fig. 13 - Variation of the unsteady lift coefficients with reduced frequency for several aspect ratio one foils in fully wetted flow at 1.7 chords submergence (second group of runs).

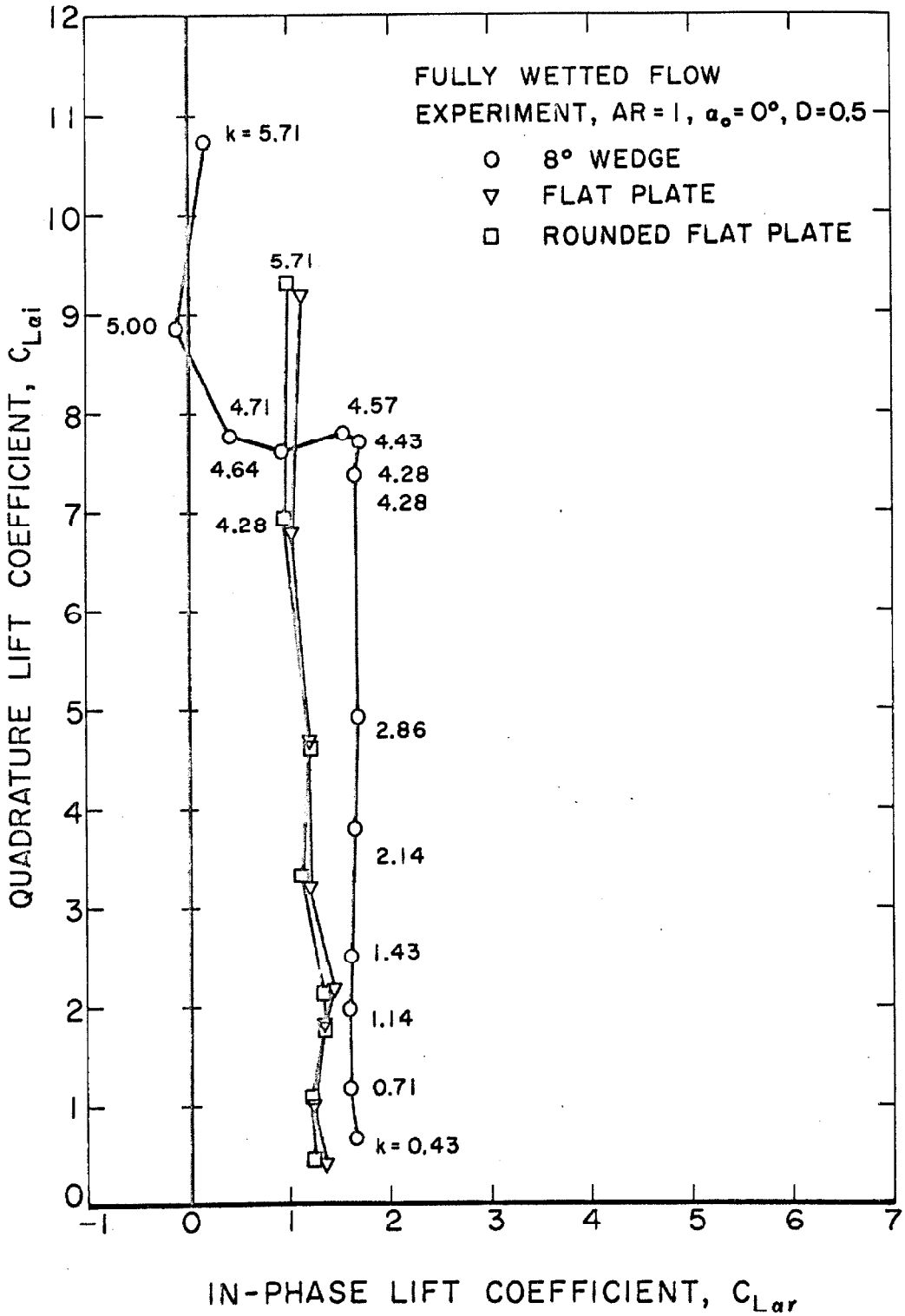

Fig. 14 - Variation of the unsteady lift coefficients with reduced frequency for several aspect ratio one foils in fully wetted flow at 0.5 chords submergence.

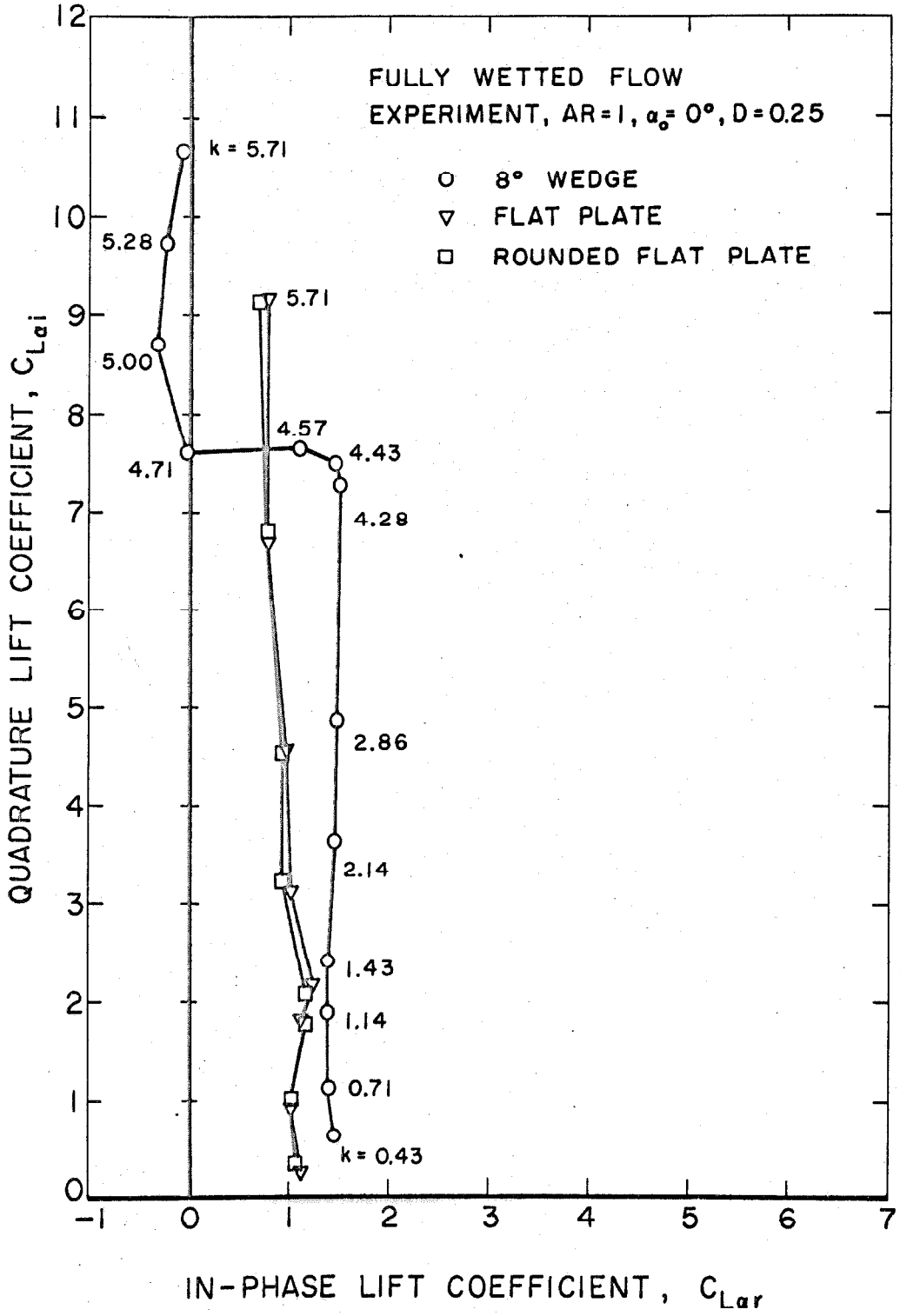

Fig. 15 - Variation of the unsteady lift coefficients with reduced frequency for several aspect ratio one foils in fully wetted flow at 0.25 chords submergence.

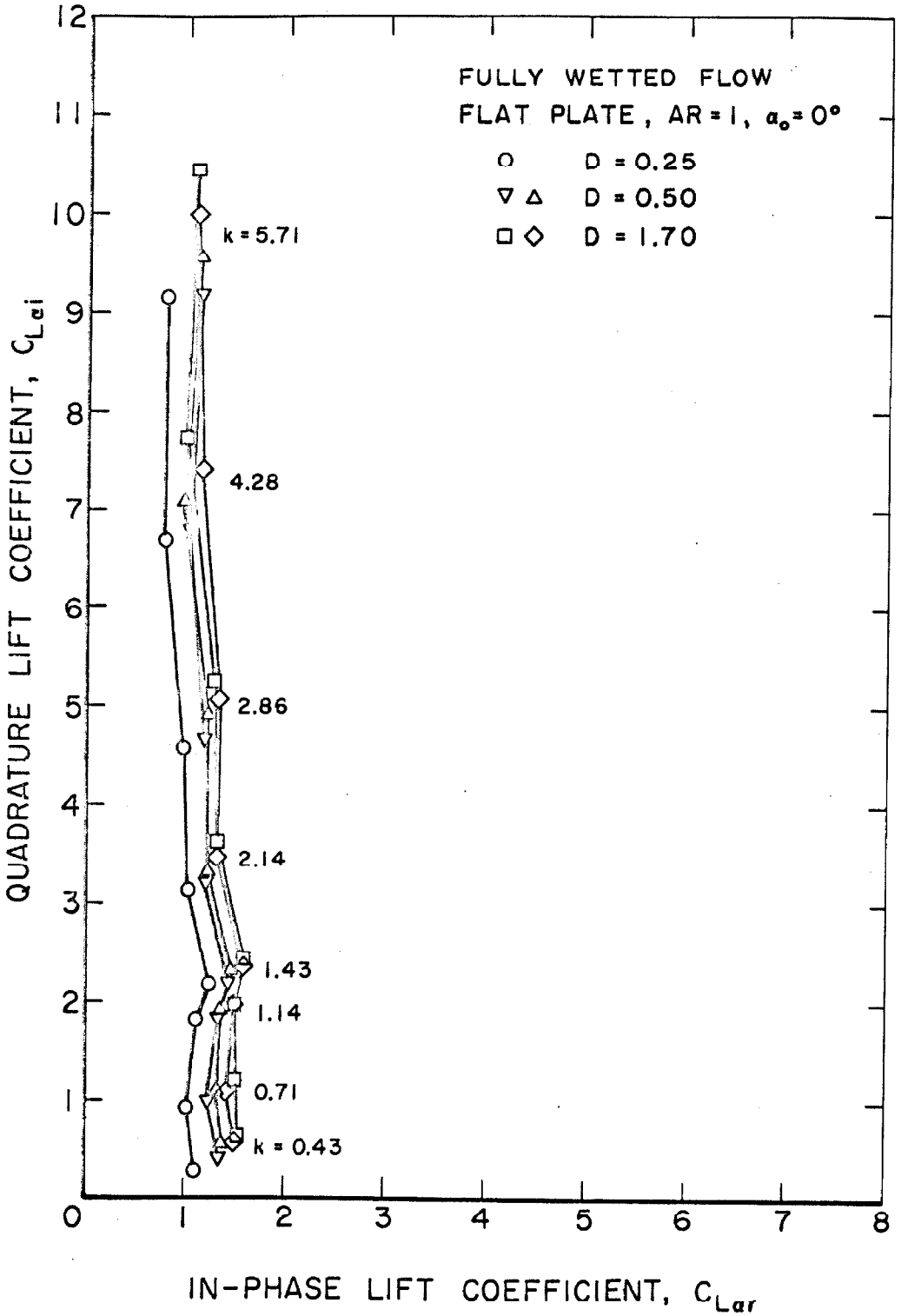

Fig. 16 - Variation of the unsteady lift coefficients with reduced frequency for the aspect ratio one flat plate in fully wetted flow, showing the effect of submergence.

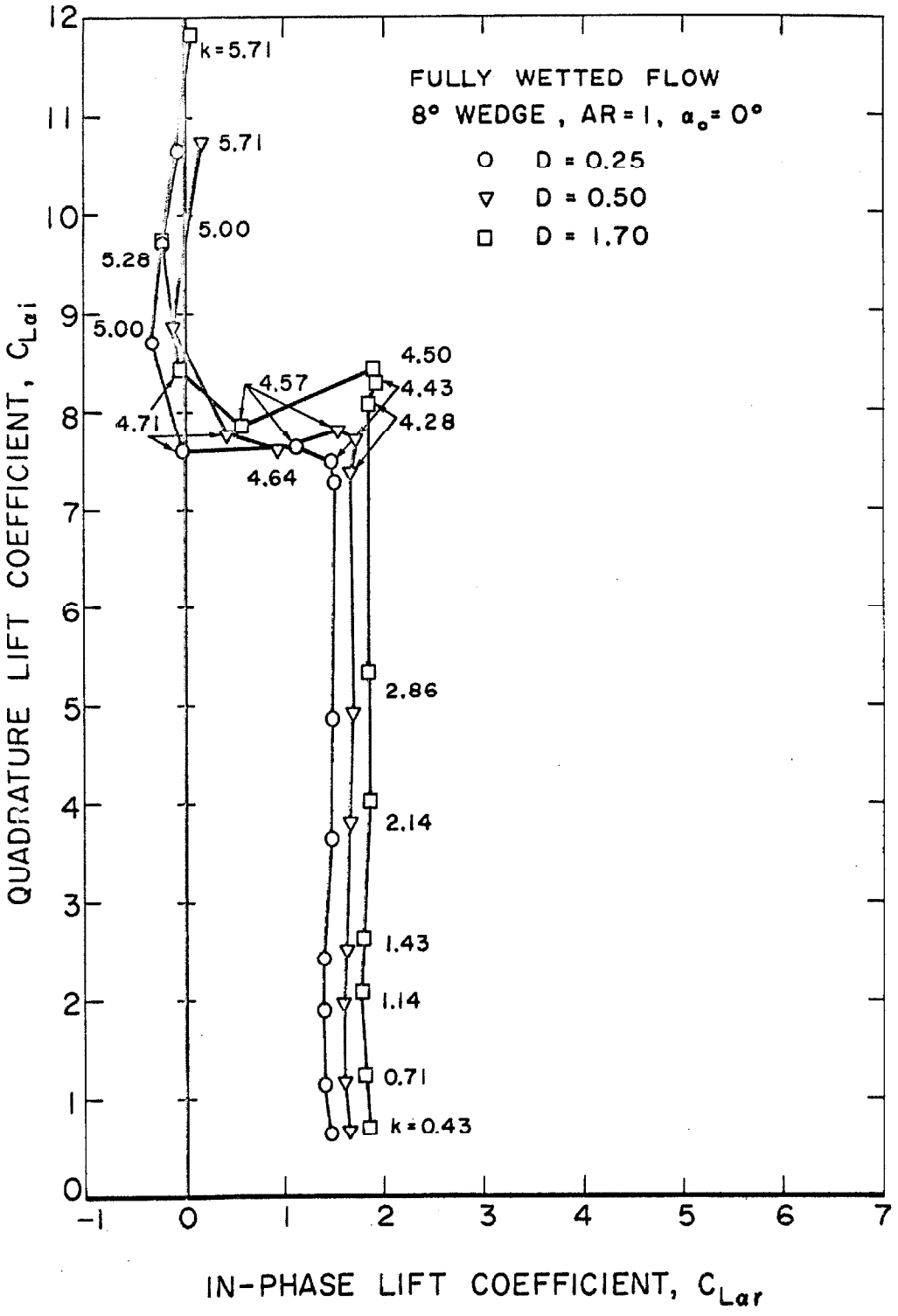

Fig. 17 - Variation of the unsteady lift coefficients with reduced frequency for the aspect ratio one wedge in fully wetted flow, showing the effect of submergence.

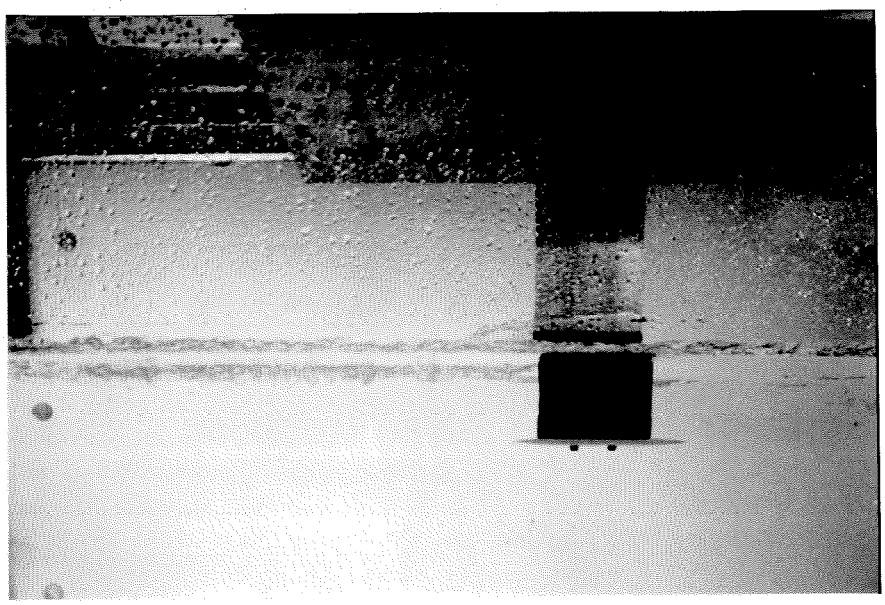

a. Foil stationary.

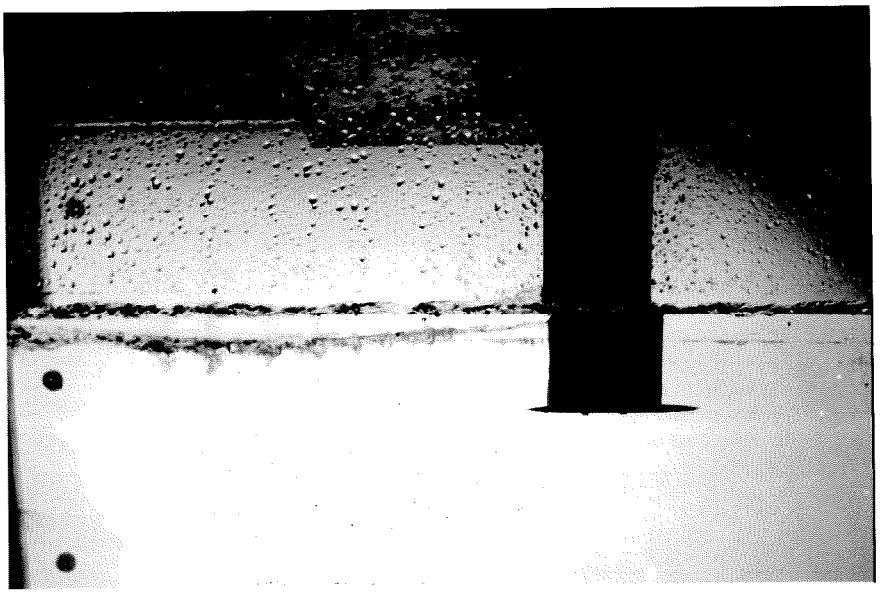

b. Foil oscillating; reduced frequency = 0.71.

Fig. 18 - Displacement of the free surface due to the heaving motion of a fully wetted hydrofoil.

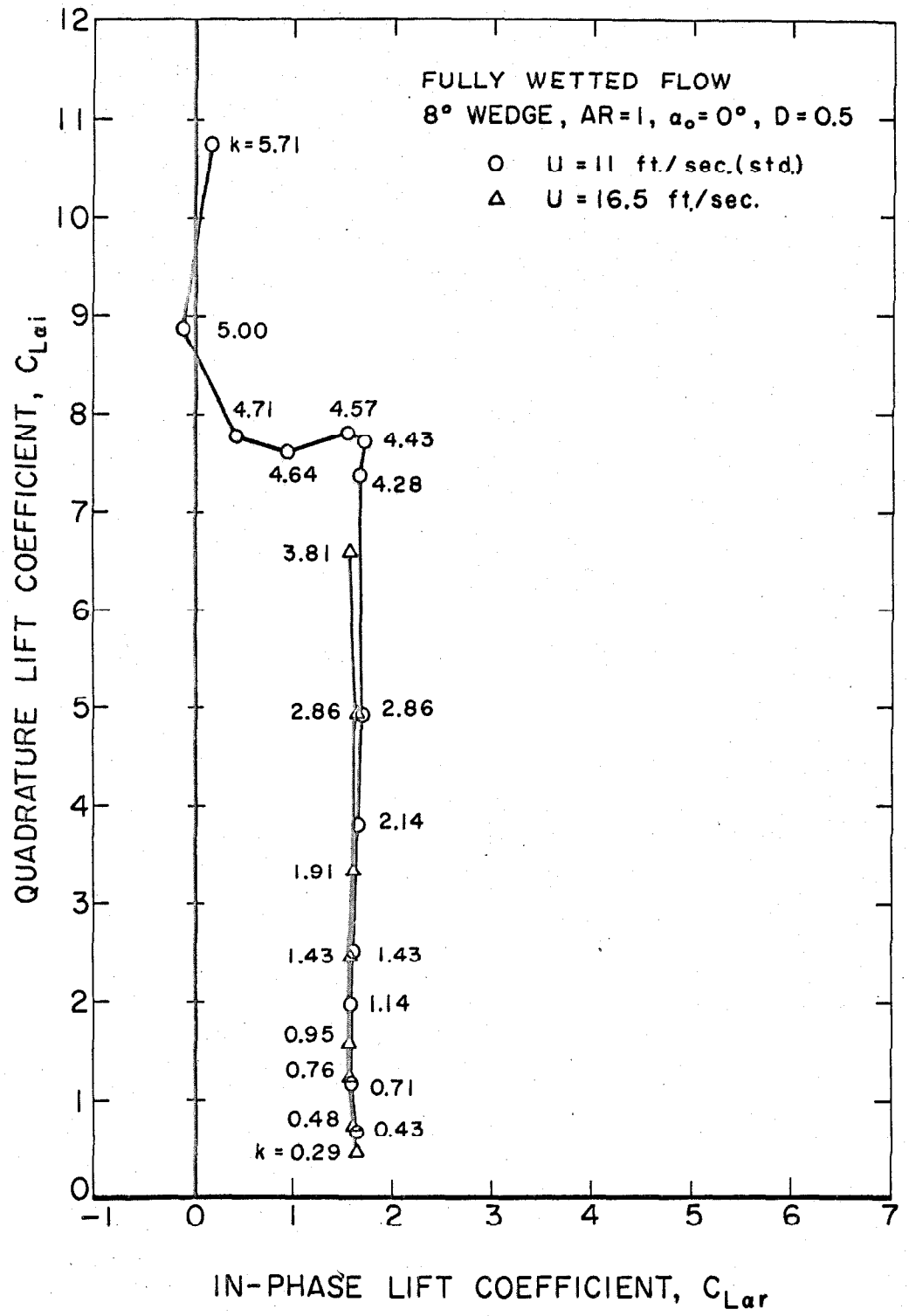

Fig. 19 - Variation of the unsteady lift coefficients with reduced frequency for the aspect ratio one wedge in fully wetted flow, showing the effect of flow velocity.

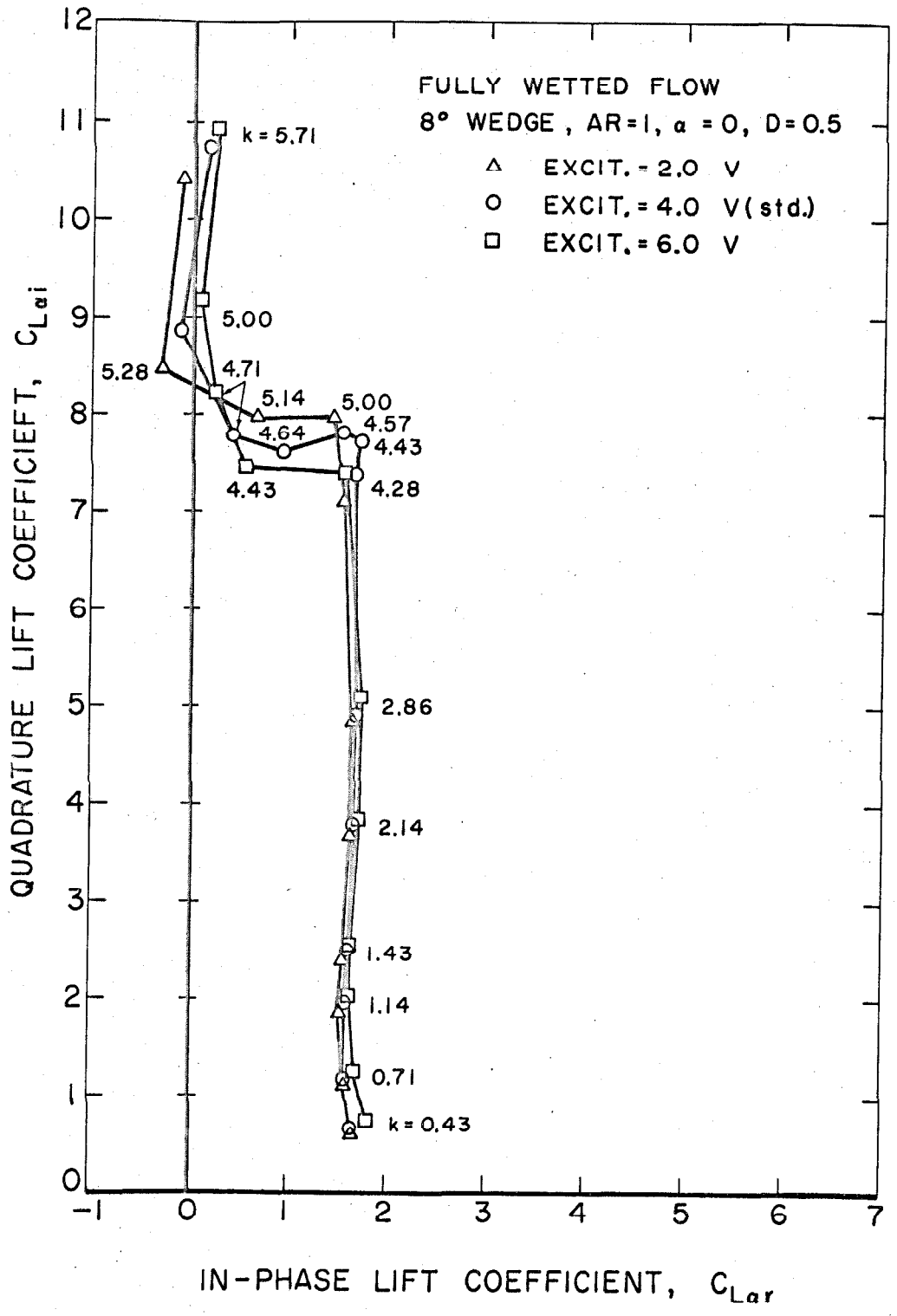

Fig. 20 - Variation of the unsteady lift coefficients with reduced frequency for the aspect ratio one wedge in fully wetted flow, showing the effect of oscillation amplitude.

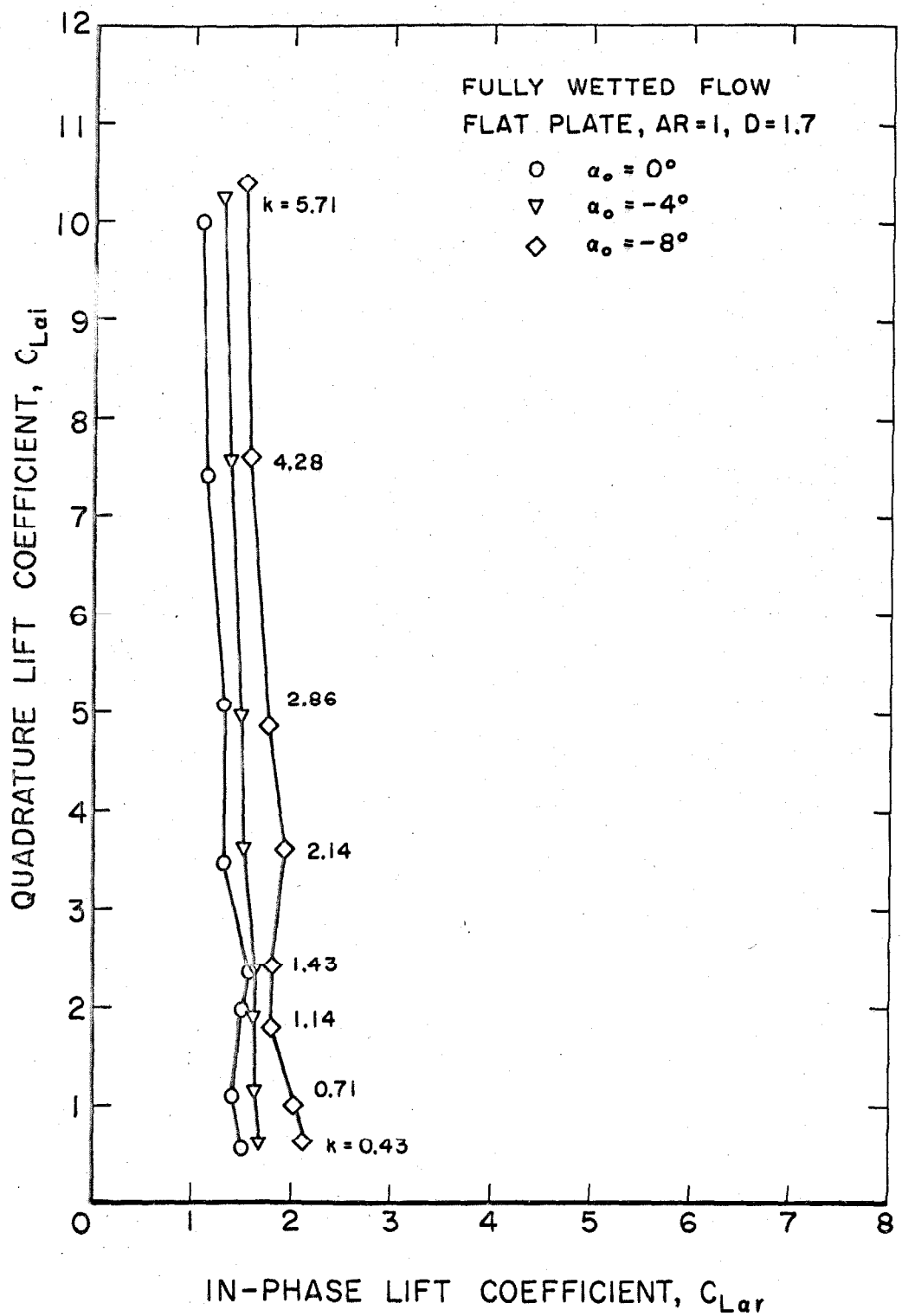

Fig. 21 - Variation of the unsteady lift coefficients with reduced frequency for the aspect ratio one flat plate in fully wetted flow, showing the effect of angle of attack.

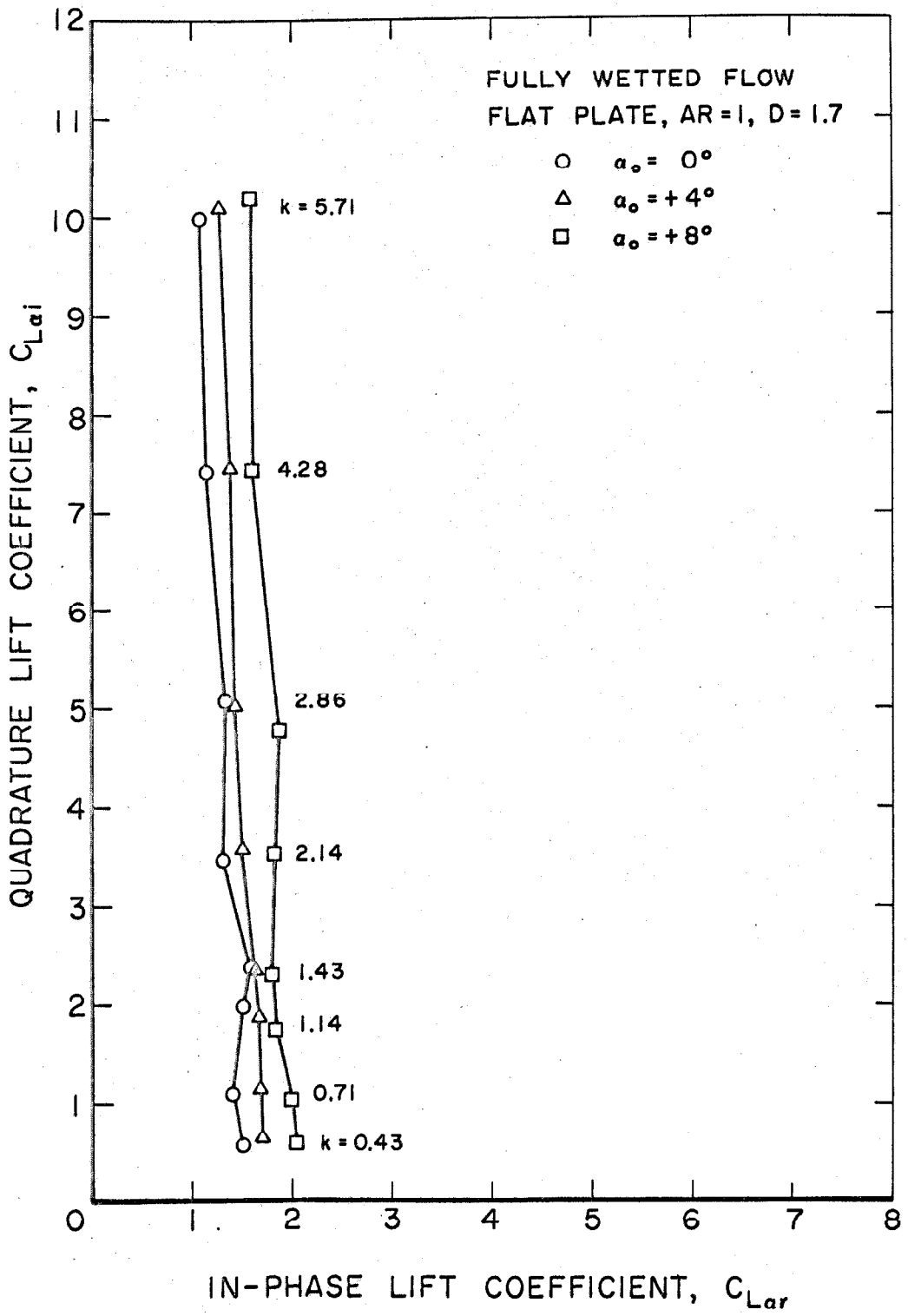

Fig. 22 - Variation of the unsteady lift coefficients with reduced frequency for the aspect ratio one flat plate in fully wetted flow, showing the effect of angle of attack.

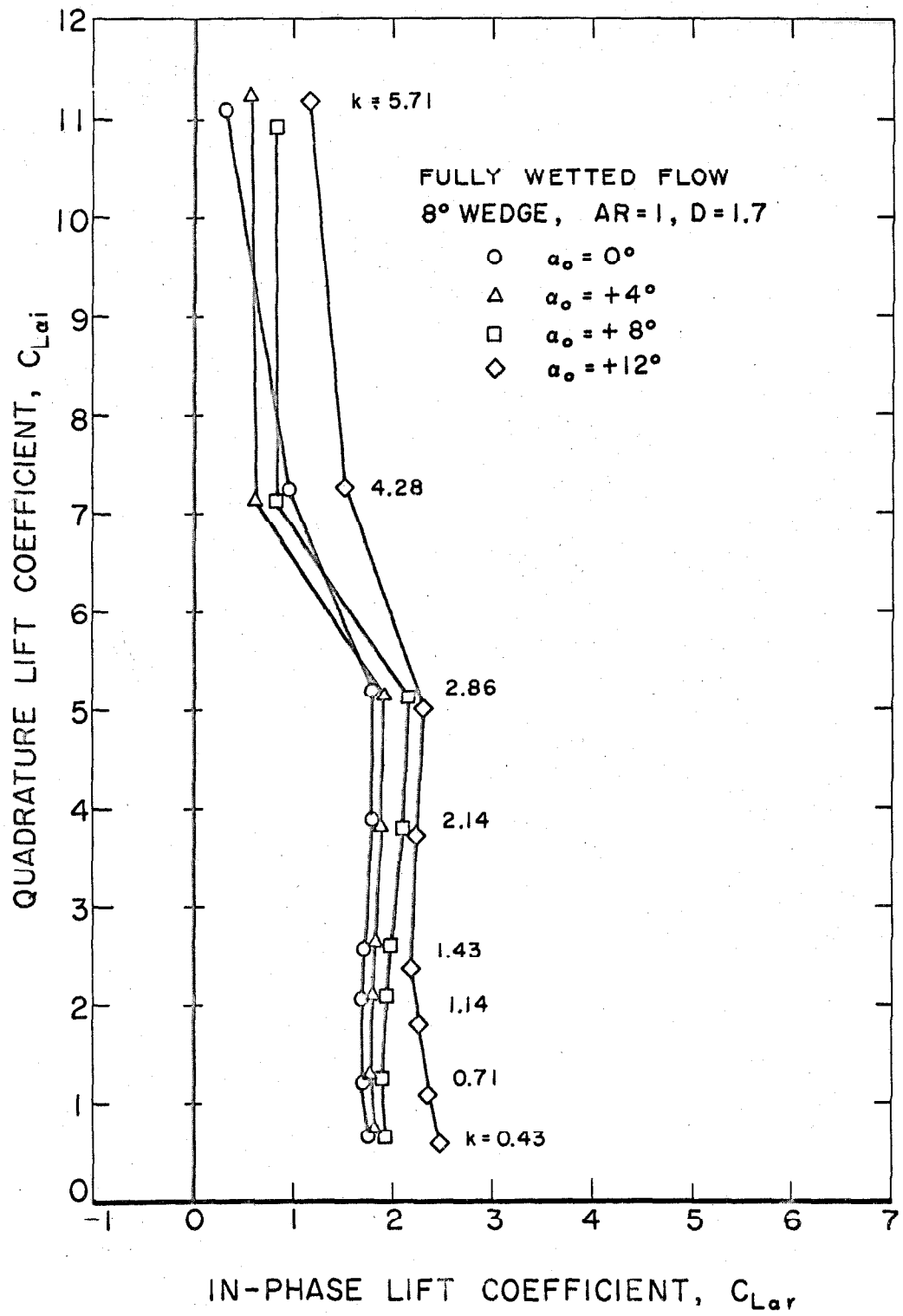

Fig. 23 - Variation of the unsteady lift coefficients with reduced frequency for the aspect ratio one wedge in fully wetted flow, showing the effect of angle of attack (first group of runs).

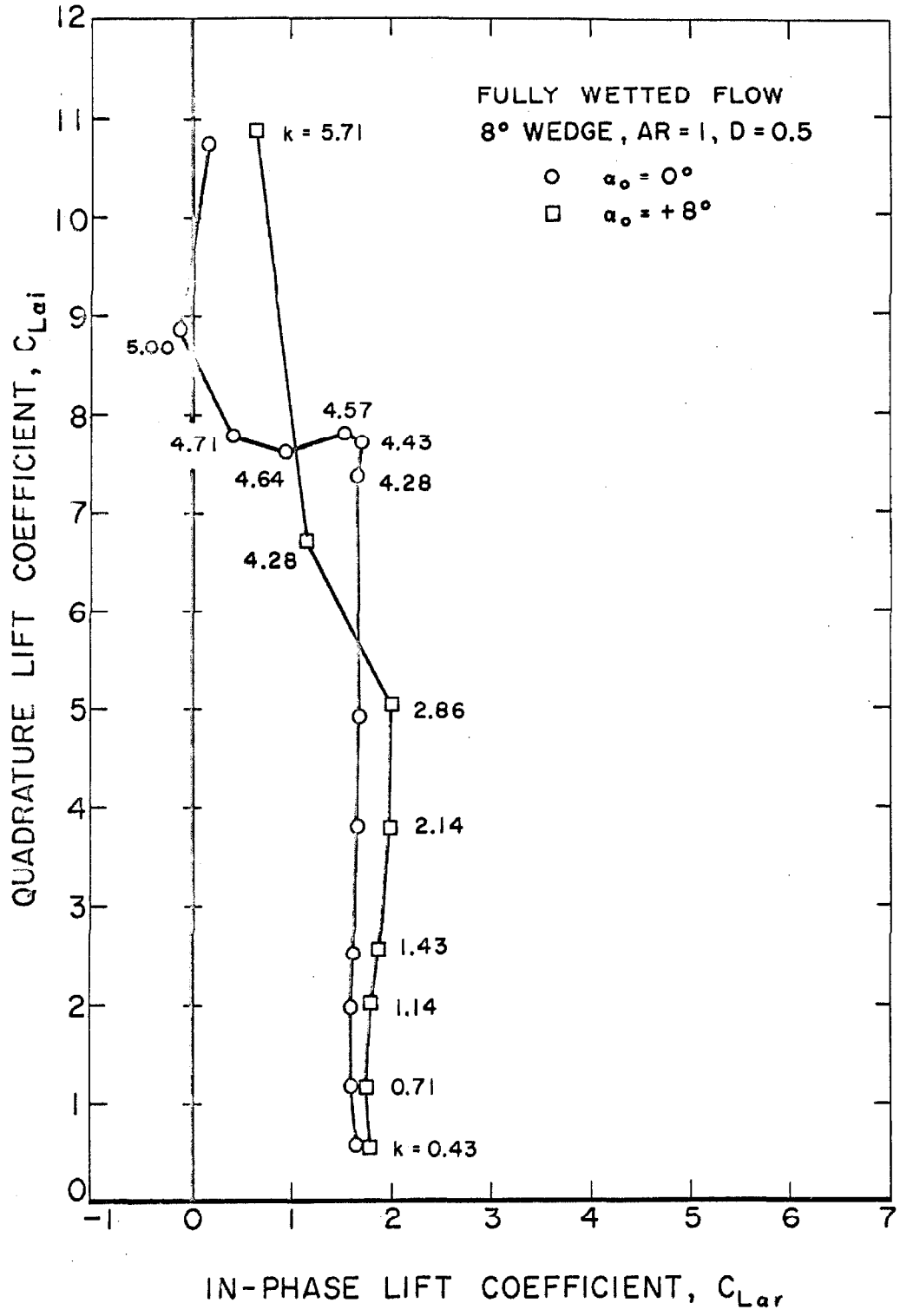

Fig. 24 - Variation of the unsteady lift coefficients with reduced frequency for the aspect ratio one wedge in fully wetted flow, showing the effect of angle of attack (second group of runs).

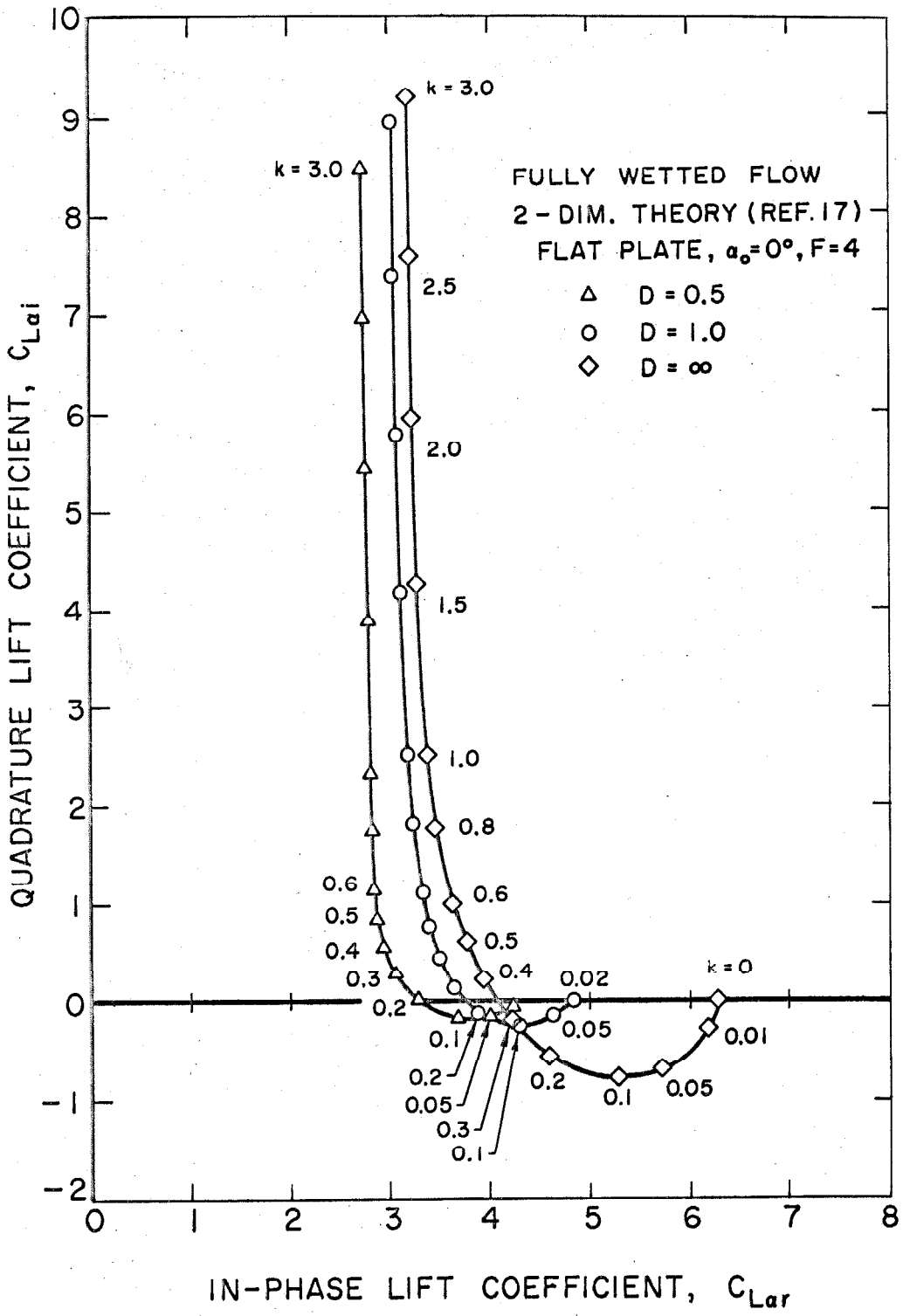

Fig. 25 - Theoretical variation of the unsteady lift coefficients with reduced frequency for a two-dimensional fully wetted flat plate, showing the effect of submergence.

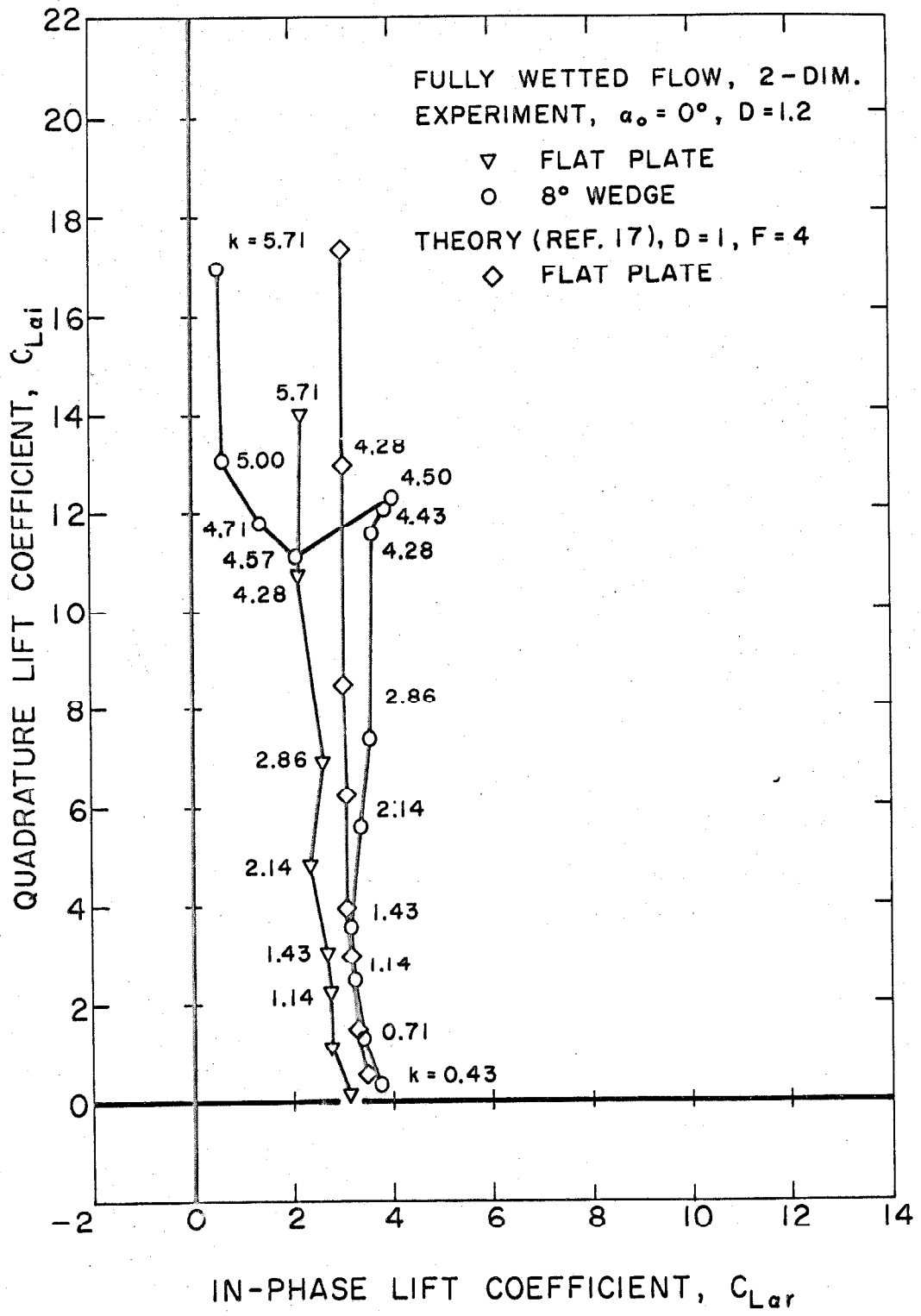

Fig. 26 - Variation of the unsteady lift coefficients with reduced frequency for the two-dimensional fully wetted flat plate and wedge.

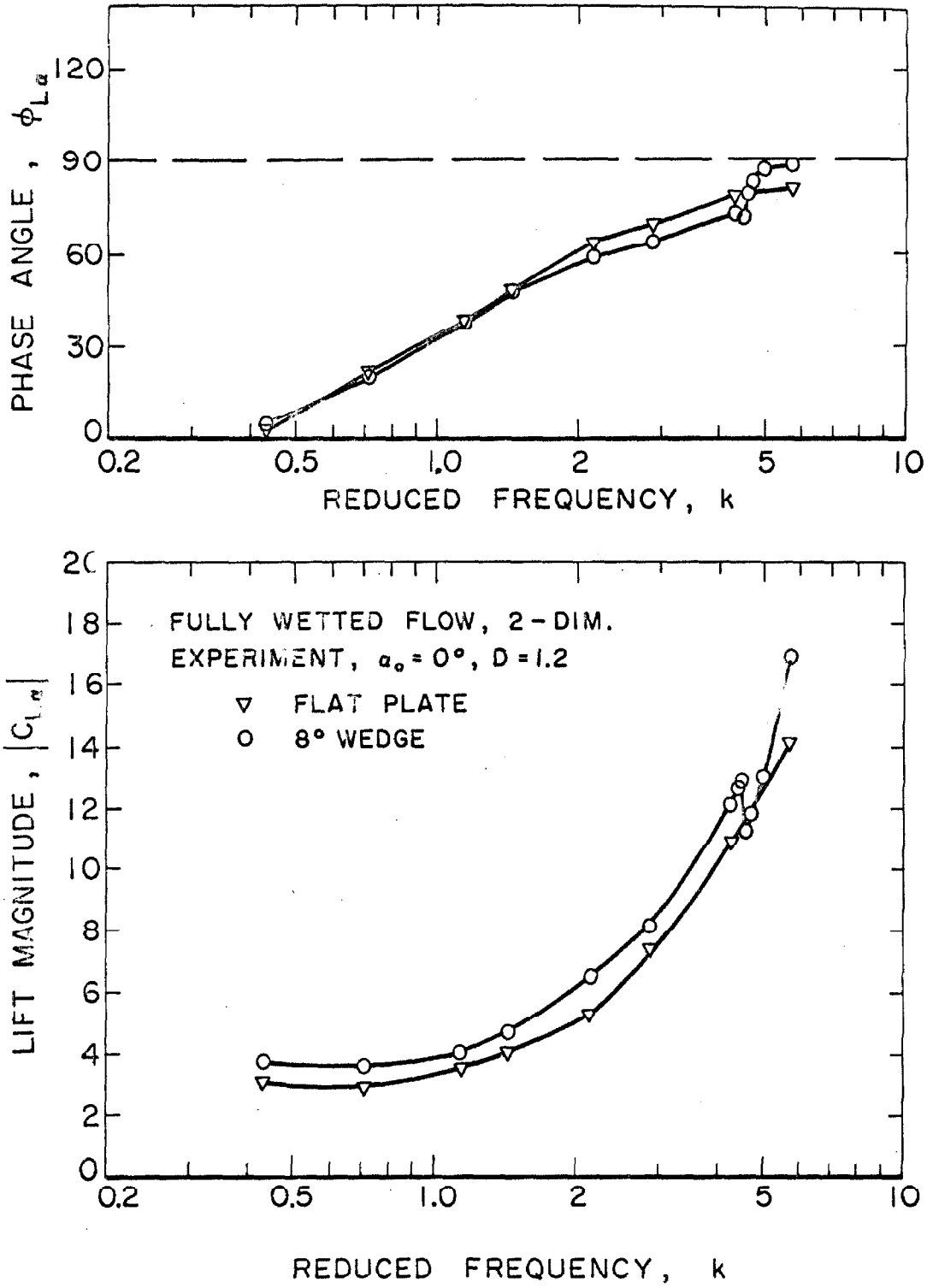

Fig. 27 - Magnitude-and-phase plot of the variation of the unsteady lift coefficients with reduced frequency for the two-dimensional fully wetted flat plate and wedge of Fig. 26.

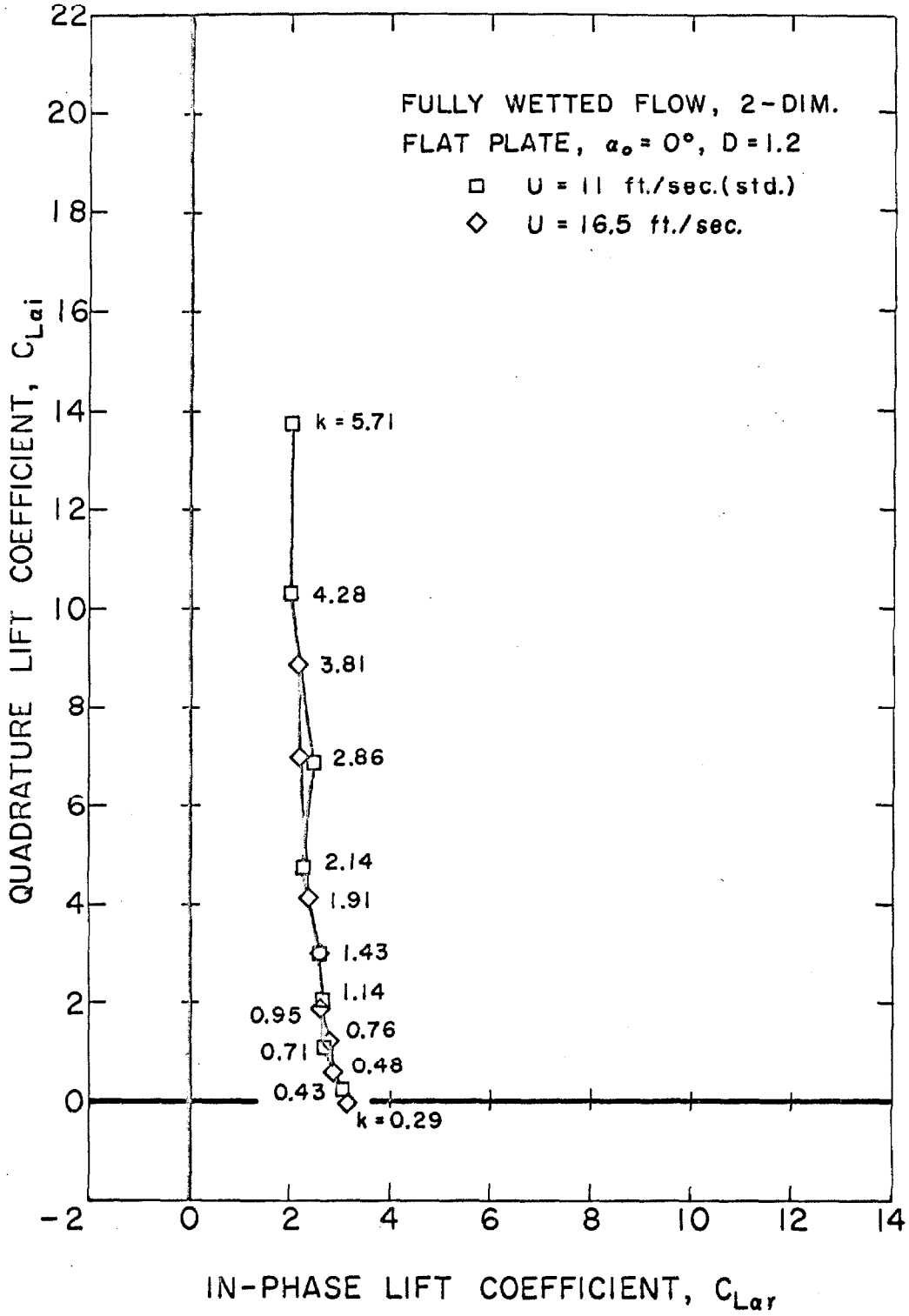

Fig. 28 - Variation of the unsteady lift coefficients with reduced frequency for the two-dimensional fully wetted flat plate, showing the effect of flow velocity.

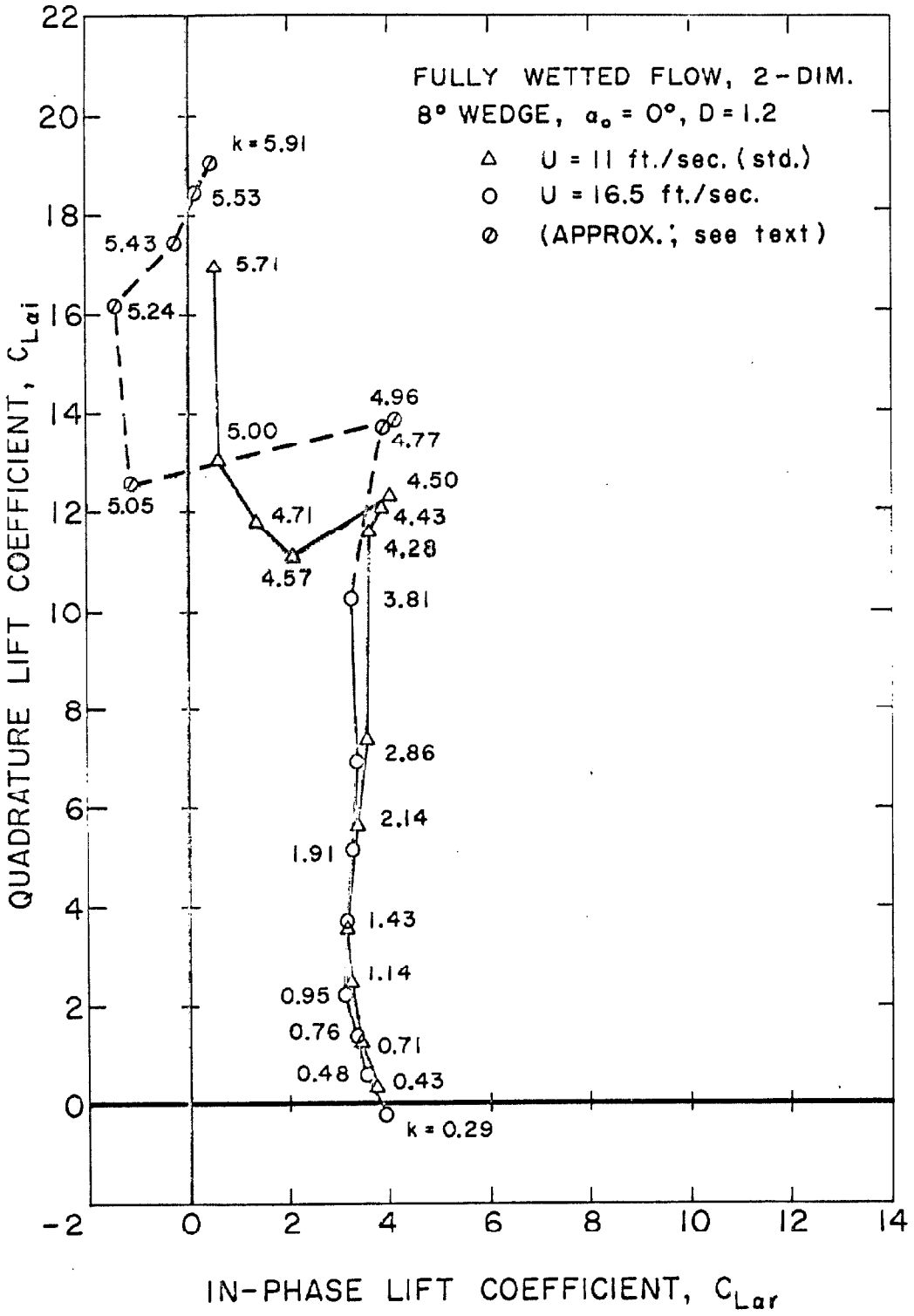

Fig. 29 - Variation of the unsteady lift coefficients with reduced frequency for the two-dimensional fully wetted wedge, showing the effect of flow velocity.

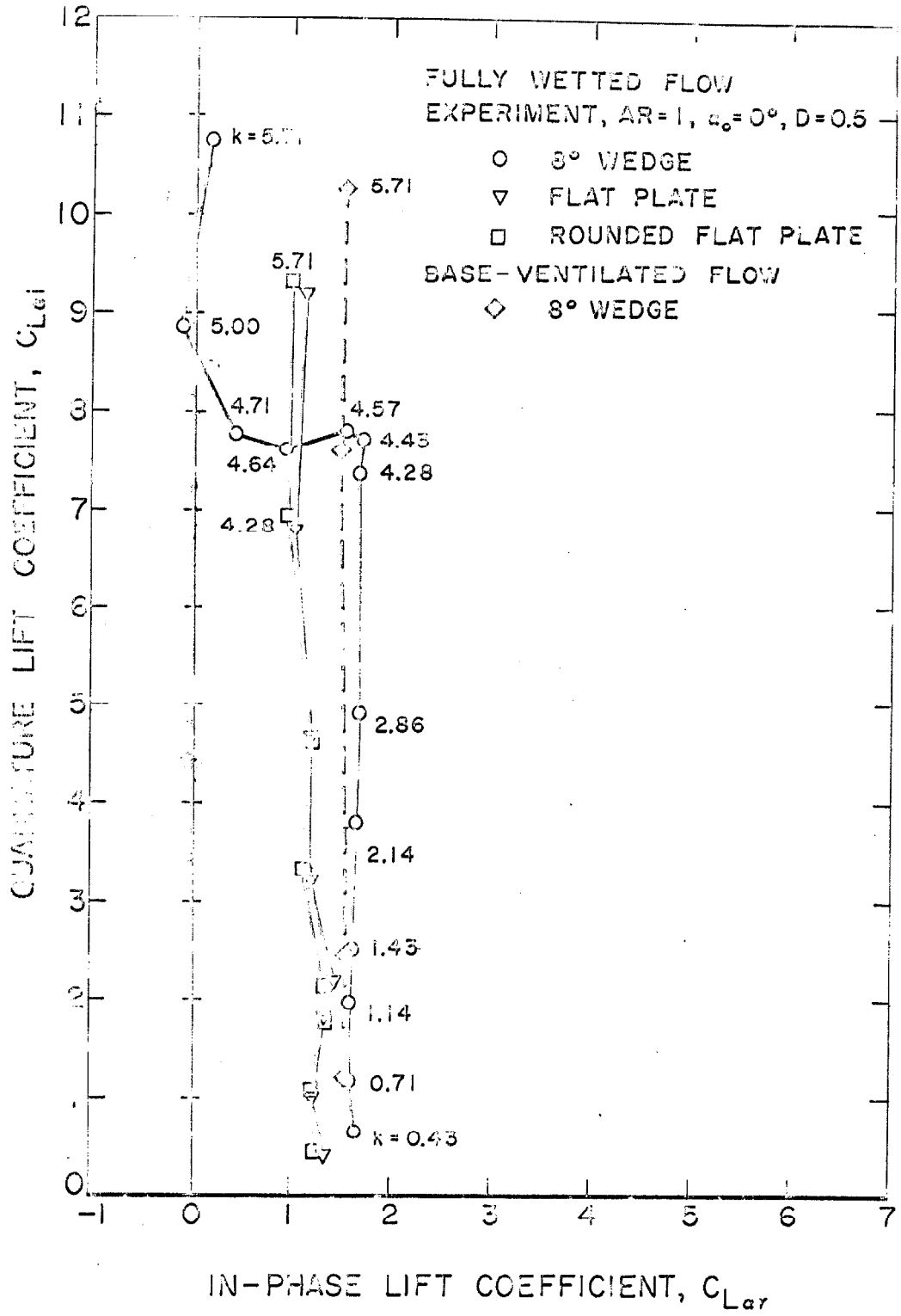

Fig. 30 - Variation of the unsteady lift coefficients with reduced frequency for the aspect ratio one wedge with base ventilation, and comparison with fully wetted results.

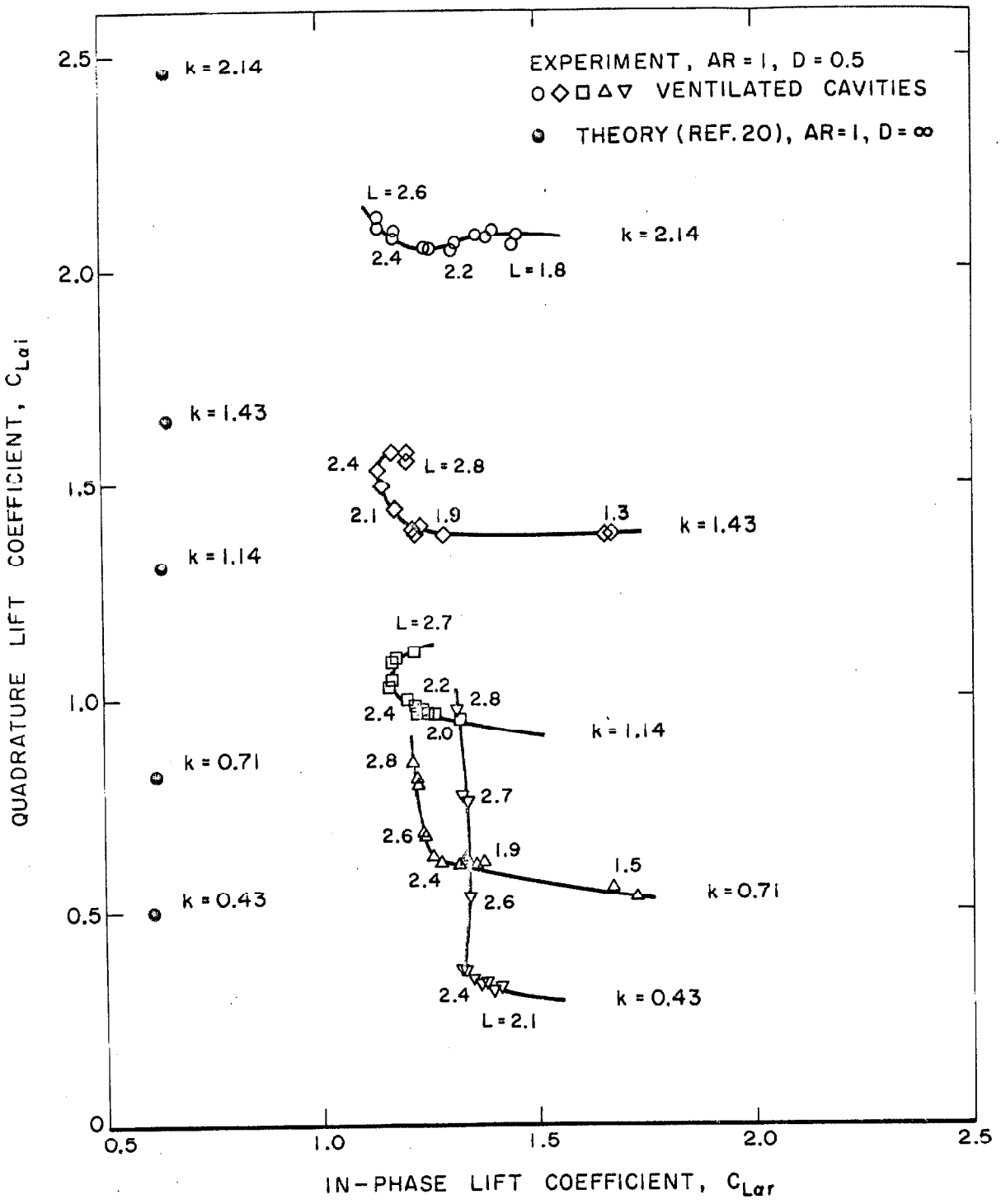

Fig. 31 - Variation of the unsteady lift coefficients with cavity length at several values of reduced frequency for the supercavitating aspect ratio one wedge.

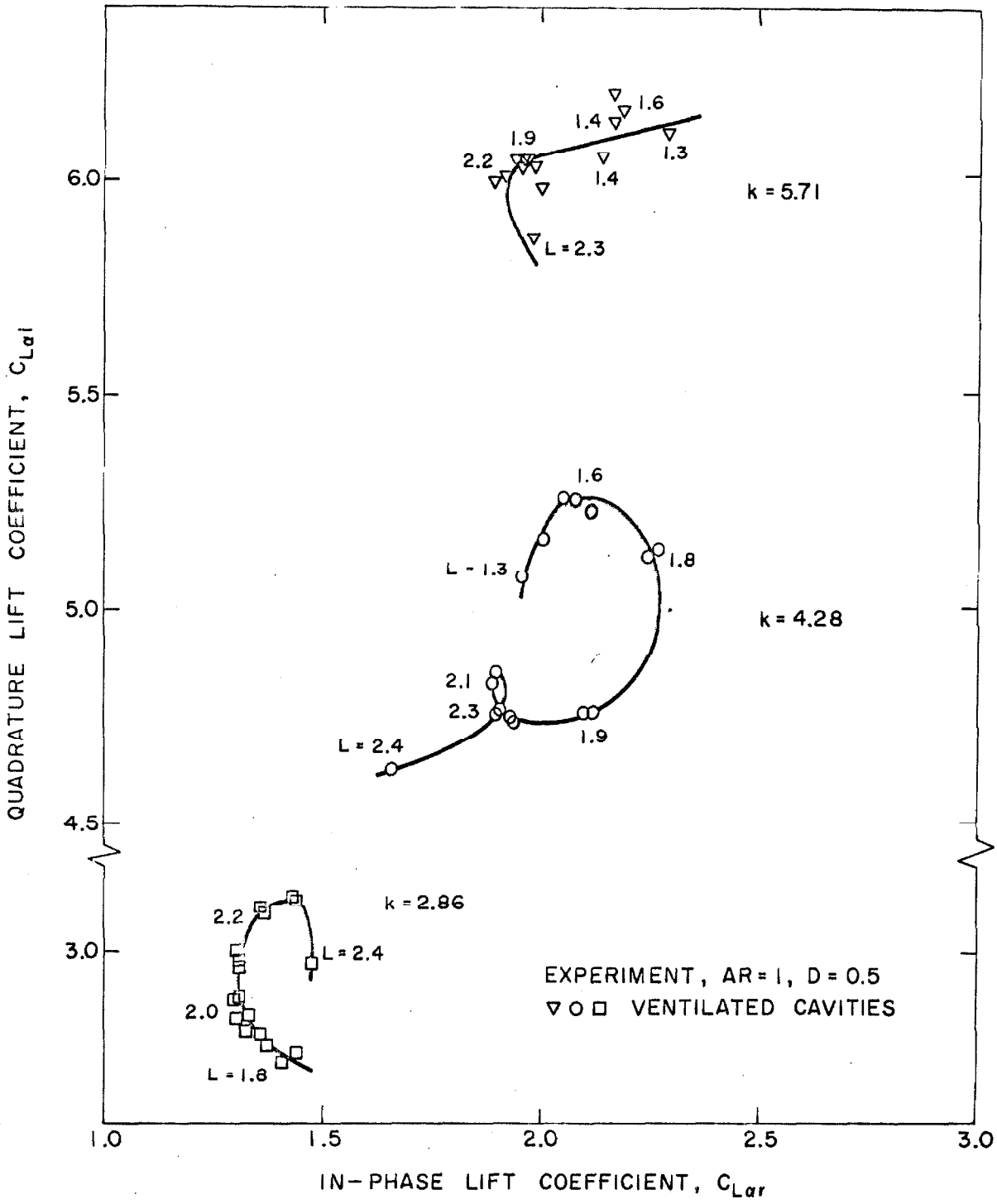

Fig. 32 - Variation of the unsteady lift coefficients with cavity length at several values of reduced frequency for the supercavitating aspect ratio one wedge.

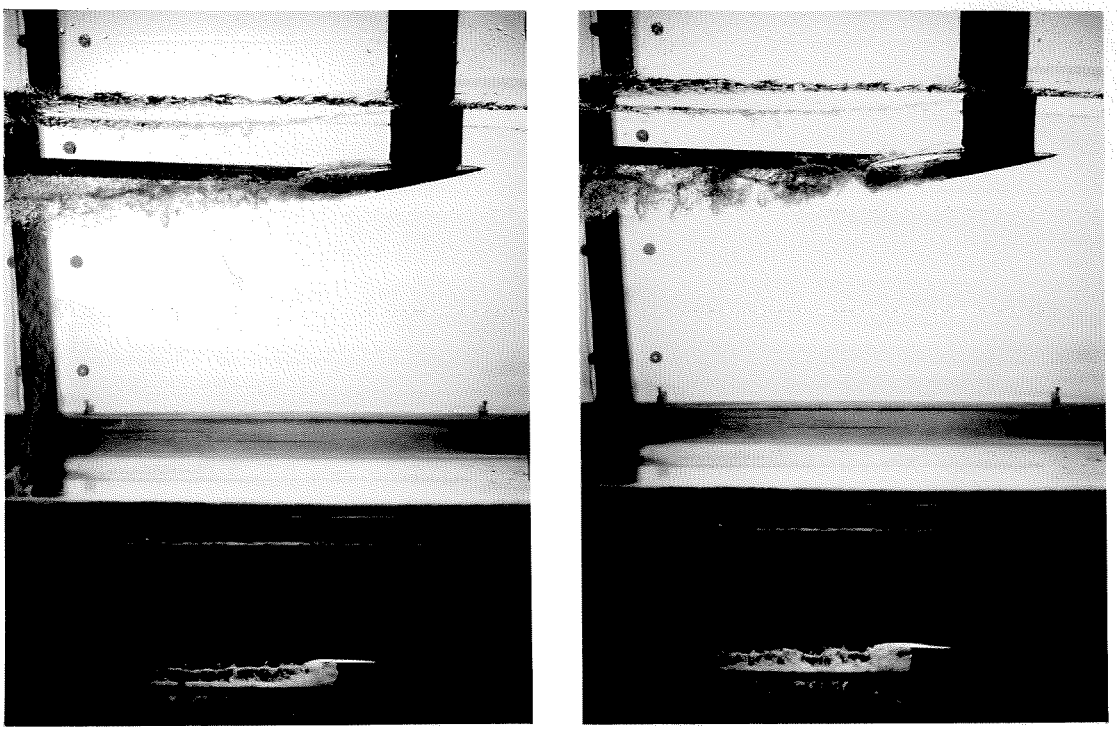

a. Foil stationary; $C_Q = 0.029$, $\sigma_k = 0.168$. b. $C_Q = 0.051$, $\sigma_k = 0.163$.

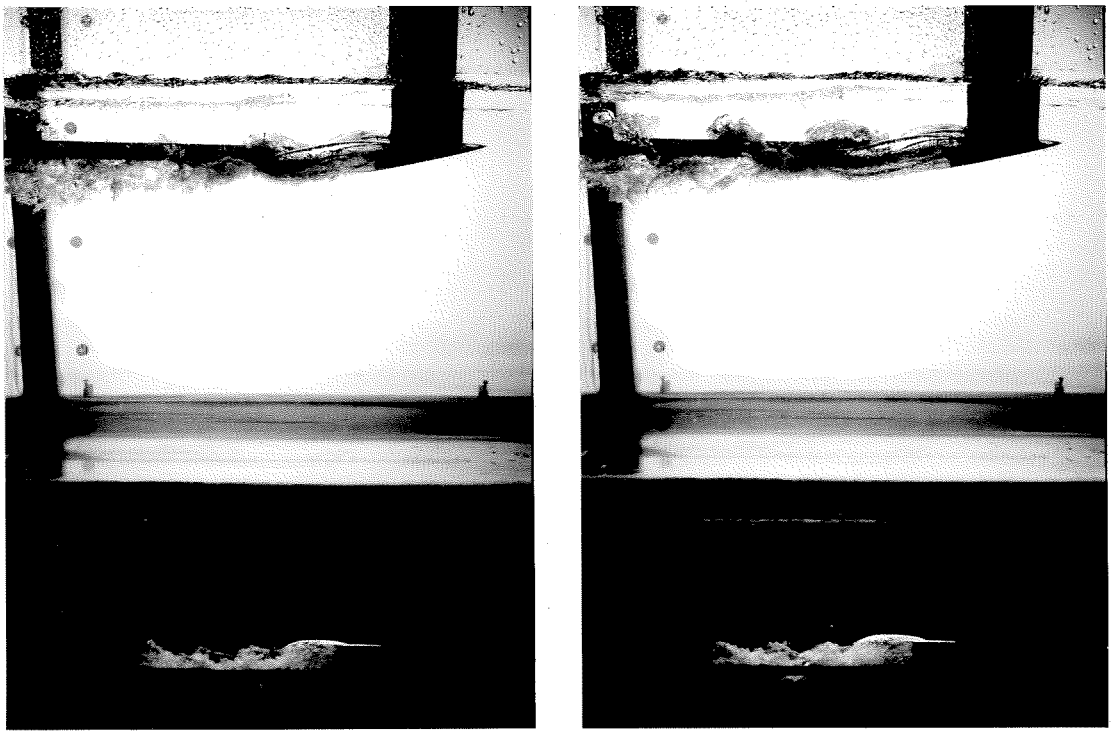

c. $C_Q = 0.067$, $\sigma_k = 0.142$. d. $C_Q = 0.172$, $\sigma_k = 0.116$.

Fig. 33 - High-speed flash photographs of the ventilated cavity behind the aspect ratio one wedge; k = 2.86.

a. $C_Q = 0.047$, $\sigma_k = 0.163$.

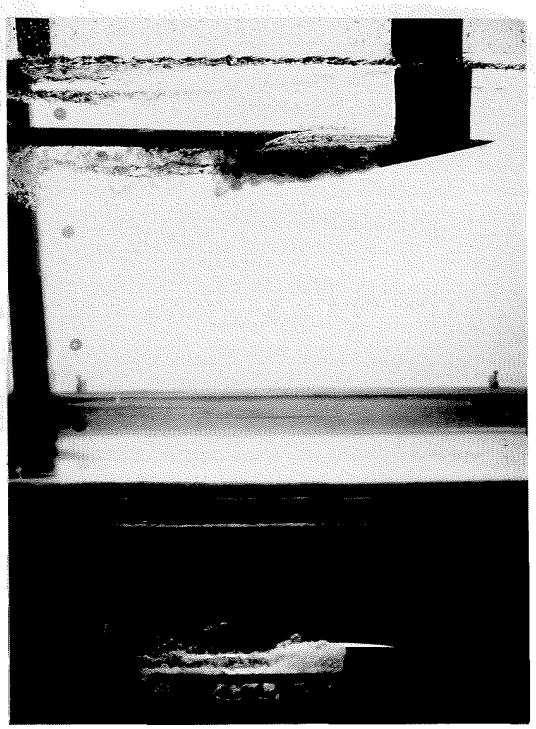

b. $C_Q = 0.093$, $\sigma_k = 0.132$.

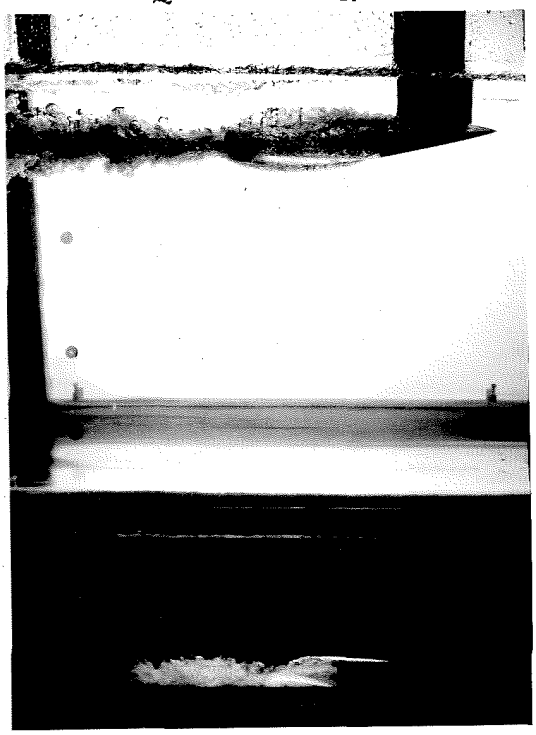

c. $C_Q = 0.093$, $\sigma_k = 0.132$.

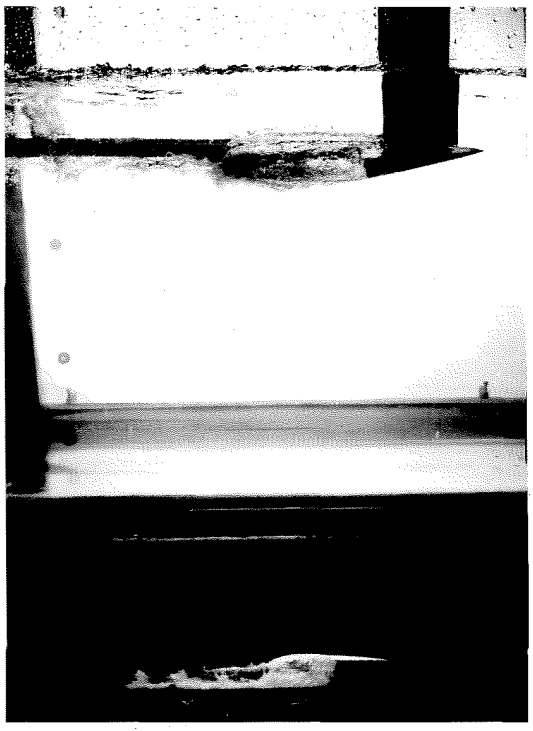

d. $C_Q = 0.113$, $\sigma_k = 0.111$.

Fig. 34 - High-speed flash photographs of the ventilated cavity behind the aspect ratio one wedge; k = 0.43.

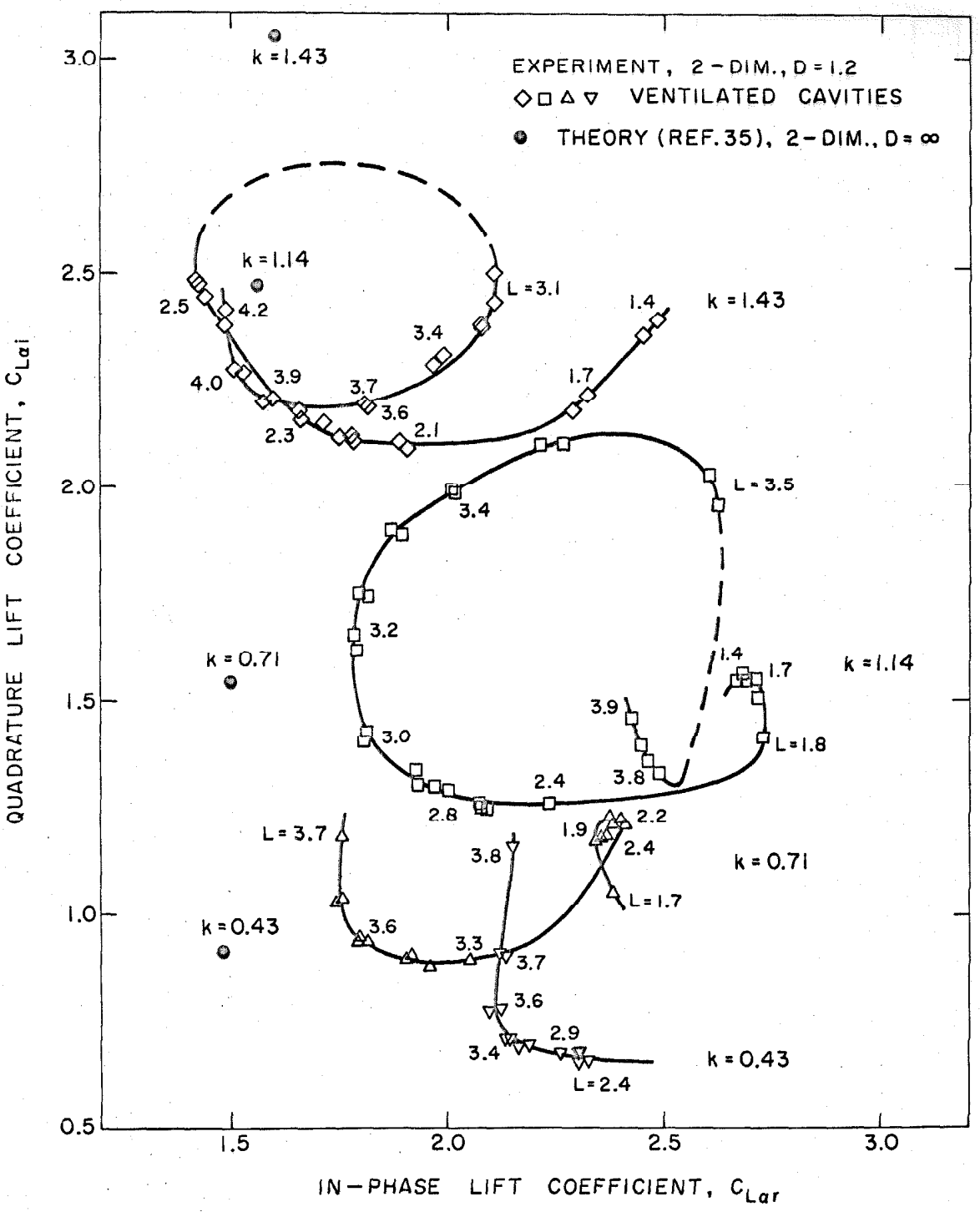

Fig. 35 - Variation of the unsteady lift coefficients with cavity length at several values of reduced frequency for the supercavitating wedge in two-dimensional flow.

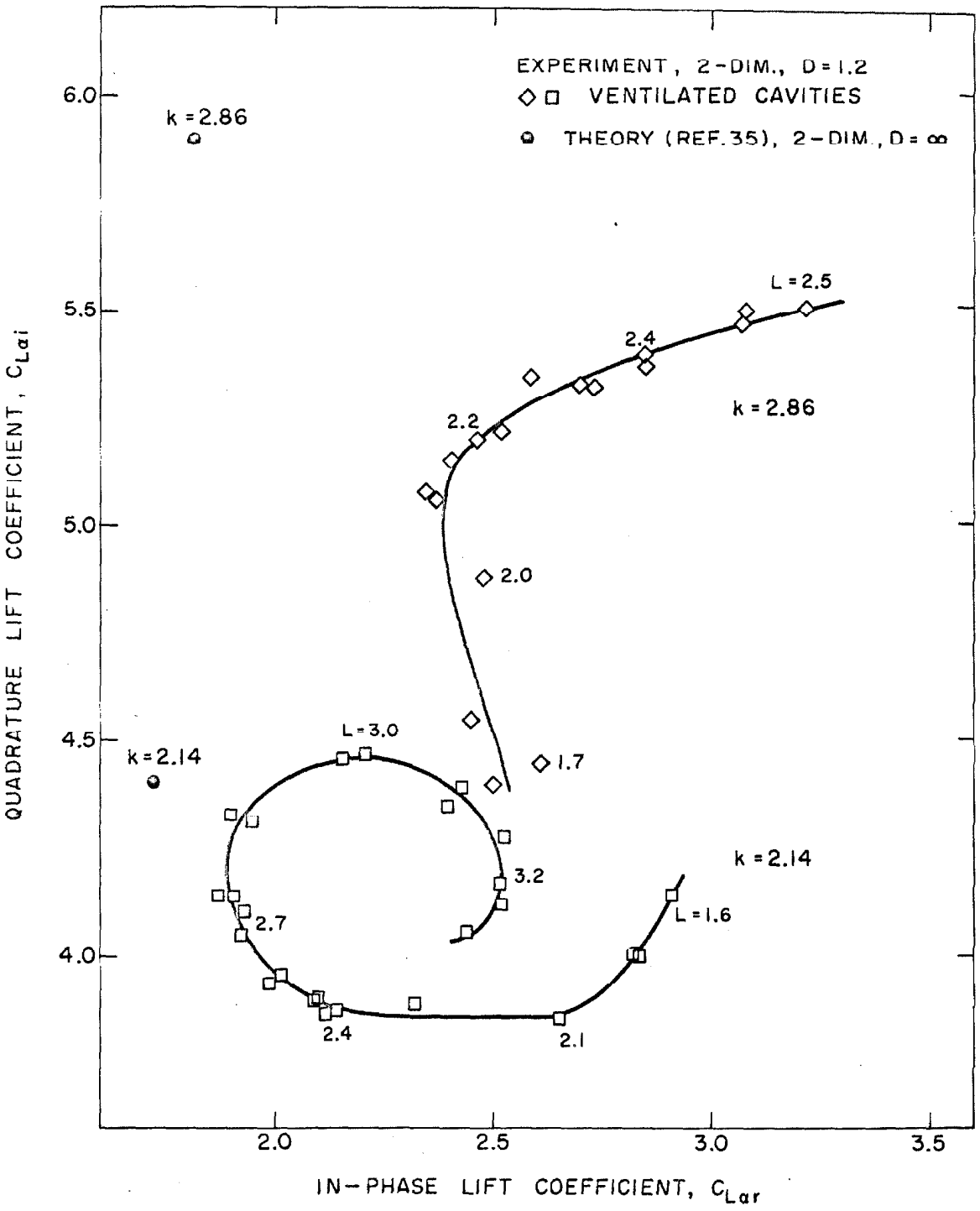

Fig. 36 - Variation of the unsteady lift coefficients with cavity length at several values of reduced frequency for the supercavitating wedge in two-dimensional flow.

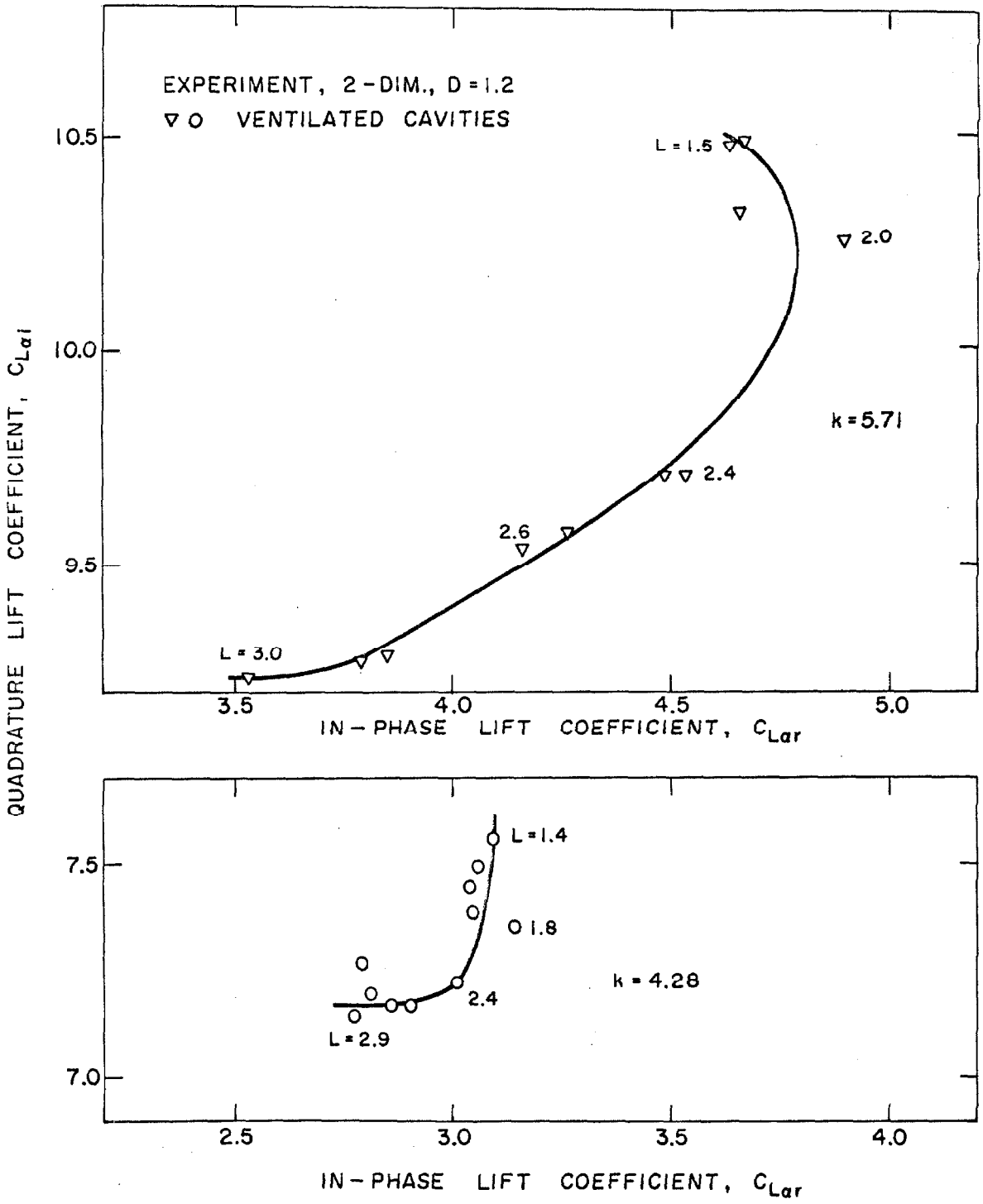

Fig. 37 - Variation of the unsteady lift coefficients with cavity length at several values of reduced frequency for the supercavitating wedge in two-dimensional flow.

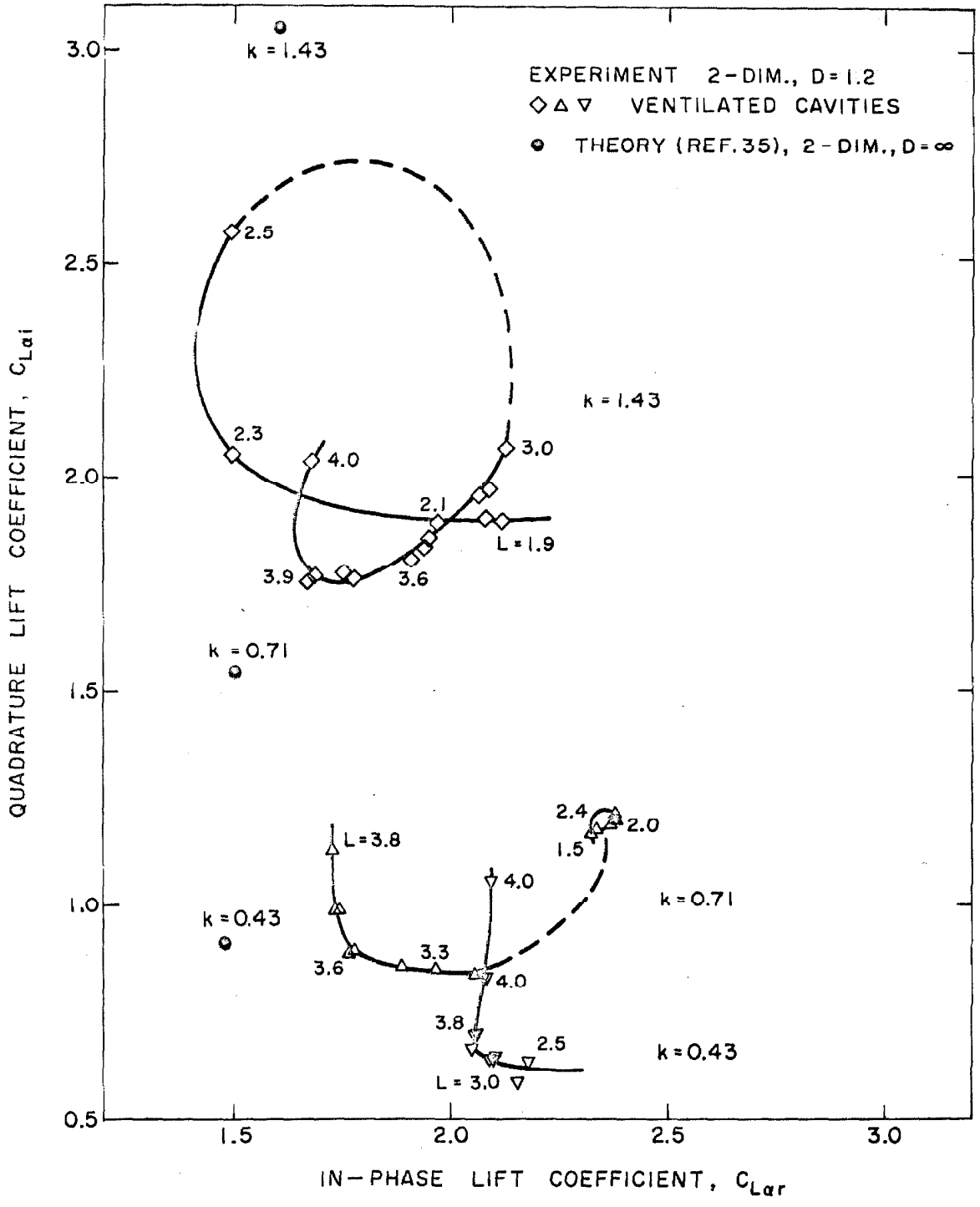

Fig. 38 - Variation of the unsteady lift coefficients with cavity length at several values of reduced frequency for the supercavitating wedge in two-dimensional flow. (Repeat of runs in Fig. 35)

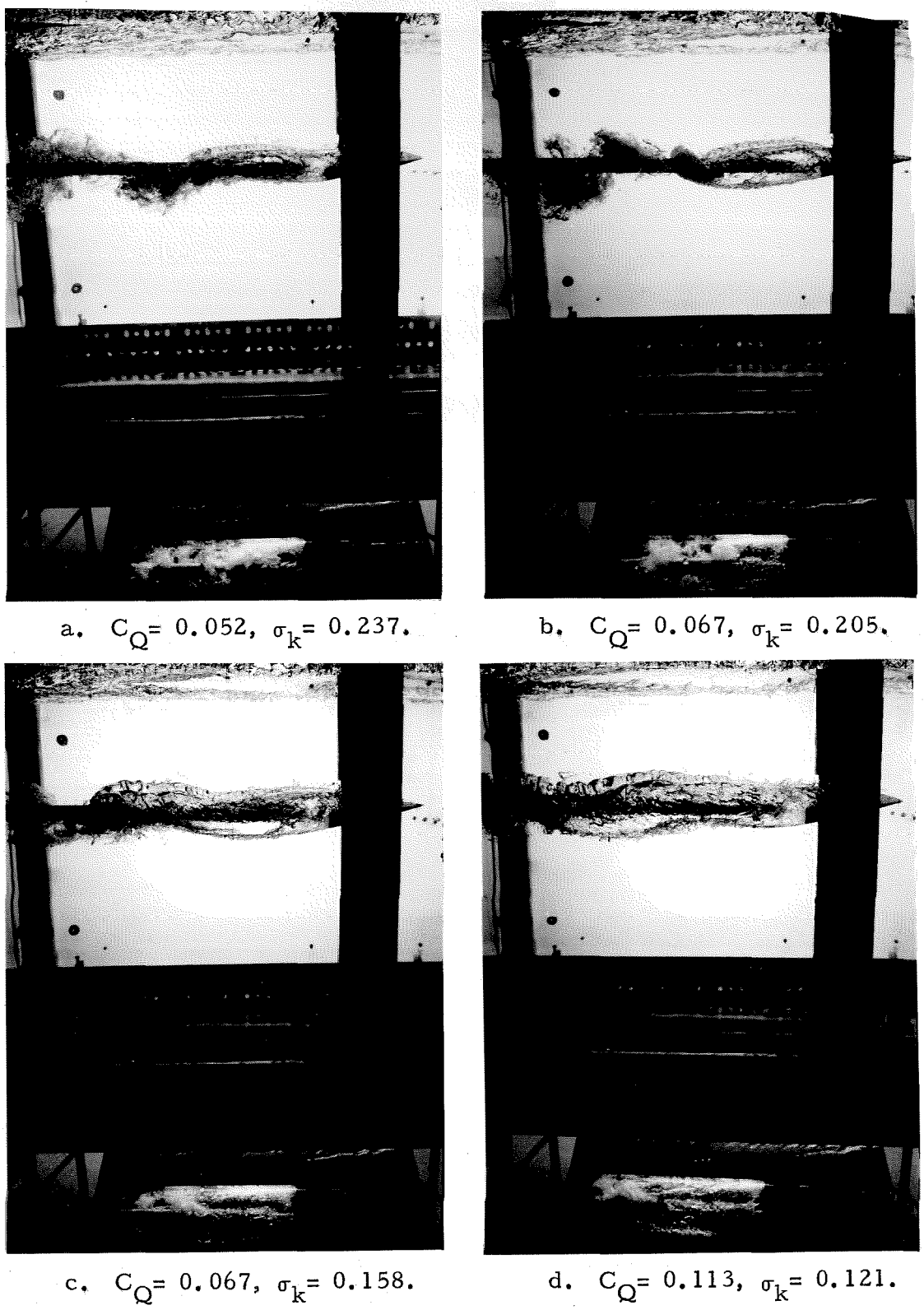

a. $C_Q = 0.052$, $\sigma_k = 0.237$.

b. $C_Q = 0.067$, $\sigma_k = 0.205$.

c. $C_Q = 0.067$, $\sigma_k = 0.158$.

d. $C_Q = 0.113$, $\sigma_k = 0.121$.

Fig. 39 - High-speed flash photographs of the ventilated cavity behind the wedge in two-dimensional flow; k = 1.43.

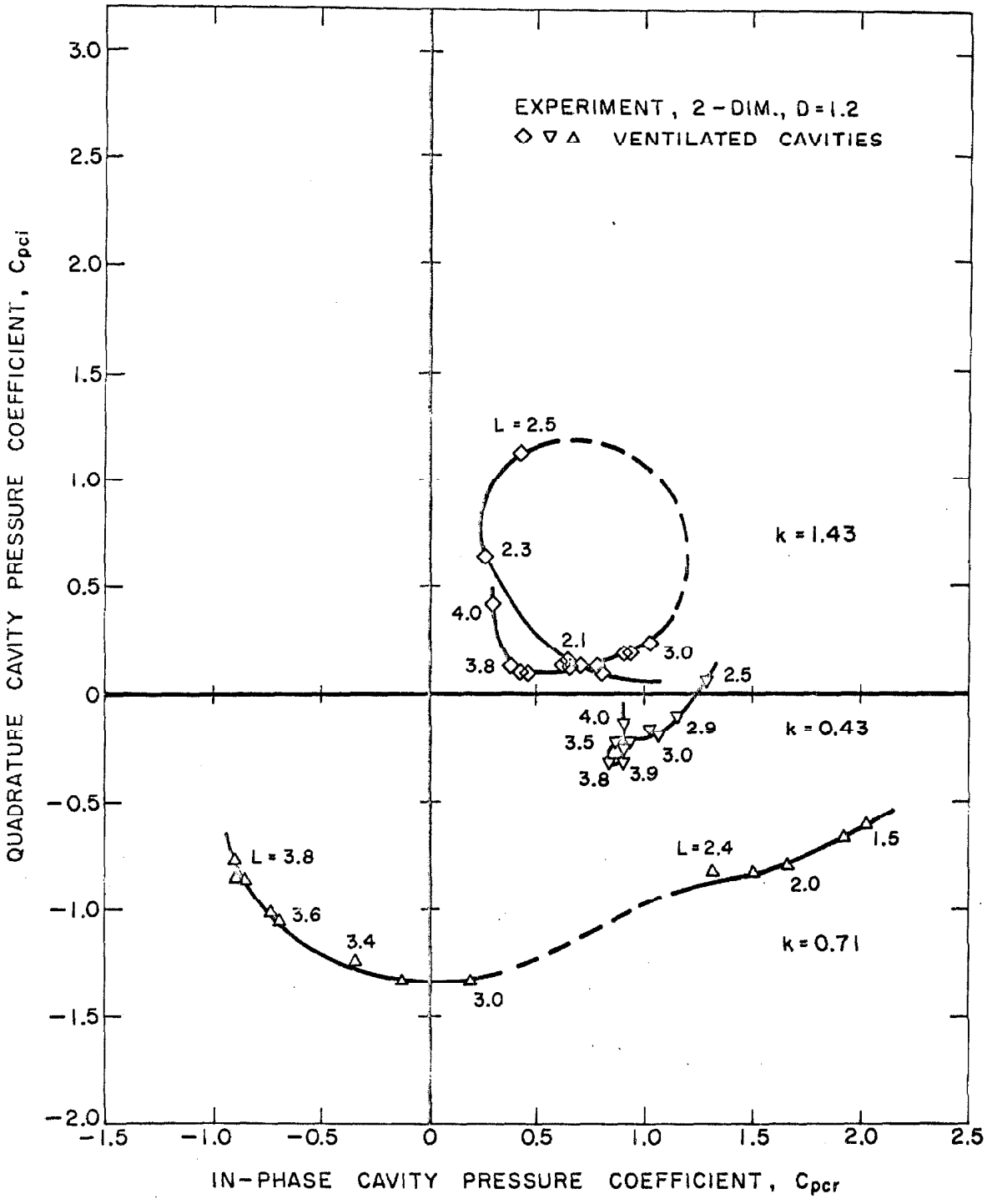

Fig. 40 - Variation of the unsteady cavity pressure with cavity length for the tests shown in Fig. 38.

APPENDIX

SYMBOLS AND NOTATION

A	foil planform area, $= 2bs = cs$
A_p	projected foil area normal to the flow
AR	aspect ratio, $= s/c$
b	foil semi-chord
c	foil chord
$C_{L\alpha r}$	in-phase lift coefficient (see p. 47)
$C_{L\alpha i}$	quadrature lift coefficient (see p. 47)
$C_{L\alpha}$	vector magnitude of unsteady lift coefficient, $= \sqrt{C_{L\alpha r}^2 + C_{L\alpha i}^2}$
C_{pcr}	in-phase cavity pressure coefficient (see p. 49)
C_{pci}	quadrature cavity pressure coefficient (see p. 49)
C_Q	air flow rate coefficient, $= Q/A_pU$ (see p. 47)
D	submergence depth in terms of the hydrofoil chord
f	frequency in cycles per second, $= \omega/2\pi$
F	Froude Number based on semi-chord, $= \frac{U}{\sqrt{bg}}$
g	acceleration due to gravity
k	reduced frequency, $= \frac{\omega b}{U} = \frac{\omega c}{2U}$
L	cavity length in terms of the hydrofoil chord
p_o	ambient static pressure
p_c	cavity pressure

Q air flow rate, corrected to atmospheric pressure

Re Reynolds Number, $= \frac{Uc}{\nu}$

V_{osc} transverse velocity due to the heaving oscillation

w base height of wedge

α_o stationary angle of attack

ν kinematic viscosity

ρ density of water

σ_k cavitation number, $= \frac{p_o - p_c}{\frac{1}{2}\rho U^2}$

$\phi_{L\alpha}$ phase angle of unsteady lift coefficient,

$$= \tan^{-1}\left(\frac{C_{l\alpha i}}{C_{L\alpha r}}\right)$$

ω frequency in radians per second, $= 2\pi f$